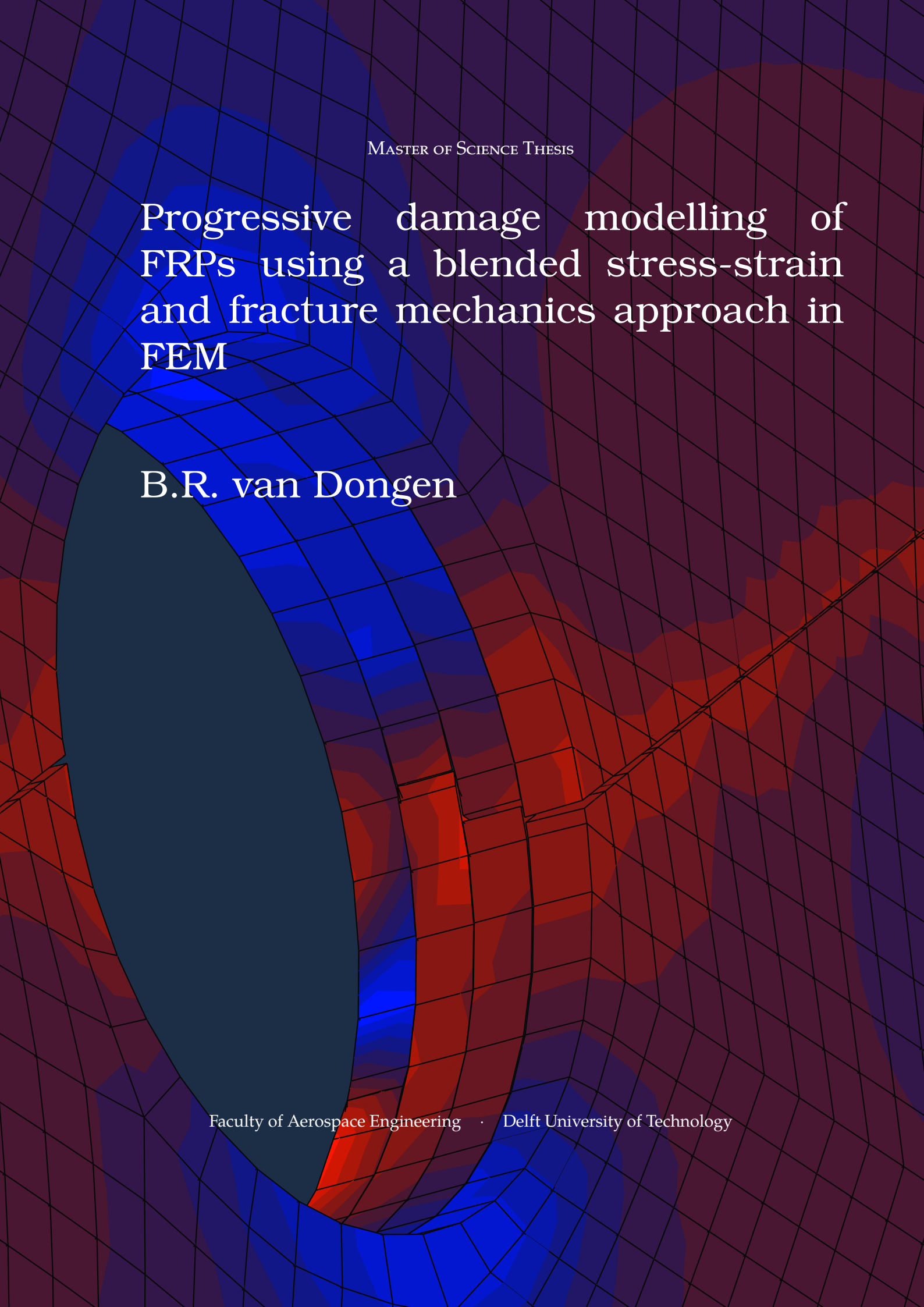

Master of Science Thesis

Progressive damage modelling of FRPs using a blended stress-strain and fracture mechanics approach in FEM

B.R. van Dongen

Faculty of Aerospace Engineering · Delft University of Technology

Progressive damage modelling of FRPs using a blended stress-strain and fracture mechanics approach in FEM

Master of Science Thesis

For obtaining the degree of Master of Science in Aerospace Engineering
at Delft University of Technology

B.R. van Dongen

June 29, 2017

Faculty of Aerospace Engineering · Delft University of Technology

Delft University of Technology
Faculty of Aerospace Engineering
Department of Aerospace Structures and Materials

GRADUATION COMMITTEE

Dated: June 29, 2017

Chair holder:

Dr.ir. R.C. Alderliesten

Committee members:

Dr.ir. D.S. Zarouchas

Dr. C.D. Rans

Dr.ir. F.P. van der Meer

Abstract

Fiber Reinforced Polymers (FRPs) have found widespread application in numerous industries, foremost among which the aerospace industry. The advent of FRPs is propelled by advantages in structural efficiency, performance, versatility and cost. However, despite great strides made over the past decades in understanding and modelling FRPs, the full potential of FRPs is held back by an inability to accurately predict and describe failure, made glaringly obvious by first and second installments of The World-Wide Failure Exercise.

Academia is struggling to found new failure theories upon a physical basis, but understanding is lacking and current design practice suffers. Opinions are divided on the appropriate basis for prediction, and past attempts have been focused on isolated application of stress-strain arguments on one hand and fracture mechanics on the other hand. Contrary to these attempts, this research builds upon the existing framework by combining failure theories. In this light, this study provides a critical evaluation of stress-strain based methods for Progressive Damage Analysis (PDA) of FRPs and practical Finite Element Model (FEM) implementation thereof as well as alleviating shortcomings by blending in fracture mechanics, validated by numerous case studies and experimental campaigning.

Over the years, remarkable efforts have been made to predict damage initiation on a stress-strain basis. Conducting a failure analysis and trade-off on a variety of cases selected from The First World-Wide Failure Exercise confirmed Cuntze, Puck and LaRC05 criteria as top-performing damage initiation criteria, evaluated in terms of predictive accuracy, computational effort and versatility. A key consideration in achieving accurate predictions are in-situ strengths that reflect the experimentally observed effect of ply thickness and embeddedness on the apparent resistance to fracture.

Stress-strain based theories for propagating damage operate uniformly on the basis of stiffness degradation, either suddenly or gradually. Critical assessment and trade-off of leading theories based on test cases selected from The First World-Wide Failure Exercise offered little basis for distinction. Rather, numerical considerations formed a key reason for selecting a bilinear softening model and two sudden degradation models, those by McCarthy et al. and Camanho and Matthews, to complement LaRC05, Puck and Cuntze criteria respectively.

Selected theories were implemented, along with full constitutive modelling, in a UMAT subroutine in ABAQUS. A trio of study cases were analysed, covering a variety of material, lay-up and loading configurations. Results show remarkable capability in predicting laminate failure, particularly consistent for bilinear softening in conjunction with LaRC05 initiation (errors to within 6 %). Comparison to X-ray Computed Tomography (CT) scans shows significant discrepancies of the sudden degradation models with respect to experimental failure patterns, as one of the stress-strain based models pertain to a strong physical basis. Only the bilinear softening model shows decent correspondence, although damage is excessively smeared.

To alleviate this key shortcoming of stress-strain approaches in predicting failure patterns, a fracture mechanics approach was adopted to model matrix failure using the Extended Finite

Element Method (XFEM) and a UDMGINI subroutine. The use of XFEM yields great versatility, allowing cracks to grow and propagate at any location, as opposed to inserting cohesive interfaces at known crack locations. Moreover, the lack of satisfactory stress-strain methods for predicting delaminations led to the adoption of a Cohesive Zone Model (CZM) to model interlaminar failure. This blended approach displays good capability in modelling cases with strong matrix cracking - delamination interaction, reproduced to a better extent than on a purely stress-strain basis, confirmed both in terms of final failure load and failure patterns acquired by X-ray CT scans.

An experimental campaign conducted on a set of Carbon Fiber Reinforced Polymer (CFRP) Open Hole Tension (OHT) specimens shows good predictive capability of both blended and stress-strain models in terms of final failure. Failure patterns, however, are relatively poorly predicted from a stress-strain point of view, and the stiffness degradation is disputed by Digital Image Correlation (DIC) observations of in-plane strains. Acoustic Emission (AE) observations indicate good prediction of the damage growth rate throughout the loading process.

The developed blended model is promising, showing global predictive capability on par or superior to state-of-the-art implementations and a strong basis for predicting experimental failure patterns. Still, there is a lot of headway to be made in the field of FRP failure prediction. In particular, this relates to the following recommendations:

- Current approaches have a limited physical basis and evaluate failure deterministically on a mesolevel, whereas FRP failure processes are inherently stochastic and the accumulation of individual failure processes on a microlevel. Therefore, it is recommended to firstly investigate failure on a microscale, guided by extensive experimental campaigning, and secondly to take a stochastic approach towards mesolevel modelling, for example in a Stochastic Finite Element Method (SFEM) framework.
- Although the notion and effect of in-situ strength has been investigated to some extent, this remains relatively unexplored. In particular, the applicability thereof to fracture mechanics based approaches, such as the XFEM approach taken, is questionable. Further research into the estimation, effect and applicability thereof is as such a key recommendation.
- Numerical convergence remains problematic for the blended method. An explicit scheme may offer improved convergence. Alternatively, a more robust convergence framework may be adopted.
- Regardless of the direction taken in further studies, extensive validation with respect to experimental results is an absolute necessity. Strong dependency of composites on the specific case evaluated necessitates a wide set of test cases. Moreover, the possibility of predictions showing good global agreement in terms of final failure but poor local agreement in terms of failure patterns warrants assessment of the local damage state, for example through X-ray CT scans.

Preface

Dear reader,

The advent of Fiber-Reinforced Polymers (FRPs) has yielded great benefits in terms of structural efficiency, performance and versatility. Still, a lot of the physical behaviour of these materials remains unknown and unpredictable - arguably in no respect more so than in terms of damage. The approaches that have been taken in the past are mostly pragmatic formulated for ease of use, yielding a plethora of models, none of which are fully dependable, and current industry practice suffers. This study provides a valuable characterization and evaluation of current stress-strain based approaches to Progressive Damage Analysis (PDA) of FRPs, provides practical Finite Element Model (FEM) implementations and addresses shortcomings through a blend with fracture mechanics.

Throughout this journey, the guidance and support of my supervisor Dr.ir. D. Zarouchas have been invaluable, for which I am eternally grateful. Moreover, thanks go out to Alexander van Oostrum, without whose constructive criticism and the endless discussions we have had, my journey would have been much less eventful and much more arduous. Lastly, I would like to thank all of my friends and family for their continuous love and support.

Delft, University of Technology
June 29, 2017

B.R. van Dongen

"I always avoid prophesying beforehand because it is much better to prophesy after the event has already taken place."

— *Winston Churchill*

Table of Contents

Acronyms

AE Acoustic Emission.

CDM Continuum Damage Model.

CFRP Carbon Fiber Reinforced Polymer.

CLT Classical Laminate Theory.

CT Computed Tomography.

CV Coefficient of Variation.

CZM Cohesive Zone Model.

DCB Double Cantilever Beam.

DIC Digital Image Correlation.

DL Delamination.

ECT Edge-Cracked Torsion.

ENF End-Notched Flexure.

ESL Equivalent Single Layer.

FEM Finite Element Model.

FF Fibre Failure.

FFC Compressive Fibre Failure.

FFT Tensile Fibre Failure.

FMC Failure Mode Concept.

FML Fibre Metal Laminate.

FRP Fiber Reinforced Polymer.

GFRP Glass Fiber Reinforced Polymer.

GLARE GLass REinforced Aluminum.

LW Layer-wise.

MDM Material Degradation Model.

MF Matrix Failure.

MFC Compressive Matrix Failure.

MFT Tensile Matrix Failure.

NDT Non-Destructive Testing.

OHT Open Hole Tension.

PDA Progressive Damage Analysis.

RVE Representative Volume Element.

SFEM Stochastic Finite Element Method.

VCCT Virtual Crack Closure Technique.

XFEM Extended Finite Element Method.

List of Symbols

Symbol	Unit	Description
A	$[m^2]$	Area associated with integration point
$b_{\perp\parallel}$	$[-]$	Curve parameter (Cuntze)
$b_{\perp}^{\tau}$	$[-]$	Curve parameter (Cuntze)
$b_{\perp\parallel}^{\tau}$	$[-]$	Curve parameter (Cuntze)
$\mathbf{C}$	$[Pa]$	Stiffness matrix
C_{ij}	$[Pa]$	Stiffness matrix element (i, j)
E_{f1}	$[Pa]$	Elastic fibre modulus in fibre direction
Eff	$[-]$	Stress effort (Cuntze)
E_1	$[Pa]$	Elastic modulus in fibre direction
E_2	$[Pa]$	Elastic modulus in matrix direction
E_3	$[Pa]$	Elastic modulus in through-thickness direction
g	$[-]$	Ratio of mode I and mode II fracture toughness
G_{ffc}	$[N/m]$	Intralaminar compressive fiber failure fracture energy
G_{fft}	$[N/m]$	Intralaminar tensile fiber failure fracture energy
G_{mfc}	$[N/m]$	Intralaminar compressive matrix failure fracture energy
G_{mft}	$[N/m]$	Intralaminar tensile matrix failure fracture energy
G_{12}	$[Pa]$	In-plane ply shear modulus
G_{13}	$[Pa]$	Out-of-plane longitudinal shear modulus
G_{23}	$[Pa]$	Out-of-plane transverse shear modulus
L	$[m]$	Characteristic element length
$\mathbf{M}$	$[-]$	Ply rotation matrix
m_{Cuntze}	$[-]$	Empirical fitting parameter strength envelope Cuntze
$m_{\sigma f}$	$[-]$	Mean magnification factor for fiber transverse stress
$p_{\perp\parallel}^{c}$	$[-]$	Slope of the (σ_n, τ_{n1}) fracture envelope for $\sigma_n \leq 0$ at $\sigma_n = 0$
$p_{\perp\perp}^{c}$	$[-]$	Slope of the (σ_n, τ_{nt}) fracture envelope for $\sigma_n \leq 0$ at $\sigma_n = 0$
$p_{\perp\parallel}^{t}$	$[-]$	Slope of the (σ_n, τ_{n1}) fracture envelope for $\sigma_n > 0$ at $\sigma_n = 0$
$p_{\perp\perp}^{t}$	$[-]$	Slope of the (σ_n, τ_{nt}) fracture envelope for $\sigma_n > 0$ at $\sigma_n = 0$
$\mathbf{Q}$	$[Pa]$	Ply stiffness matrix
$R_{\perp\perp}^{A}$	$[Pa]$	Transverse-transverse action plane fracture resistance
$R_{\perp\psi}^{A}$	$[Pa]$	Action plane fracture resistance in fracture plane
$\mathbf{S}$	$[1/Pa]$	Compliance matrix
S_{12}	$[Pa]$	In-plane shear strength
S_{23}	$[Pa]$	Out-of-plane transverse shear strength
ν_{f12}	$[-]$	In-plane Poisson's ratio of fiber
ν_{13}	$[-]$	Longitudinal out-of-plane major Poisson's ratio

Symbol	Unit	Description
ν_{21}	$[-]$	In-plane minor Poisson's ratio
ν_{23}	$[-]$	Transverse out-of-plane major Poisson's ratio
X_T	$[Pa]$	Tensile strength along fibers
X_C	$[Pa]$	Compressive strength along fibers
Y_C	$[Pa]$	Compressive transverse strength
Y_T	$[Pa]$	Tensile transverse strength
α	$[rad]$	Fracture plane angle (LaRC)
α_1	$\begin{bmatrix}\circ C^{-1}\end{bmatrix}$	Coefficient of thermal expansion in fiber direction
α_2	$\begin{bmatrix}\circ C^{-1}\end{bmatrix}$	Coefficient of thermal expansion in transverse direction
β	$[Pa^{-3}]$	Shear non-linearity parameter Hahn-Tsai fit
χ	$[Pa/rad]$	In-plane shear stress-strain operator
ΔT	$[\circ C]$	Temperature change
ε_1	$[-]$	Strain in fiber direction
ε_1^{cu}	$[-]$	Ultimate compressive strain in fiber direction
ε_1^{tu}	$[-]$	Ultimate tensile strain in fiber direction
$\varepsilon_{eq,f}$	$[-]$	Equivalent failure strain (bilinear softening)
η	$[s]$	Viscosity
η_{BK}	$[-]$	Benzeggagh-Kenane interaction coefficient
η^L	$[-]$	Coefficient of longitudinal influence
η_{Puck}	$[-]$	Degradation factor (Puck)
η^T	$[-]$	Coefficient of transverse influence
γ_{12}^u	$[-]$	Ultimate in-plane shear strain
Λ_{22}^0	$[1/Pa]$	Parameter dilute crack growth
Λ_{23}^0	$[1/Pa]$	Parameter dilute crack growth
Λ_{44}^0	$[1/Pa]$	Parameter dilute crack growth
φ	$[rad]$	In-plane fiber misalignment angle
φ_0	$[rad]$	Initial fiber misalignment angle
φ_C	$[rad]$	Fiber misalignment angle in pure compression
ψ	$[rad]$	Out-of-plane fiber misalignment angle
σ_1	$[Pa]$	Stress in fiber direction
σ_2	$[Pa]$	Stress in transverse in-plane direction
$\sigma_{eq,f}$	$[Pa]$	Equivalent failure stress (bilinear softening)
σ_n	$[Pa]$	Normal fracture plane stress
τ_{12}	$[Pa]$	In-plane shear stress
τ_{13}	$[Pa]$	In-plane-through-thickness shear stress
τ_{23}	$[Pa]$	Transverse-transverse shear stress
τ_L	$[Pa]$	Transverse in-plane fracture plane stress
τ_T	$[Pa]$	Transverse out-of-plane fracture plane stress
θ	$[rad]$	Fracture plane angle (Puck)
ζ	$[rad]$	Ply angle

List of Figures

List of Tables

Chapter 1

Introduction

Driven by advantages in structural efficiency, performance, versatility and cost, Fiber Reinforced Polymers (FRPs) have seen numerous application in a variety of industries, foremost among which the aerospace industry. However, in spite of decades of application and research, composite behaviour is still not fully understood [1, 2]. Inherent heterogeneity and anisotropy complicate the dependency of composite behaviour on a large number of parameters, significantly more so than for conventional materials. A glaring shortcoming in the current knowledge of FRPs is Progressive Damage Analysis (PDA) of FRPs, demonstrated by first and second installments of The World-Wide Failure Exercise [2, 3]. An overall lack of agreement between current failure theories and experimental results in these installments benchmark the lacking state-of-the-art in composite failure prediction. Although industry has placed little reliance on this predictive capability thus far, this view is changing, promoting the development of methods of higher fidelity to take greater advantage of the possibilities offered by FRPs.

Consensus on the appropriate approach for PDA of FRPs remains out of reach. On one hand, a stress-strain approach to PDA has been in wide use [4]. On the other hand, fracture mechanics forms a strong basis for PDA, in particular for interlaminar damage[5]. Academia is struggling to found new failure theories upon a physical basis, but understanding is lacking and current design practice suffers [2]. Contrary to these attempts, this research builds upon the existing framework of theories by blending current approaches to PDA. This research aims to improve the fidelity of PDA of FRPs by the development of a numerical Finite Element Method (FEM) implementation using a blended stress-strain and fracture mechanics approach. Since this research is part of a combined effort, this part of the research is centered around the stress-strain approach and its combination with a fracture mechanics approach.

The thesis commences with an overview of the main research questions, goals and objectives in Chapter 2. A basis for PDA is set by an abridged overview of the fundamentals of FRP mechanical behaviour in Chapter 3. After a review of the theoretical foundation of stress-strain based PDA of FRPs in Chapter 4, a preliminary analysis is conducted for the purpose of a critical comparison and trade-off of stress-strain models in Chapter 5. Chapter 6 ensues with FEM implementation of selected theories following from the trade-off, accompanied by a series of study cases to benchmark and compare the models. Thereafter, a blended model is proposed in Chapter 7 and implemented in FEM. A critical evaluation using an experimental Open-Hole Tension (OHT) test aims to quantify the impact of the blended model. Lastly, conclusions and recommendations are given in Chapter 8.

Appendices are included for a more elaborate treatment where appropriate. Appendix A gives

an abridged overview of Classical Laminate Theory (CLT). Appendix B shortly treats the experimental determination of material properties. Appendix C provides an in-depth overview in the theory and equations behind intralaminar damage initiation criteria. Test cases for the preliminary analysis are discussed in Appendix D, including a detailed overview of input parameters. Lastly, input parameters for FEM test cases are given in Appendix E.

Chapter 2

Research scope

This Chapter provides a roadmap for this research. As such, the problem statement is firstly given and research questions are presented and worked out. Thereafter, research objectives are defined and the approach taken is outlined. The Chapter is concluded by a section on the limitations in scope.

Contents

2.1 Problem statement

The problem statement of this research is the following:

> To bridge the gap towards high-fidelity PDA of FRPs by combining and building upon the existing bodies of knowledge (contrary to founding new theories on a physical basis) through critical evaluation and FEM implementation of stress-strain approaches and a blended stress-strain and fracture mechanics method for PDA of FRPs.

2.2 Research questions and hypothesis

This section outlines research questions and the main hypothesis. After presenting the main research question and hypothesis, research subquestions are worked out. These research questions define directions for research activities and are ultimately answered to fulfill the problem statement.

2.2.1 Main research question

The main research question is:

Does a blended stress-strain and fracture mechanics approach implemented in Finite Element Model (FEM) offer improved predictive accuracy of PDA in FRPs, as compared to an isolated stress-strain approach?

Ultimately, this research question allows a statement on the relative performance of a blended versus an isolated approach to PDA of FRPs. This statement can be turned towards directing further developments in PDA theories and, if the question is positively answered, provide a direct improvement over current methods in place.

2.2.2 Hypothesis

It is hypothesized that a blend of stress-strain and fracture mechanics approaches will improve predictive capability over an isolated stress-strain approach, since blending judiciously by predicting damage initiation from a stress-strain perspective and damage propagation from a fracture mechanics perspective will use the predictive strengths of each approach in conjunction.

2.2.3 Research subquestions

Research subquestions branch out from the main research question, such that answering all subquestions yields the answer to the main research question as a result. These subquestions follow hereafter, divided into the theoretical foundation, numerical FEM implementation and the comparative predictive performance.

Theoretical foundation

A number of research subquestions pertains to the theoretical foundation of PDA of FRPs. These are the following.

A precise definition of PDA is firstly in order, yielding the first research question

(a) Which failure modes are defined for a FRP laminate?

Second and third research questions concern prediction using the individual theories, namely:

(b) By which methods is damage defined and predicted for a FRP laminate using current stress-strain approaches?

(c) By which methods is damage defined and predicted for a FRP laminate using current fracture mechanics approaches?

Each of these previous questions entails two subquestions, regarding the two key steps of damage initiation and propagation in PDA

(b1/c1) By which methods is damage initiation defined and predicted for a FRP laminate using current stress-strain (b1) / fracture mechanics (c1) approaches?

(b2/c2) By which methods is damage propagation defined and predicted for a FRP laminate using current stress-strain (b2) / fracture mechanics (c2) approaches?

The distinguishing feature of this research, blending the theories, requires the answer to the following research question

(d) By which methods is damage defined and predicted for a FRP laminate using a blend of current stress-strain and fracture mechanics approaches?

Answering these questions yields a theoretical foundation for implementation. Without a theoretical foundation, numerical implementation is out of the question.

Numerical implementation

With the theoretical foundation captured in the previous questions, numerical implementation in a FEM framework remains. Therefore the following research question is to be answered:

(e) By which methodology can PDA of FRP laminates be performed in FEM?

with corresponding subquestions

(e1) By which methodology can PDA of FRP laminates using a stress-strain approach be performed in FEM?

(e2) By which methodology can PDA of FRP laminates using a fracture mechanics approach be performed in FEM?

(e3) By which methodology can PDA of FRP laminates using a blended stress-strain and fracture mechanics approach be performed in FEM?

Comparative studies

To fully answer the main research question, a set of candidate theories needs to be implemented and results analysed with respect to predictive capability and computational effort. A key first step therein is narrowing down candidates:

(f) Which three selected stress-strain approaches are most promising in terms of prediction accuracy, computational effort and versatility?

Followed by application to study cases of OHT specimens:

(g) How do numerical results as obtained by three selected stress-strain approaches and a blended approach compare in terms of prediction accuracy with respect to experimental campaigns on OHT specimens?

This research question instigates investigation of the advantages and disadvantages offered by three selected stress-strain approaches and a combined approach to formulate a judgment on the relative performance, in terms of prediction accuracy.

2.3 Research objectives

The research questions that have been formulated in the previous section are translated into research objectives. Similar to the research questions, these are structured in three categories.

Theoretical foundation

For the theoretical foundation, the following objectives follow from the research questions:

- Overview of failure modes in FRP laminates
- Overview of current stress-strain approaches for damage initiation
- Overview of current stress-strain approaches for damage progression

- Overview of current fracture mechanics approaches for damage initiation
- Overview of current fracture mechanics approaches for damage progression
- Formulation of a blended stress-strain and fracture mechanics approach

The first objective is contained in Chapter 3. Second and third objectives are contained in Chapter 4 and Appendix C. Lastly, the formulation of a blended approach is treated in Chapter 7. Fracture mechanics methods are treated in a parallel study [6].

Comparative studies

Prior to numerical implementation, stress-strain approaches are filtered. The outcome is captured in the following objective, treated in Chapter 5:

- Select the three stress-strain approaches most suitable in terms of maximum predictive capability and versatility at minimum computational effort

Models are implemented with the goal of obtaining:

- Verification of the developed algorithms using available analytical solutions and reference literature
- Outline and execution of an experimental campaign on an Open Hole Tension (OHT) Carbon Fiber Reinforced Polymer (CFRP) laminate
- Validation of the developed algorithms using study cases from literature and an experimental campaign
- A comparison of predictive capability of stress-strain and blended models

The first three follow indirectly from the research questions, namely from the necessity of verifying and validation the implemented models. These validation cases are treated in Chapters 6 and 7.

Numerical implementation

For the numerical implementation, the following objectives apply:

- Overview of FEM implementation methods for PDA of FRPs
- Selection of a FEM implementation method
- Implementation of three isolated stress-strain approaches and a blended approach for PDA of FRPs in a commercial FEM package

Numerical implementation is treated in Chapter 6 for stress-strain methods and Chapter 7 for the blended method.

2.4 Research approach

To answer the research questions and fulfill the ensuing research objectives, the following approach is taken. This approach is split into a number of parts:

1. A literature survey on the theoretical foundation and numerical implementation of stress-strain based approaches for PDA of FRPs

2. Selection of stress-strain based approaches for implementation in FEM
3. Implementation of three selected stress-strain based approaches in FEM
4. Implementation of a blended stress-strain approach with fracture mechanics in FEM
5. Validation and analysis of results with study cases from literature and an experimental campaign

A research was run in parallel that performs the first three tasks on the topic of fracture mechanics based PDA of FRPs [6]. The results thereof are referenced and used in the blended PDA implementation.

2.5 Limitations in scope

A number of limitations apply to this study, foremostly the following:

- Although attempts have been made to include as many failure theories as possible, the study is limited to leading failure theories (in terms of both damage initiation and propagation modelling).
- In recognition of the importance of numerous different (in terms of loading, material and geometry) validation cases for FRPs, multiple study cases have been included. Still, these form a limited subset in quantity as well as in nature, limited to mostly OHT test cases under quasi-static loading.
- Only a plenary treatment is given of in-situ strengths, input parameters and fundamentals of composite modelling, for a working knowledge of these principles and application thereof. As such, detailed investigations are left out and pending further research.
- Fracture mechanics based methods are treated in a study conducted in parallel [6], and consequently not subject to an equally extensive treatment as stress-strain methods in this study.

Chapter 3

Mechanics and failure of FRP composites

Although FRP composites have been researched and applied for decades, physical understanding of their mechanics and behaviour is still incomplete [1, 2]. Still, efforts to understand these materials have yielded a number of valuable insights and powerful tools to analyze them. This Chapter gives an overview of the fundamental methodologies and insights by which FRPs are commonly analyzed.

Firstly, an overview is given of constitutive models applied to FRPs. Secondly, failure modes are defined and characterized briefly. Lastly, governing material properties that are central in each of the different approaches to PDA of FRPs are discussed - primarily in relation to the use of in-situ strengths.

Contents

3.1 Constitutive modelling

Constitutive models represent the stress-strain relationship of a material. This is a key relation, considering that FEM implementation centers around this relation and especially in view of the stress and strain basis of many approaches to PDA. It is therefore key that constitutive models are inventarised and their complications listed. To this end, this section lists three- and two-dimensional constitutive models followed by a discussion on the main complicaticating feature of material non-linearity.

3.1.1 Three-dimensional constitutive model

Traditionally, computational considerations have played a large role in the selection of constitutive models. Consequently, constitutive models for FRP composites are primarily linear elastic [7]. By far the most widely used linear constitutive relationship for FRPs is that for an orthotropic material in terms of engineering constants (1 in fiber direction, 2 transverse in-plane

and 3 through-thickness) [4, 7]

$$\begin{bmatrix} \sigma_1 \\ \sigma_2 \\ \sigma_3 \\ \tau_{23} \\ \tau_{13} \\ \tau_{12} \end{bmatrix} = \begin{bmatrix} C_{11} & C_{12} & C_{13} & 0 & 0 & 0 \\ & C_{22} & C_{23} & 0 & 0 & 0 \\ & & C_{33} & 0 & 0 & 0 \\ & & & C_{44} & 0 & 0 \\ & \text{Symmetric} & & & C_{55} & 0 \\ & & & & & C_{66} \end{bmatrix} \begin{bmatrix} \varepsilon_1 \\ \varepsilon_2 \\ \varepsilon_3 \\ \gamma_{23} \\ \gamma_{13} \\ \gamma_{12} \end{bmatrix} \tag{3.1}$$

This constitutive model has been applied in a large number of studies, either in its full linear elastic form or by accounting for material non-linearity [7–12]. This relation models out-of-plane as well as in-plane stress and strain components. This inclusion allows modelling of out-of-plane phenomena, of which Delaminations (DLs) are a key example, and a more accurate representation of material behaviour [7]. This does come at increased computational effort, a key consideration explaining a history of models applying a two- rather than three-dimensional constitutive model.

Elements C_{ij} can be defined in terms of engineering constants as follows [7]

$$\begin{cases} C_{11} = E_1 \frac{1-\nu_{23}\nu_{32}}{\nu} \\ C_{22} = E_2 \frac{1-\nu_{13}\nu_{31}}{\nu} \\ C_{12} = E_2 \frac{\nu_{12}+\nu_{32}\nu_{13}}{\nu} \\ C_{33} = E_2 \frac{\nu_{13}+\nu_{12}\nu_{23}}{\nu} \\ C_{23} = E_2 \frac{\nu_{23}+\nu_{21}\nu_{13}}{\nu} \\ C_{13} = E_2 \frac{\nu_{13}+\nu_{12}\nu_{23}}{\nu} \\ C_{44} = G_{23} \\ C_{55} = G_{13} \\ C_{66} = G_{12} \\ \nu = 1 - \nu_{12}\nu_{21} - \nu_{23}\nu_{32} - \nu_{13}\nu_{31} - 2\nu_{32}\nu_{21}\nu_{13} \end{cases} \tag{3.2}$$

Moreover, through application of Maxwell's theorem [7]

$$\begin{cases} \nu_{32} = \frac{E_3}{E_2}\nu_{23} \\ \nu_{31} = \frac{E_3}{E_1}\nu_{13} \\ \nu_{21} = \frac{E_2}{E_1}\nu_{12} \end{cases} \tag{3.3}$$

and the assumption of transverse isotropy in view of matrix homogeneity [12]

$$\begin{cases} E_3 = E_2 \\ G_{13} = G_{12} \\ \nu_{13} = \nu_{12} \\ G_{23} = \frac{E_2}{2(1+\nu_{23})} \end{cases} \tag{3.4}$$

the number of independent material constants can be reduced to five ($E_1, E_2, G_{12}, \nu_{12}$ and ν_{23}). When evaluating damaged composite materials, transverse isotropy does not hold [13] and use of the more general relationship for orthotropic materials is warranted.

3.1.2 Two-dimensional constitutive model

When out-of-plane stresses are not a key factor, the above three-dimensional model can be reduced to two dimensions. In this state of plane stress, the traditional and most widely used constitutive model is the following [7, 8]

$$\begin{bmatrix} \sigma_1 \\ \sigma_2 \\ \tau_{12} \end{bmatrix} = \begin{bmatrix} C_{11} & C_{12} & 0 \\ C_{12} & C_{22} & 0 \\ 0 & 0 & C_{66} \end{bmatrix} \begin{bmatrix} \varepsilon_1 \\ \varepsilon_2 \\ \gamma_{12} \end{bmatrix} \tag{3.5}$$

Many early PDA studies were conducted using the above two-dimensional constitutive model for its simplicity and computational ease [7]. Moreover, this constitutive model features prominently in the widely applied Classical Laminate Theory (CLT) for FRP laminate analysis [14]. A brief overview of CLT is given in Appendix A.

3.1.3 Non-linearity

Failing to account for constitutive non-linearity introduces errors in stress and strain prediction. It is thereby key that non-linearity is addressed.

Non-linearity in the stress-strain relation of FRPs stems from two main factors:

1. Inherent material non-linearity
2. Damage

A brief discussion follows on these factors and the means by which to address the effects thereof. In both cases, stress-strain curves are approximated by a piecewise linear fit. This fit results from expressing engineering constants as a function of strains, to account for material non-linearity, and a function of damage parameters, to account for damage non-linearity.

Addressing material non-linearity

Material non-linearity primarily exhibits itself in transverse and shear moduli [8, 15, 16]. Depending on the material, a judicious selection of non-linearity approximations in the various directions can be made if errors induced are limited, to alleviate computational effort.

Material non-linearity is modelled by fitting experimental stress-strain curves. In possession of experimental stress-strain curves, Ramberg-Osgood [17] and spline interpolation[15] are common tools to find the tangent stiffness in the response. In case of plane stress, shear non-linearity can be implemented through Hahn's relationship [18, 19]. This approach is, however, more limited and Ramberg-Osgood or spline fits are preferable for generality and limited additional computational effort (the fit is only performed once).

In spite of the fact that stress-strain curves in different directions interact, a strong absence of multi-axial test data prevents modelling of this interaction in many cases. An equivalent strain has been proposed to take this into account to some extent [15].

Extrapolation, in addition to the aforementioned interpolation, may be necessary in view of the fact that composites can sustain higher stresses and strains under combined loading than suggested by uni-axial test data [20]. This is particularly pronounced in transverse elastic and shear moduli [13]. Ideally, extrapolation would be guided by multi-axial data. The scarcity of such data has necessitated extrapolation on a subjective basis [13, 20]. Although semi-empirical

functions for secant moduli exist to guide this extrapolation, with good agreement with experimental data, these are not fit for FEM implementation due to a dependence on stresses incompatible with FEM formulations [13].

Addressing damage non-linearity

Damage degradation is almost exclusively handled by a degradation of engineering constants upon localized damage. The degradation can occur either suddenly or gradually and effects a decrease in slope in stress-strain diagrams [7–11, 15]. This is discussed in more detail in Chapter 4 on stress-strain based approaches to damage modelling.

3.2 Failure modes

For a full and proper account of PDA, it is of crucial importance that the failure modes in FRPs are characterized. A multitude of failure modes results from the heterogeneity of composites, on one hand within plies (intralaminar failure) and on the other hand between plies (interlaminar failure) [4]. Intralaminar failure modes are Fibre Failure (FF) and Matrix Failure (MF), whereas DLs are an interlaminar failure mode. These failure modes have differing detrimental effects and modelling these judiciously is key in simulating physically based damage propagation. To this end, this section discusses the main failure modes encountered in FRPs and incorporated in failure theories.

3.2.1 Tensile matrix failure

The presence of matrix cracks under transverse tension is commonly denoted as Tensile Matrix Failure (MFT). The stiffness loss due to tensile matrix cracking is relatively small, hence this failure mode is sometimes considered benign as compared to Compressive Matrix Failure (MFC) and FF [21]. Since the matrix is not the main load-carrying component, MFT can be preferred to FF. Upon growth of these cracks, however, detrimental effects can be severe and can induce additional damage modes.

Matrix cracks progress through the thickness of a ply. They are mostly constrained and stopped at ply boundaries for surrounding plies of different orientations. At a certain saturation level or sufficient crack opening, a DL starts from the transverse cracks [11].

3.2.2 Compressive matrix failure

MFC exhibits itself similar to MFT in the presence of matrix cracks. Different to MFT, these are induced by transverse compression and the resulting matrix cracking is not necessarily in through-thickness direction. Rather, the matrix fails in shear, as evidenced by the angle under which it occurs [12, 21]. This necessitates a distinction between MFC and MFT, first recognized by Hashin [22].

3.2.3 Tensile fibre failure

Tensile Fibre Failure (FFT) is generally regarded as a catastrophic failure mode, since the main load-carrying constituents, namely the fibres, are lost [4] and it is accompanied by a large en-

ergy release [12]. This phenomenon is relatively well-established as the accumulation of individual fibre failures and evaluation of this failure mode has not changed significantly over the years.

3.2.4 Compressive fibre failure

Contrary to FFT, Compressive Fibre Failure (FFC) is not a well-understood phenomenon [23]. FFC is mostly attributed to multiple mechanisms. Firstly, failure of fibres themselves can be a cause although only for very weak fibers, like Kevlar [24]. Secondly, and in general, FFC can exhibit itself as the collapse of fibers due to shear kinking and surrounding matrix failure. A kink band forms locally and is followed upon by fiber fracture at the kink band boundaries [23, 24].

3.2.5 Delamination

DLs are the result of shear stresses at ply interfaces and/or out-of-plane tensile stresses, causing separation of adjacent plies [25]. Interlaminar shear can result from ply stiffness mismatching, notches, ply drops and bonds or bolted joints [26]. In addition, DLs can originate from the coalescence or saturation of matrix cracks [27]. At locations of matrix cracks, DLs can jump between different interfaces [13].

A fracture mechanics approach is traditionally taken to DL prediction, modelling discrete cracks [13]. Three fracture modes are typically distinguished: mode I opening in tension, mode II in-plane longitudinal shear and mode III in-plane transverse shear (longitudinal being in fiber direction, transverse perpendicular to fiber direction).

3.3 In-situ strength

Transverse tensile and shear strength of plies have been observed to differ depending on thickness and orientation of plies as well as whether these are embedded, an effect first observed by Parvizi et al. [28]. Transverse and shear strengths increase upon decreasing ply thickness and moreover upon embedding plies due to the constraining effects of surrounding plies [29]. This dependency is captured in the use of in-situ strengths, governing crack growth, as opposed to the strengths measured from uniaxial testing of unidirectional laminates. A brief overview of the latter is given in Appendix B.

In-situ strengths are readily implemented in a stress-strain theory in the failure criteria, namely by replacing the shear and transverse tensile strengths by their in-situ values for each ply. Their use is less obvious, however, when considering a fracture mechanics approach to crack propagation [11].

Experimental determination

The experimental determination of in-situ strengths, such as performed by Chang and Chen [30] and Flaggs and Kural [31], is a prohibitive approach for widespread use in design and analysis. A reasonably accurate approximation of in-situ strengths will require extensive and expensive experimental campaigning on a case-by-case basis. As such, analytical determination is deemed preferable.

Analytical determination

The most predominant prediction theory was developed by Camanho et al. [29], implemented in the LaRC03/04/05 failure criteria [15, 20, 21]. Use thereof has yielded good agreement with experimental results [15, 20, 32].

This theory [29] is based on a crack analysis in thick, thin and embedded plies in the wake of Dvorak and Laws [33]. A slit crack is considered as a macroscopic representation of a number of microdefects and crack growth based on a fracture mechanics perspective.

Expressions for in-situ strength Premise for the theory is a Hahn-Tsai fit of the (experimentally determined) in-plane shear stress-strain curve that allows finding an analytical solution conveniently while incorporating shear non-linearity. This fit is of the form [18]

$$\gamma_{12} = \frac{1}{G_{12}}\tau_{12} + \beta\tau_{12}^3 \tag{3.6}$$

and fitted on a least-squares basis. The decency of this fit is illustrated in Appendix D for a number of materials.

Analytical solutions for the in-situ strengths are then attained on the basis of expressions for the critical fracture energy, taking into consideration the embeddedness and thickness of a ply. Two general conclusions are reached. Firstly, the strength of an embedded ply is higher than that of an outer ply. This can be explained by the fact that surrounding plies, of different ply orientations, function as crack stoppers. At ply boundaries, fibers change direction and a growing crack traversing the ply boundary will have to change its growth direction. Absence of such a ply boundary on one side removes this obstruction.

Secondly, reasoned on a similar basis, the strength of a thin ply is higher than that of a thicker ply. Thinner plies mean less space for a crack to grow unobstructed. In the model, the transition from thin to thick ply is at the intersection of the solutions for thin and thick plies, i.e. the thick ply strength is a lower bound for embedded plies.

These considerations appear in the form of stress-concentrations and geometry-dependent factors, to yield the following expressions for the in-situ in-plane shear and transverse compression strength.

In-situ in-plane shear strength is given by [29]

$$S_{12,\,\text{in situ}} = \sqrt{\frac{\sqrt{1+\beta\phi G_{12}^2}-1}{3\beta G_{12}}} \tag{3.7}$$

where [29]

$$\phi = \begin{cases} 12\frac{S_{12}^2}{G_{12}} + 18\beta S_{12}^4 & \text{for a thick (embedded) ply} \\ \frac{48 G_{IIc}}{\pi t} & \text{for a thin (embedded) ply} \\ \frac{24 G_{IIc}}{\pi t} & \text{for an outer ply} \end{cases} \tag{3.8}$$

The in-situ transverse tensile strength is given by [12, 15, 29]

$$Y_{T,\,\text{in situ}} = \begin{cases} 1.12\sqrt{2}Y_T & \text{for a thick (embedded) ply} \\ \sqrt{\frac{8 G_{Ic}}{\pi t \Delta_{22}^0}} & \text{for a thin (embedded) ply} \\ 1.79\sqrt{\frac{G_{Ic}}{\pi t \Delta_{22}^0}} & \text{for an outer ply} \end{cases} \tag{3.9}$$

with

$$\Delta_{22}^{0} = 2(\frac{1}{E_2} - \frac{\mu_{21}^2}{E_1}) \tag{3.10}$$

The above model, rather than the adapted model by Pinho et al. [20, 32], is chosen since the presented model has been validated with good results [29, 34] whereas the model by Pinho et al. offers less validation and explanation. However, a detailed study into the effect and estimation of in-situ strengths is warranted in the future. These in-situ parameters largely affect the results, as shown hereafter, and a proper estimation will offer improved model accuracy without necessarily requiring a reformulation or improvement of current PDA models. Since a detailed study of in-situ strengths is outside the scope of the current research, this is left as a recommendation for further work.

Effect of using in-situ strength To motivate that in-situ strengths, via the proposed expressions, benefit the accuracy of PDA using stress-strain based models, the sixth test case of the first World-Wide Failure Exercise [2] is ran with and without in-situ strength as input. Results are obtained both for initial and final failure, for a number of initiation criteria and propagation models as outlined in the next Chapter. This test case is described in more detail in Appendix D.

Initial failure predictions show improved correspondence when considering in-situ strength, see Figure 5.5 versus Figure 3.1, for all of the models considered in this study. Without taking into account in-situ strength, initial failure predictions are overly conservative. With the increase of strength in embedded plies, captured in the in-situ expressions, predictions of all models more closely resemble the experimental data. In terms of final failure, in-situ strength does not noticeably increase predictive accuracy.

3.4 Conclusions and recommendations

The linear constitutive model forms the basis for representation of material behaviour, described by a number of engineering constants. For a full description, however, non-linearity is to be included by inter- and extrapolation of stress-strain curves. Current best practice is a subjective extrapolation and interpolation based on uniaxial test data, whereas interaction effects are preferably described by biaxial test data. In the absence of such data, spline fits or closed-form expressions such as Hahn-Tsai fits are suitable for describing material non-linearity.

The heterogeneity induces a number of failure modes in FRP composites, namely MF, FF and DLs. A distinction thereof is critical in any evaluation, necessitating the use of mode-dependent failure criteria. In spite of years of application, many of the mechanisms behind these failure modes remain not fully known.

A number of parameters govern damage initiation and growth, captured by the use of material strengths and fracture toughnesses. Although material strengths are often straightforwardly extracted from unidirectional lamina, this overlooks the effect that ply thickness and its embeddedness have on the experimentally observed strengths for multidirectional laminates. This effect necessitates a treatment of in-situ strength. A fracture mechanics based crack analysis offers an analytical estimation method thereof.

Understanding of FRP composites and practical application of this knowledge is riddled with unknowns. Particularly, the following fundamental issues are to be addressed:

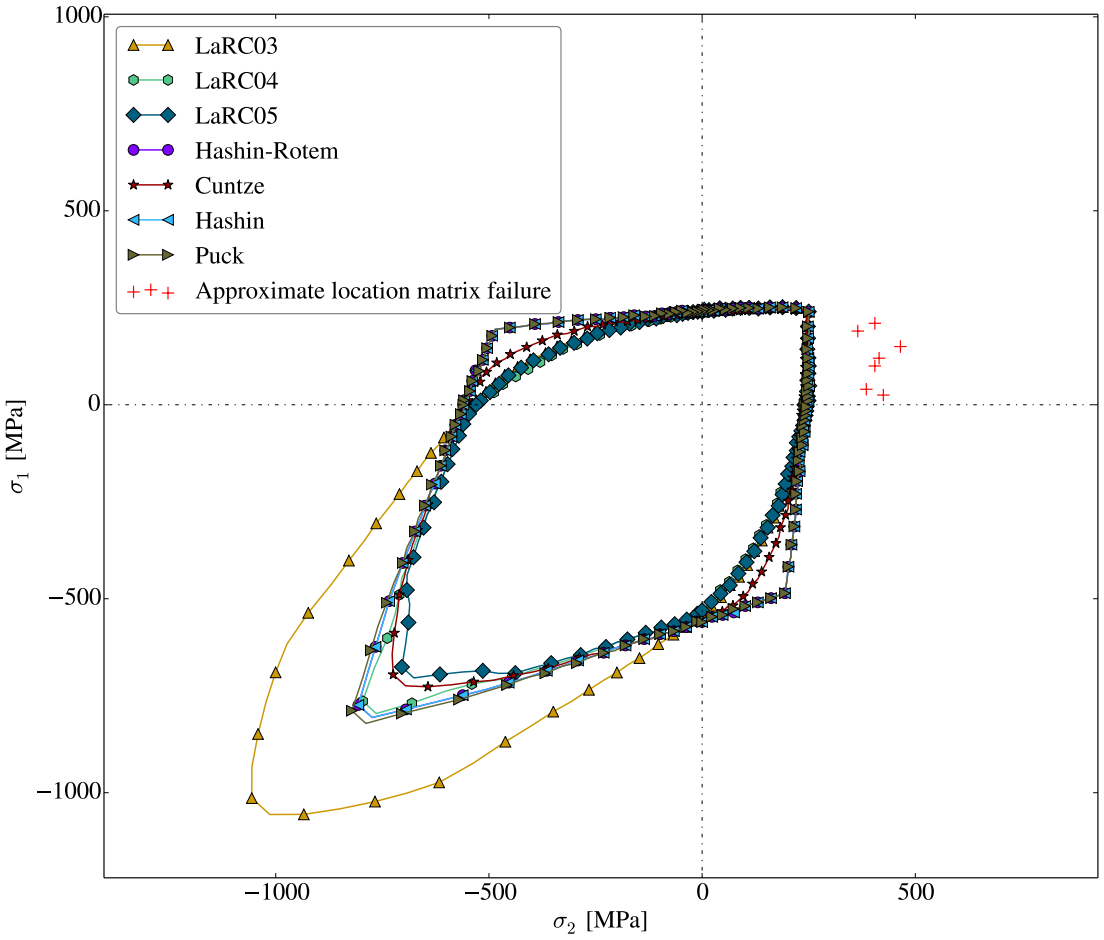

Figure 3.1: Initial failure envelope (σ_2, σ_1) of symmetric $[0°/\pm 45°/90°)_s]$ AS4/3501−6 laminate without in-situ strength (Test case 6)

- A better physical understanding of mechanisms governing the various damage modes in FRP composites is in order. There is, however, no straightforward path to this insight. Extensive testing and evaluation on a micromechanical level are recommended activities.
- Interaction effects between stress and strain in various directions are to be explored and addressed. Reliance on uniaxial test data overlooks the interaction effect and leads to a subjective interpretation of stress-strain behaviour, potentially inducing significant errors in modelling material non-linearity.
- Although analytical models exist for in-situ strength estimation, the effect of ply thickness and embeddedness on composite strength remains relatively unexplored. Investigation, guided by extensive experimental campaigning, is recommended.
- Current practice relies on deterministic input data, whereas parameters are inherently stochastic. Uncertainty is associated with the determination of experimental parameters, such as material strengths, and ideally this uncertainty is taken into account in the evaluation. A stochastic approach could offer improved results.

Moreover, specific to this studies, the scope is limited. A general treatment of composite behaviour and failure would necessitate exploring effects such as thermal behaviour and pressure dependency.

Chapter 4

Overview of stress-strain based methods

Traditionally, stress-strain based damage models, or Continuum Damage Models (CDMs), have been employed for PDA of FRPs. This line of models was initiated by Tsai and Hill's extension of the Von Mises yield theory, producing the first damage criterion in the form of the Tsai-Hill criterion [35]. Since this proposition, a number of models has been developed to predict the initiation and propagation of damage sites in FRPs on the basis of the local stress and strain state. These models follow the same general approach of initiating damage on the basis of the actual stress and strain state and, upon damage initiation, degrading material properties accordingly to reflect the detrimental effect of damage [7]. To define a theoretical methodology for PDA of FRPs, a treatment of damage initiation criteria and propagation or degradation models is in order.

To this end, this chapter discusses and outlines past and current stress-strain based initiation criteria and propagation models subsequently. Within each category, the failure modes presented in the previous chapter are considered. Initiation and propagation criteria are expressly treated separately, since these are distinctly separate components. This distinction allow mixing and matching of various model components.

Contents

4.1 Damage initiation criteria

The advent of stress-strain based damage initiation is marked by the proposition of the Tsai-Hill criterion [35, 36]. This criterion initiated a long series of stress-strain based models to damage initiation in FRPs. This series is riddled with flaws originating from this initial proposition, extrapolating the available knowledge on metals to composites in spite of composite heterogeneity and anisotropy. Over the years, remarkable efforts have been made to improve the quality of PDA on FRP composites. This section gives an overview of the most prominent stress-strain based damage initiation criteria.

Generally speaking, these criteria can be divided into mode-independent and mode-dependent criteria. The former are criteria following directly in the wake of the Tsai-Hill criterion [35, 36] and characterized by an inability to distinguish failure modes. The latter, in contrast, specifically distinguish failure modes on the physical basis of composite heterogeneity. It should not come as a surprise that criteria have moved from mode-independent to mode-dependent criteria, to better capture the physical basis and composite heterogeneity.

This section gives a brief excerpt of mode-independent criteria and then moves on to the most prominent and promising mode-dependent criteria currently in place. Since many of the criteria do not offer a solution for DL prediction, initiation criteria for DLs are treated separately at the end. In view of the extensive nature of the theory behind the mode-dependent criteria, an abridged overview is given in Appendix C and the current section focuses on the main characteristics of each model.

4.1.1 Mode-independent criteria

Although easy to use, these failure criteria suffer from a limited physical basis and yield little to no information on the failure mode, a requisite for PDA [4]. These criteria have been of historical significance, however, and the Tsai-Wu and Tsai-Hill criteria are still used in industry and FEM codes for their decent accuracy [1, 37].

First to propose a failure criterion for composites were Tsai and Hill [35], on the basis of the Von Mises yield criterion extended to anisotropic metals [38]. While this theorem was thought to account for the differences between metals and composites in their (an)isotropy, it fails to distinguish the multitude of failure modes. As a result, this theorem can be seen as fundamentally wrong, failing to capture the heterogeneity of FRPs. Still, however, this theorem has found extensive use, even after this deficiency became apparent [39], and it is still used today for its decent agreement in some cases and its conservativeness for design purposes [1].

In the wake of Tsai and Hill, a series of mode-independent criteria were formulated on the same false basis. Hoffman extended on Hill's yield condition [38], but accounts for the brittle nature through differing tension and compression strengths [40]. Chamis proposed an adaptation of Tsai-Hill's failure condition, adding an empirical factor to take different values in the differing quadrants of axial and transverse in-plane normal stresses, thereby accounting for the discontinuous failure in composite materials [41]. This improves accuracy slightly, but the impracticality of estimating the additional coefficient makes the expression less versatile. Tsai and Wu proposed their criterion similar to the Tsai-Hill and Hoffman criteria on the basis of a curve fit of strength tensors [36]. The Tsai-Wu criterion is fundamentally wrong same as the previous criteria, but is one of the most widely used criteria in industry and FEM codes [4, 37]. Reason is that the agreement with experimental tests is decent, although it notably suffers in the case of fibre compression [1, 4].

Contrary to this class of models, mode-dependent criteria respect composite heterogeneity and the various failure modes exhibited by FRPs. A historical trend towards mode-dependent criteria can be distinguished [4]. Recent criteria all fall within this category and form the focus on this study. After all, the intent is to move towards high-accuracy, physically based criteria. Mode-independent criteria suffer from a lack of physical foundation and are especially inappropriate for PDA, where progression is a key component that relies on an accurate distinction of failure modes.

4.1.2 Hashin-Rotem

Hashin and Rotem were the first to make a real distinction in failure modes. Based on logical reasoning and seeing FF and MF as independent, Hashin and Rotem formulated separate criteria for MF and FF [22]. This first real contribution to mode-dependent failure criteria formed a stepping stone towards more advanced criteria. As the first real mode-dependent failure criteria, the formulation of the criteria is still based primarily on logical reasoning and a polynomial fit as opposed to insight in the failure mechanisms of FRPs.

The simplicity of the criteria promotes inaccuracy [15, 21]. Still, approximations can be decent [1, 11].

The criteria can be said to be fallacious in the sense that fracture plane angles are not considered and the difference between MFC and MFT is not addressed in terms of tractions or crack opening. Sun et al. proposed an empirical modification to yield a criterion much like Puck's (in two dimensions) by accounting for the friction caused by the normal stress, although still not considering the fracture plane angle [37].

The limit criterion used for FF, although simple, has some physical basis and interaction effects are slight. For one, Puck and Schürmann argue that differences are small with respect to their proposed criterion for FFT [42]. For the case of FFC, however, agreement can be expected to be less good in view of complex phenomena such as fiber kinking.

For more details, please refer to Appendix C. Herein, the main equations and theory underlying the criteria are outlined.

4.1.3 Hashin

In the wake of the Hashin-Rotem criteria, Hashin went on to propose failure criteria on the basis of specific failure mechanisms and stressed the need thereof. Moreover, he led a break with the traditional use of the mode-independent failure criteria, earlier discussed as being based on the fallacious premise of the Von Mises yield criterion [39, 43].

Contrary to the Hashin-Rotem criteria, the Hashin criteria have more of a physical basis. His work for MF is related to the Mohr-Coulomb theory, considering fracture to be caused solely by stresses acting on the fracture plane. Still, in the formulation of the criteria simplifications were made. The MF criterion itself is deduced on the basis of a smooth quadratic failure criterion, i.e. heuristically more so than physically grounded. The same goes for the FF criterion. Consequently, the Hashin criteria are simple, but accuracy is limited [1, 21]. As for the Hashin-Rotem criteria, the simplicity proves advantageous in terms of computational effort.

For more details, please refer to Appendix C. This Appendix summarizes the main equations and fundamentals of the Hashin criteria.

4.1.4 Puck

The first truly physically based damage initiation model for FRPs was founded by Puck and Schürmann [42]. In particular, this model (hereafter referred to as the Puck model) proposes MF criteria with a physical basis extending from the Mohr-Coulomb fracture theory for brittle materials. This hypothesis states that fracture is influenced by stresses on the fracture plane. The Puck model initiated a series of models founded thereafter on a similar basis, predominantly in the form of the LaRC criteria, and is well-regarded as state-of-the-art [4].

Its strong physical foundation lends strength to its predictions and past implementations have found good agreement with experimental results, underlined by the good correspondence achieved in the Worldwide Failure Exercise [2, 3]. Compared to the more simplistic Hashin and Hashin-Rotem criteria, computational effort is greater by an iterative search for a fracture plane angle considering MF.

In spite of the strong physical basis, part of the criteria is still supplemented heuristically. In particular, the approach to FFC neglects underlying physical phenomena. Moreover, a drawback is the requirement of additional experimentally determined inclination parameters. However, guidelines for the selection of the latter are available for CFRP and GFRP laminates [13, 16], yielding a relatively easy way of obtaining good results. This is demonstrated by the fact that no additional fitting has been done in the Worldwide Failure Exercises and good results were still obtained [3].

For more details, see Appendix C. Herein, a detailed description of the Puck treatment of MF and FF is given.

4.1.5 Cuntze

Cuntze and Freund describe damage on the basis of the Failure Mode Concept (FMC). Five modes are distinguished, FFT, FFC and the other three corresponding to MF, on the basis of material symmetry [44]. With each mode corresponding to one failure mechanism and one failure condition, each mode is governed by one strength. The criteria are then formulated on the basis of invariants, in analogy to Hashin's work [43].

Cuntze's theory is based on the same premises of fracture planes being affected only by the stresses acting on that plane and brittle failure as Puck's [44, 45]. Whereas Puck derives criteria more on a physical basis, Cuntze turns to probabilistic curve fitting.

Although Cuntze's results display good accuracy [2, 3], the curve fitting aspect means that this theorem is less easily applicable without the fitting parameters. In terms of versatility, the Cuntze criteria are thereby more limited. The empirical nature does alleviate computational efficiency, obviating the iterative procedure to find fracture plane angles.

For specifics on the FMC and governing equations, see Appendix C. This Appendix contains the key components of Cuntze's formulation of the FMC.

4.1.6 LaRC03

The proposition by Puck et al. [16, 45] initiated the development of the LaRC damage criteria for FRP composites [15, 20, 21]. These criteria have a strong physical foundation and commenced with the proposition of the LaRC03 criteria. The LaRC03 criteria were followed up by LaRC04 and LaRC05 criteria to address shortcomings or take a different approach. LaRC03 displays a number of similarities to the Puck model, including the adoption of Mohr-Coulomb theory for MFC [21].

The strong physical basis necessitates a more extensive approach as compared to more simplistic Hashin and Hashin-Rotem criteria, with relatively higher associated computational effort. Principally, however, this is expected to incur a higher degree of accuracy. Still, the LaRC03 formulation suffers from a fallacy in the MFC criterion overestimating friction stresses and yielding a less conservative failure envelope for biaxial compression. Moreover, the LaRC03 formulation is limited to two-dimensional application. Extension to three dimensions is performed in successive LaRC04 and LaRC05 installments [15, 20].

MF is analysed by means of the Mohr-Coulomb fracture hypothesis and a slit crack analysis. Notable is that the LaRC03 criterion for FFC is the first to consider the mechanism behind fiber kinking in detail. The theory and equations behind LaRC03 are discussed more extensively in Appendix C.

4.1.7 LaRC04

In the wake of LaRC03, Pinho et al. proposed LaRC04 to extend LaRC03 to three dimensions and address some of the shortcomings, most notably the overestimation of friction stresses in MFC and neglecting shear non-linearity [15]. With the increased physical basis, relative to LaRC03, comes additional computational effort. This effort is mostly concentrated in the need to determine misalignment and kinking angles iteratively. Good predictive capability is projected for this criterion, largely attributed to the strong physical basis [15].

Refer to Appendix C for a more in-depth overview of the LaRC04 criteria. This overview contains the main equations and fundamental theory underlying LaRC04, linked to LaRC03.

4.1.8 LaRC05

The LaRC05 criteria follow upon LaRC04 and are highly similar. Main difference lies in the treatment of MFT and MFC and the iterative search for the out-of-plane kink angle. The same physical basis underlies this criterion as the LaRC04 criterion. Correspondingly, the two installments share mostly the same characteristics.

The crack treatment in LaRC04 is omitted in preference for a single expression indicating both MFC and MFT failure, distinguishing the cases by considering the normal traction opening a matrix crack if it is positive only [20], and yielding MF criteria highly similar to those formulated by Puck. For FFC, LaRC05 considers the same three-dimensional kinking as LaRC04. Overall, the simplification in primarily MF formulation yields much improved computational effort over LaRC04.

Good predictive capability was achieved using the LaRC05 criteria in the second Worldwide Failure Exercise [3]. The implementation proved one of the top performing models in terms of three-dimensional failure analysis. Appendix C discusses the criteria in more detail, giving an abridged overview of the underlying theory and equations.

4.1.9 Delamination criteria

Criteria for DL initiation are mostly not considered in the criteria presented before. DLs are currently best modelled using decohesion elements [12] and stress-strain approaches are few. Criteria that have been formulated, such as those by Lee [46], Ochoa and Engblom [47], Long [48], Shokrieh et al. [49] and Tong [50], have a very limited physical basis and are highly similar. Moreover, a detailed treatment is left out since DLs occur between plies and the interaction between different plies is difficult to model using a stress-strain approach. In particular, this applies to propagation of DLs.

4.2 Damage propagation models

When damage is present, predicted through the criteria presented above, the progression thereof is modelled using propagation models. Current stress-strain based practice focuses exclusively on degradation of material stiffness parameters to reflect the loss in load-carrying capability [7], thereby allowing a designation of these models as Material Degradation Models (MDMs).

A distinction can be made in degradation models. On one hand, instantaneous degradation has found numerous application for ease of use [7]. These sudden MDMs are mostly posed heuristically, with limited physical basis. On the other hand, gradual degradation has found increasing application in state-of-the-art models to better capture the physical basis of the damage process [7]. Moreover, a key advantage of gradual degradation is the possibility for crack smearing to alleviate mesh dependency [9].

In both cases, however, true physical understanding of the damage mechanisms is lacking. Noteworthy is that DLs in particular are poorly modelled using current stress-strain based approaches. Sudden and gradual degradation models are discussed subsequently hereafter.

4.2.1 Sudden material degradation models

Most sudden MDMs are simplistic propositions posed without justification other than limited comparison with experimental campaigns. As such, an in-depth discussion is difficult. However, part of the degradation factors can be logically reasoned. To this end, the models are discussed per failure mode.

Fiber failure

Fibres are the main load-carrying components, predominantly affecting the stiffness in longitudinal direction. The criticality of this failure mode has led to the use of a total-ply discount method, as used by Lee [46] and Pachajoa [51]. The loss of all components in the stiffness matrix is, however, not entirely realistic. Consequently, a number of models have been introduced that degrade material properties more selectively. A particular instance thereof is the model introduced by McCarthy et al., distinguishing FFT and FFC for the differing failure mechanisms thereof. FFC was accounted for by an additional reduction (to zero) of G_{23} with respect to FFT. Agreement with experimental results was good [52]. In the wake of this, Camanho and Matthews [53] and Tserpes et al. models [54] distinguish FFT and FFC by applying a stronger reduction factor in E_1 for the former, leaving all other properties intact. Results were reported in close correspondence to experimental data [54].

A number of other models can be distinguished, their degradation factors documented by Garnich and Akula [7]. These do not require further treatment as they are highly similar to the ones discussed. Commonality exists in the degradation of E_1 to zero, reflecting that the fibers do not carry any load in this direction. This is deemed necessary especially for FFT, since load transfer is discontinued by fiber breakage, and for FFC a logical consideration in view of experimental data confirming fiber breakage at the kink boundaries or fiber splitting (see e.g. [20]). While full property degradation might not be fully realistic, for partial property reduction experimental data are required, not always within practicality or easy reach [7]. In view of the commonly observed large energy release with FFT [12], surrounding matrix failure and concurrent loss of properties in transverse (matrix-dominated) properties is reasonable.

Table 4.1: Overview of sudden MDMs for FF

Mode	Implemented by	E_1	E_2	E_3	G_{12}	G_{23}	G_{13}	ν_{12}	ν_{23}	ν_{13}
FF	Lee	0	0	0	0	0	0	0	0	0
FFT	McCarthy et al.	0.10	-	-	0.10	-	0.10	0.10	-	0.10
	Camanho and Matthews	0.07	-	-	-	-	-	-	-	-
FFC	McCarthy et al.	0.10	-	-	0.10	0.10	0.10	0.10	-	0.10
	Camanho and Matthews	0.14	-	-	-	-	-	-	-	-

An overview of these sudden MDMs is given in Table 4.1. The model used by McCarthy et al.[52] is deemed most realistic. A total ply-discount, as used by Lee [46], is unrealistic whereas Camanho and Matthews [53] and Tserpes et al. [54] do not consider any effect on shear moduli, something contrasting with the fact that the matrix is locally affected by FF, be it FFT or FFC [11]. Still, all considered models are formulated for practicality rather than on a physical basis.

Matrix failure

Matrix failure is associated with a loss of stiffness in transverse directions. Most MDMs consider a complete degradation of E_2, G_{23} and G_{12} [7]. G_{13} and E_3 are not always reduced, considering that fibres contribute in this direction. A reduction in transverse properties due to MF, either MFC or MFT, is reasonable due to the formation of matrix cracks discontinuing the load path and thereby local load transfer within the matrix.

An overview of sudden MDMs for MF is given in Table 4.2. A distinction between MFC and MFT is difficult to make, main difference lying in the opening mode (hence also angle of matrix cracking). A compressive crack is assumed to carry still some load, as opposed to an opening (MFT) crack, leading to the differentiation by Camanho and Matthews [53] and Tserpes et al. [54]. Absence of a G_{12} degradation in the model of McCarthy et al. [52] is deemed unrealistic, due to the fact that shear load transfer is inhibited by the formation of matrix cracks.

Table 4.2: Overview of sudden MDMs for MF

Mode	Implemented by	E_1	E_2	E_3	G_{12}	G_{23}	G_{13}	ν_{12}	ν_{23}	ν_{13}
MF	Lee	-	0	-	0	0	-	0	0	-
	McCarthy et al.	-	0.10	0.10	-	0.10	-	-	0.10	-
MFT	Camanho and Matthews	-	0.20	-	0.20	0.20	-	-	-	-
MFC	Camanho and Matthews	-	0.40	-	0.40	0.40	-	-	-	-

Delaminations

Degradation models for DLs are especially scarce, few studies using a stress-strain approach to model DLs. Consensus amongst the existing models is a degradation of out-of-plane properties, reasonable in view of losing the interface between adjacent plies while still retaining the ability to carry loads within the ply, i.e. in plane [7]. The models by Lee [46] and Tserpes et al. [54] consider a degradation of E_3, G_{23}, G_{13}, with reported good correspondence to experiments. Ochoa and Engblom propose $C_{13} = C_{23} = C_{33} = C_{44} = C_{55} = 0$ after DL in analogy to the former models, although formulated directly in terms of stiffness matrix elements [47]. An overview of the degradation factors is given in Table 4.3.

This approach to degrading DLs is considered physically ungrounded and fallacious. Although it is a simple way of taking into account damage, adopting the same procedure as for the intralaminar mechanisms of FF and MF is not appropriate for the interlaminar mechanism of DL. DLs occur at the interface and the sudden MDM fails to capture this, instead discounting a number of intralaminar properties that are likely retained in the case of DLs occurring. Consequently, this can be seen as a key point for improvement when it comes to damage propagation.

Table 4.3: Overview of sudden MDMs for DL

Implemented by	E_1	E_2	E_3	G_{12}	G_{23}	G_{13}	ν_{12}	ν_{23}	ν_{13}
Lee, Tserpes et al., Ochoa and Engblom	-	-	0	-	0	0	-	0	0

4.2.2 Gradual material degradation models

Contrary to instantaneous or sudden MDMs, a number of models has been proposed to gradually degrade properties after damage detection. A bilinear softening model is presented (in the wake of work by Lapczyk [9], Pinho et al. [12, 20] and Zhang et al. [55]) as well as the gradual MDM proposed by Puck and Schürmann [45].

Models that are highly similar, such as exponential softening laws [11], are omitted. This omission leads to little loss in accuracy or quality of the study in view of the similarity. After all, this merely changes the shape of the softening portion of stress-strain curves, but the general trend remains the same.

Puck degradation

Puck adopts a purely phenomenological approach for degrading stiffness after MF through degradation factor η_{Puck}. This factor reduces secant moduli E_2 and G_{12}, G_{23}. Initially, a Poisson's ratio reduction was used but based on experimental evidence this was considered false [13, 42]. For mode B and C fracture, i.e. MFC, E_2 is not degraded [13]. This follows on the basis that for mode B and C, i.e. MFC, cracks do not open.

In principle, this degradation factor η_{Puck} is to be determined experimentally but in its absence, it was proposed that it is to be taken such that the factor on left-hand sides of the MF criteria featured in Puck are equal to one (i.e. at the initiation threshold), using the inverse of the current value thereof as an estimate for η_{Puck} until the condition is satisfied. This essentially entails keeping the stresses in the damaged region constant after fracture.

This is associated with increased computational effort, since for each stress increment the degradation factor must be recalculated by iteration. Noteworthy is, however, that this approach does not require determination of additional parameters, as is the case for the bilinear softening laws relying on the critical fracture energy of failure modes.

Bilinear softening

Bilinear softening is characterized by a linear softening after failure. The softening relates, however, not necessarily to one of the principal stresses or strains, but rather to equivalent forms thereof. In the bilinear softening law by Pinho et al. [12, 20], this is taken care of by considering stresses and strains in the kink and misalignment frame. For a generally applicable theory, however, one must step away from this notion since this only applies to LaRC criteria.

Consequently, the notion of equivalent stresses and strains is adopted as per the work by Lapczyk [9]. Essentially, this entails formulating a combination of principal stresses and strains to calculate equivalent forms, one for each failure mode. Although a precise definition thereof is impossible without a deeper physical knowledge of the failure processes, a pragmatic definition can be taken in likeness to Lapczyk [9]. Adopting the same polynomial trends as Hashin criteria [43] yields the following equivalent stresses and strains [55]

$$\varepsilon_{eq} = \begin{cases} \sqrt{(\langle\varepsilon_1\rangle^+)^2 + \gamma_{12}^2 + \gamma_{13}^2} & \text{if FFT} \\ \langle -\varepsilon_1\rangle^+ & \text{if FFC} \\ \sqrt{(\langle\varepsilon_2\rangle^+)^2 + \gamma_{12}^2 + \gamma_{23}^2} & \text{if MFT} \\ \sqrt{(\langle -\varepsilon_2\rangle^+)^2 + \gamma_{12}^2} & \text{if MFC} \end{cases} \tag{4.1}$$

$$\sigma_{eq} = \begin{cases} \frac{\langle\sigma_1\rangle^+\langle\varepsilon_1\rangle^+ + \tau_{12}\gamma_{12} + \tau_{13}\gamma_{13}}{\varepsilon_{eq}} & \text{if FFT} \\ \frac{\langle -\sigma_1\rangle^+\langle -\varepsilon_1\rangle^+}{\varepsilon_{eq}} & \text{if FFC} \\ \frac{\langle\sigma_2\rangle^+\langle\varepsilon_2\rangle^+ + \tau_{12}\gamma_{12} + \tau_{23}\gamma_{23}}{\varepsilon_{eq}} & \text{if MFT} \\ \frac{\langle -\sigma_2\rangle^+\langle -\varepsilon_2\rangle^+ + \tau_{12}\gamma_{12}}{\varepsilon_{eq}} & \text{if MFC} \end{cases} \tag{4.2}$$

Although this is not entirely physically based, it should be noted that in particular for damage propagation all theories suffer from a lack of physical basis. Physical meaning to the notion of equivalent strains and stresses is that these determine the direction of crack propagation.

The bilinear softening relation defines the slope of the portion between damage initiation, at $(\varepsilon_{eq,0}, \sigma_{eq,0})$, and failure, at $(\varepsilon_{eq,f}, \sigma_{eq,f})$. To calculate $\varepsilon_{eq,f}$, the crack band method of Bažant and Oh [56] is adopted. This is advantageous in terms of relieving mesh dependency by the introduction of a characteristic element length L. This yields [9, 12, 20]

$$\varepsilon_{eq,f} = 2\frac{G_c}{\sigma_{eq,0}L} \tag{4.3}$$

The fracture toughness in the above equation is to be determined for each of the damage modes separately (G_{fft}, G_{ffc}, G_{mft} and G_{mfc}), determined from Compact Tension and Compact Compression specimens [12].

The characteristic length can be calculated using a number of different measures [9, 12, 20], but generally it can be calculated as [9, 34]

$$L = \frac{\sqrt{A}}{\cos\omega} \tag{4.4}$$

with ω the angle of the mesh lines with respect to the crack direction. If this is unknown, the average of the expression can be used to find [34]

$$L = 1.12\sqrt{A} \tag{4.5}$$

In possession of these parameters, the softening relation then defines damage parameters for each failure mode as follows [9]

$$d = \max_{\text{time}} \langle \min(1, \varepsilon_f \frac{\varepsilon - \varepsilon_0}{\varepsilon(\varepsilon_f - \varepsilon_0)}) \rangle^+ \tag{4.6}$$

where the maximum in time effects irreversibility of the damage process.

These damage parameters are then used to degrade moduli, although not directly in terms of engineering constants as for the sudden MDMs considered and Puck's degradation model. Rather, the Matzenmiller damaged compliance matrix is turned towards. The corresponding stiffness matrix with degraded moduli is calculated as (extended to three dimensions)[9, 57]

$$\boldsymbol{C} = \begin{bmatrix} (1-d_f)E_1 & -\frac{\nu_{21}}{E_2} & -\frac{\nu_{21}}{E_2} & 0 & 0 & 0 \\ -\frac{\nu_{21}}{E_2} & \frac{1}{(1-d_m)E_2} & -\frac{\nu_{23}}{E_2} & 0 & 0 & 0 \\ -\frac{\nu_{21}}{E_2} & -\frac{\nu_{23}}{E_2} & \frac{1}{(1-d_m)E_2} & 0 & 0 & 0 \\ 0 & 0 & 0 & \frac{1}{(1-d_m)G_{23}} & 0 & 0 \\ 0 & 0 & 0 & 0 & \frac{1}{(1-d_m)G_{12}} & 0 \\ 0 & 0 & 0 & 0 & 0 & \frac{1}{(1-d_m)G_{12}} \end{bmatrix} \tag{4.7}$$

implemented by Van der Meer [57], Zhang et al. [55] and Camanho et al. [58].

4.3 Conclusions and recommendations

A plethora of stress-strain based methods for damage initiation exists. To respect composite heterogeneity, models have moved from mode-independent to mode-dependent criteria. Whereas early theories were proposed simplistically, a trend towards more physically based models, such as Puck and LaRC criteria, is observable. Commonality of recent criteria exists in their basis, being the Mohr-Coulomb hypothesis that fracture is governed by stresses acting on the fracture plane, as well as the fact that damage is treated on a mesolevel. The increasing physical basis is generally accompanied by an increase in model complexity and computational effort, as well as an increase in the number of involved parameters.

Damage propagation suffers particularly from a lack of reliable experimental data and physical understanding. Simplistic sudden degradation has traditionally found the most use, although the recent advance of gradual degradation models, particularly bilinear softening, offers an alternative. The latter offer a more physical basis and moreover a means to mitigate mesh dependency in FEM applications.

Both initiation and propagation models suffer from a severe lack of DL modelling. The investigated stress-strain based models for DLs are mostly heuristical propositions.

Regardless, however, of the leaps in physically based damage models for FRP composites, a number of issues remains overlooked or unaddressed. Moreover, the current study is limited in scope, focusing on generally applicable stress- and strain-based approaches. In particular, the following issues deserve further study:

- The Mohr-Coulomb fracture hypothesis states that fracture is only influenced by stresses acting on the fracture plane angle. Experimental evidence suggests, however, a decrease in strength prior to failure designation due to damage processes on a microlevel and stresses not directly acting on the fracture plane [13]. Correspondingly, a correction or extension beyond the Mohr-Coulomb hypothesis is warranted to account for this pre-failure degradation.
- Propagation models presented in this study follow mostly heuristically with a limited physical basis. This is particularly true for the sudden degradation models. One way to address the limitations thereof is to turn towards fracture mechanics. Another possibility opens up when considering micromechanical modelling. Particularly DLs are poorly modelled by stress-strain based approaches, whereas fracture mechanics offers many possibilities through Cohesive Zone Models (CZMs) and the recent advance of Extended Finite Element Method (XFEM) techniques [11, 12, 25, 57, 59, 60].
- On a more general level, an investigation on the effect of the micromechanical features of damage is recommended, for example by conducting Representative Volume Element (RVE) studies. For one, the influence of the fracture plane angle on material degradation remains relatively uninvestigated.
- All models suffer from the common flaw of evaluating failure deterministically. In reality, however, a statistical component is strongly present in composites due to the multiple constituents and interaction thereof on a number of levels. One way to address this is a statistical approach to FRP failure.

Chapter 5

Preliminary analysis and stress-strain method selection

The plethora of available stress-strain based models for PDA necessitates thorough selection. Part of this selection is done prior to FEM implementation, by means of a preliminary analysis on a select number of test cases and available literature. This selection serves the purpose of evaluating model performance in a number of aspects and cases at less implementation effort than a full-fledged PDA routine in FEM. Ultimately, this selection results in three stress-strain based models for FEM implementation.

The express distinction between initiation criteria and propagation models comes in here, in order to select firstly initiation criteria and thereafter propagation models to formulate combined models. This two-stage selection is performed by means of two successive trade-offs, both based upon the same criteria although using a different set of test cases. This chapter describes the selection process, commencing with a definition of the trade-off set-up, proceeding with analysis and trade-off results and concluding with a final model selection.

Contents

5.1 Trade-off set-up

It is essential that models are evaluated on the basis of representative cases and filtered on the basis of a consistent set of criteria. To this end, the trade-off method is defined firstly followed upon by motivation of the trade-off criteria. Thereafter, a discussion on the preliminary analysis and selection of candidate stress-strain models follow.

5.1.1 Trade-off method

Selecting an appropriate methodology for PDA of FRPs requires judicious selection of initiation criteria and propagation modelling. The plethora of available models necessitates an effective trade-off method. To this end, method selection is performed using a two-stage trade-off procedure.

Trade-off sequence

The trade-off sequence is as follows:

- Firstly, a trade-off amongst initiation criteria on the basis of test cases governed by initial failure. On the basis of model performance in these cases and qualitative considerations on the basis of method formulation, three criteria are selected.
- Secondly, a trade-off amongst propagation models on the basis of a second set of cases governed by damage propagation. On the same selection basis as for the first trade-off, three propagation models are selected - one for each of the initiation criteria.

This two-stage approach is taken for the following reasons. Firstly, a single trade-off amongst all initiation and propagation models would incur significant work and clutter in results. Dividing the trade-off into two parts makes the process more manageable, reducing the number of model evaluations and allowing a near-independent evaluation of the two model components, being damage initiation and propagation modelling. Secondly, related to the latter, performing a single trade-off would hamper insight in the two model components. After all, initiation and propagation models are essentially independent components that each govern a part of model performance. Consequently, it is preferable to evaluate these components as independently as possible - for the dual purpose of an effective comparison and for gaining additional insight in the damage mechanisms.

This approach comes with the requirement that test cases for each trade-off ideally isolate one of the model components (initiation or propagation). To this end, initial failure is evaluated for the first trade-off and final failure (of multidirectional lamintes) for the second stage. For the first stage, selecting initiation criteria, initial failure is of primary interest whereas for the second stage final failure is of primary interest. Although initiation criteria play a role after initial failure in defining intermediate and final failure, progression does not play a role in initial failure.

A drawback of this approach is that only a subset of all possible model combinations is evaluated. Moreover, since initiation criteria play a role in intermediate and final failure as well as in initial failure, this part of initiation criteria performance is left unevaluated. The selection of a trio of models in each stage mitigates these drawbacks to some extent.

Ranking of models

Models are ranked per trade-off criterion with a score on a scale of five, A being the highest and E being the lowest score. Within each criterion, several remarks with individual scores can apply and the average thereof determines the score on that criterion.

Criteria are combined in an aggregated score, obtained as the weighed average. Weights are dictated by the priorities given to the criteria. The aggregated score determines the overall performance of each model.

This process aids in objectifying the trade-off, although precise quantification is impossible. The quality of the trade-off hinges on a proper designation of trade-off criteria and assessment thereof.

5.1.2 Trade-off criteria

Models are consistently compared on the basis of judiciously selected criteria, intended to reflect model performance on a number of key areas. As such, the criteria are intended to cover all relevant model aspects. Moreover, for an efficient trade-off differences between models in these aspects should be readily apparent.

By this philosophy, the following criteria were formulated. To facilitate and apply consistency to the process, measurement points are outlined for each criterion. For each criterion, these (criterion-specific) points are evaluated to yield a consistent scoring of models.

Predictive accuracy

Key consideration in improving the state-of-the-art in PDA of FRPs is an improvement of predictive accuracy. Although this evaluation centers around existing models as opposed to founding a new (physically based) stress-strain based model, it is essential that accurate predictions are obtained. This is highly relevant for both initiation and propagation models, since errors accumulate in PDA. To reflect this need, predictive accuracy is selected as the first and key parameter with a relative weight of 50 %.

The weight is higher than that attributed to computational effort, in order to effect the choice of a method that is at the forefront of the state-of-the-art in delivering consistently accurate predictions. In this sense, the philosophy is adopted that, crudely stated, a high cost, high accuracy model is preferred to a low cost, low accuracy model. A key consideration in this philosophy is the fact that low cost and low accuracy models are already available (e.g. total ply discount methods [7] and polynomial initiation criteria [1]), while high accuracy models (of any cost) are still relatively scarce, exemplified by the Worldwide Failure Exercise installments [2, 3, 61]. However, since improvement in state-of-the-art also entails developing lower cost methods at comparable predictive accuracy, the weights are still kept relatively close.

Indicative measurement points of predictive accuracy are the following:

- Predictive accuracy in a preliminary two-dimensional analysis covering selected test cases from the first Worldwide Failure Exercise [2]. Part of the models has already been evaluated in this context, such as Puck [2], but a number of models has been evaluated on a very limited number of test cases, for example LaRC03 [21]. It is therefore necessary that models are evaluated on identical test cases. The preliminary analysis is outlined later in more detail.
- Reported performance of models. This is particularly relevant for three-dimensional application. Whereas the preliminary analysis covers two-dimensional application over a varied set of test cases, three-dimensional performance is evaluated on the basis of available reference literature. In case models are only applicable in two dimensions, this is discounted in the versatility trade-off criterion.

Caution should be exerted when comparing model accuracy over a limited number of test cases, since composite behaviour is highly dependent upon material, structural (lay-up and geometry) definition and applied loading. Extrapolating conclusions based on a limited number of test cases is therefore to be performed with care.

Computational effort

Widespread application of methods is hindered by excessive computational effort as well as insufficient predictive accuracy [2]. For practical application, it is essential that computational effort is kept limited. In particular, this extends to cases where sizeable, or a sizeable number of, components are analysed by means of PDA. Although a method may exhibit agreeable computational effort for a coupon-sized component, for analysis of larger structures, such as wind turbine blades [62], this effort may become excessive. To reflect the need for a practically viable method, computational effort plays a key role in the selection process. Moreover, implementation effort is evaluated since overly complicated procedures may well hamper widespread use of a model. It is thereby preferred to have an easily implemented model, not so much from an academic point of view as from a practical point of view. This reasoning is captured in the relative weight of 25 %.

The weights attached to predictive accuracy and computational effort were previously compared. Summarizing, predictive accuracy is prioritized above computational effort in view of the lacking predictive accuracy of state-of-the-art PDA methods, whereas low-cost routines are already available - although at limited accuracy. Versatility is discussed in relation to the other two criteria in the following section.

Indicative measurement points of computational effort are the following:

- Computational effort in a preliminary two-dimensional analysis covering selected test cases from the first Worldwide Failure Exercise [2]. In this context, computational effort is measured as the total time to execute a PDA routine (relative to other methods evaluated).
- Qualitative assessment of implementation effort.

Duly note that computational effort increases significantly in FEM analysis as compared to the preliminary analysis performed, since the number of integration points is significantly larger but moreover since the acquisition of stress and strain takes a significant amount of effort. Still, a first-order comparison of computational effort on the basis of the preliminary analysis is worthwhile. Differences between methods will, however, be smaller in FEM analysis where the lion's share of computational effort lies in acquiring stresses and strains and the evaluation of initiation and propagation criteria (in the post-processing stage) becomes less significant.

A consideration when measuring the computational effort is the number of increments required to proceed to final failure. A more conservative model will require less increments, thereby lowering the computational effort. Without preventive measures, this would mean the conservativeness of a criterion would appear in two trade-off criteria, namely predictive accuracy and computational effort. To this end, computational effort is corrected by normalizing with respect to the number of stress increments required up to final failure.

Versatility

Practical application requires versatility. This versatility encompasses both the ability of a PDA method to predict relevant damage phenomena and the ability to do so on the basis of a limited number of variables. This ensures firstly that methods requiring extensive fitting and determination of experimental parameters are discounted, and secondly that methods are capable of handling a diverse set of cases. The former is desirable in view of the significant work that goes into determining these parameters, especially prohibiting when it comes to design [2]. The latter is desirable primarily in view of three-dimensional application. This reasoning is captured in a relative weight of 25 %.

When distinguishing methods, versatility is easily overlooked as compared to predictive accuracy and computational effort. It is, however, essential. However accurate and low cost a method may be, if it only works for a very limited number of cases or requires a significant amount of experimentally determined parameters, it is moot. To reflect this, versatility and computational effort are weighed equally.

Indicative measurement points of versatility are the following:

- Limitations in modelling phenomena. In particular three-dimensional modelling enters into play.
- Required parameters and the attainability thereof. This relates primarily to those parameters not obtained with ease through standard uni-axial material tests, e.g. curve fitting parameters.

5.1.3 Preliminary analysis

To gauge model performance in terms of predictive accuracy and computational effort, a preliminary analysis is performed. This analysis is constructed with the following qualities in mind:

- Based on a uniform set of test cases to compare models consistently
- Experimental data is available for an objective judgment on model predictive capability (apart from errors in experimental data)
- Diverse test cases in terms of material, loading and lay-up
- Test cases suited for two-dimensional analysis on the basis of CLT

The test cases of the first Worldwide Failure Exercise [2] are ideally suited, fulfilling the above qualities and moreover allowing for comparison with past implementations to verify the methodology of implemented methods. The two-stage nature of the selection process necessitates making a distinction in the available test cases, leading to one set of cases for selecting initiation criteria and a second set of cases for selecting propagation models.

5.1.4 Test case selection

Test cases are selected from the first Worldwide Failure Exercise [2] for the aforementioned reasons. A proper selection of test cases is in order to guide the two-stage trade-off. For the first stage, selecting initiation criteria, initial failure is of primary interest whereas for the second stage final failure is of primary interest. Although initiation criteria play a role after initial failure in defining intermediate and final failure, progression does not play a role in initial failure.

On the basis of the above reasoning, the following test cases were selected. For an overview of the test cases, please see Appendix D.

For evaluation of initiation criteria (cases numbered as per the first Worldwide Failure Exercise [2]):

1-3 These cases concern unidirectional laminates without damage propagation, since initial failure implies final failure [45]. A trio of different materials and loading cases is evaluated to evaluate initiation criteria over a broad range. Moreover, the variety of failure envelopes covers a number of interaction effects.

6, 9 A multidirectional laminate is considered in both cases. Since indications for initial failure are available, a comparison can be made regarding model performance on multidirectional laminates.

For evaluation of propagation models:

4, 5 Multidirectional laminates are evaluated for final failure. Two load cases are evaluated to compare models with respect to differing distinguishing features for both cases.

6 A similar reasoning as for the previous test cases hold. Moreover, this is an interesting case since initial failure was evaluated in the first trade-off stage.

Consequently, a set of five and three test cases are respectively analysed for the first and second stage of the trade-off. Results are weighed equally for all test cases to obtain an indication of overall model performance.

5.1.5 Numerical procedure

The PDA routine is handled as depicted in Figure 5.1. The numerical routine has been implemented in Python. Stress is incremented until final failure occurs. For the global ply-by-ply analysis, final failure is defined as the occurrence of FF following the authors in the Worldwide Failure Exercise [2].

For each increment, ply strains and stresses are calculated through CLT by means of compliance matrices calculated using given and interpolated material data. Thereafter, failure criteria are evaluated. If damage is detected, properties are degraded according to the applicable propagation model. Duly note that for unidirectional laminae, initial failure means final failure.

No equilibrium step is taken to check for damage progression at each increment. Instead, stress increments are chosen small such that any inaccuracy induced is limited.

Failure envelopes are generated by varying stress ratios and incrementing. This entails moving along radial lines of constant stress ratio up to final failure. Misalignment angles are only determined once along each line, since these remain constant for a constant stress ratio. This reduces the computational effort associated with determining these angles significantly, while retaining solution accuracy.

5.1.6 Models under evaluation

Models considered are historically significant and state-of-the-art stress-strain models for PDA of FRPs. As previously stated, damage is predicted by initiation criteria and propagation models. In each category, the following models are considered. All models are used in conjunction with in-situ strengths, as outlined in Section 3.3. Input for the models is detailed in Appendix D.

Initiation criteria

The following initiation criteria are considered, underlying theory and working principles as explained previously in Section 4.1:

- Hashin-Rotem
- Hashin
- Puck
- Cuntze

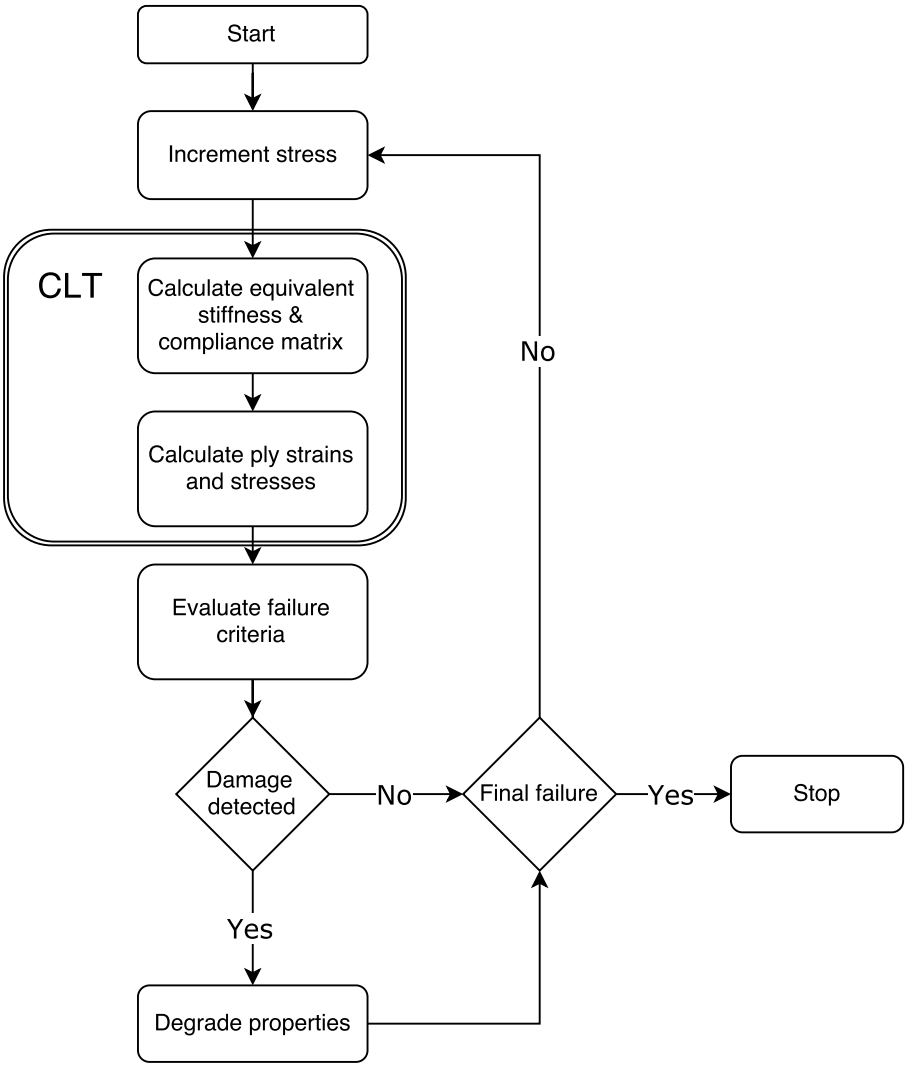

Figure 5.1: Numerical procedure PDA routine preliminary analysis

- LaRC03
- LaRC04
- LaRC05

For the implementation of these criteria, plane stress considerations (to find the fracture angle analytically, predominantly) are left out. This is done in order to provide a fair comparison for the effort of finding this angle as opposed to neglecting it (as done in Hashin-Rotem, Hashin and Cuntze criteria). Moreover, for the LaRC04 criterion, the out-of-plane kinking angle is left unconstrained in view of results by Pinho et al. [15]. Lastly, the iterative search for angles is done by searching over a number of trial angles. The number and range of trial angles is kept the same for all criteria.

Propagation models

The following propagation models are considered, underlying theory and working principles as explained previously in Section 4.2:

- Lee sudden MDM

- McCarthy (et al.) sudden MDM
- Camanho and Matthews sudden MDM
- Puck gradual MDM
- Bilinear softening gradual MDM

Since the bilinear softening model is ill-defined for the current application, in the absence of a length dimension with any physical meaning, the failure strain cannot be calculated using Equation 4.3. Instead, a pragmatic approach is taken and the bilinear model is run for $\frac{\varepsilon_f}{\varepsilon_0} = [1.50, 2.00, 4.00]$ and in the evaluation these three models are considered.

This is deemed preferable to omitting the bilinear softening model either entirely or solely in this trade-off, since the model offers a different perspective than the other implemented propagation models. Moreover, the working of the model is kept intact with the relations assumed above. Moreover, the ratio of fracture energies in MFC and MFT is respected (reported to be approximately equal [12, 34]), whereas FFC and FFT do not play a role due to termination at fiber failure.

5.1.7 Limitations of selection procedure

A number of limitations apply to the preliminary analysis and trade-off. These limitations are handled pragmatically by the selection of a trio of suitable models, as opposed to selecting a single model. Consequently, the trade-off is envisioned to yield a good impression of relative model performance. Limitations are listed hereafter, along with potential measures to address these.

Two-dimensional analysis

Two-, rather than three-dimensional analysis, limits the complexity of the analysis but at the same time incurs a loss of accuracy and moreover neglects a number of model-specific components in the trade-off. This entails that three-dimensional performance of criteria and models is to be judged on the basis of open literature. Although there is data available, such as the second Worldwide Failure Exercise [3], it would be preferable to include a fully fledged three-dimensional analysis.

To address this limitation, however, full three-dimensional analysis would have to be executed. The CLT employed will then not suffice and the analysis becomes significantly more complicated and time-intensive.

Global analysis

The analysis works on a ply-by-ply level, thereby globally, as opposed to a local analysis where damage is evaluated at a number of integration points in a specimen. Consequently, damage is smeared over entire plies. In case stresses are uniform, such as intended in the test cases, this yields a reasonably accurate representation. Still, this neglects the effect of local stress raisers and limits damage progression to the through-thickness direction (i.e. from ply to ply).

Addressing this limitation would have similar implications as for the two-dimensional analysis. A FEM-like approach would have to be taken to evaluate stress at a number of integration points throughout the specimen and identify and propagate failure accordingly.

Limited number of cases and experimental data

Evaluation based on a limited number of cases and experimental data brings two complications. Firstly, specimen-to-specimen variations can be pronounced in view of manufacturing defects or batch-to-batch differences. A limited number of specimens thereby incurs the risk of including these deviations and comparing models on the basis of false, or at the least variable, experimental data. In the first Worldwide Failure Exercise, this is only partially addressed by including multiple sets of experimental data for the test cases [2].

Secondly, composite behaviour is dependent on a large number of factors, not least among which material selection, lay-up and loading cases. A limited palette thereof necessarily limits the reflection on composite behaviour to this palette. Judging model performance objectively would strictly require investigating all possible combinations of these parameters. It is readily apparent that such an investigation would be impractical. The inclusion of multiple materials, lay-ups and load combinations in the test cases mitigates this limitation to some extent [2].

Addressing this limitation would require additional test cases on a large number of samples. Due to the costs and resources associated with the experimental testing, this rapidly becomes prohibitive. Moreover, time constraints limit the number of evaluations that can be performed.

Limited experimental data on initial failure

For a proper account of initial failure, experimental data on the mode of initial failure and the stress at which it occurs is essential. This would allow validating the predictive accuracy of initiation criteria more precisely. In addition, it would offer additional insight in the physical mechanisms of FRP failure. Although data is available for some of the test cases in the first Worldwide Failure Exercise [2], quantity and quality are limited.

Addressing this limitation would entail observing the damage state of specimens during testing using appropriate Non-Destructive Testing (NDT) techniques. The same remarks as for the previous case hold, amplified by the limitations of current NDT techniques to reliably detect damage [2].

Lack of delamination modelling

DLs are not evaluated in the preliminary analysis. For the unidirectional laminates, no accuracy is lost since these do not feature DLs in practice. For the multidirectional laminates, however, particularly the angle-ply laminates where stiffness discontinuities are large (and hence interlaminar stresses large), DLs can be expected.

However, three-dimensional stresses are essential for a proper evaluation of DLs. This has previously been discussed in the two-dimensional analysis limitation.

Final failure designated at fiber failure

Designating FF as final failure, in line with authors in the Worldwide Failure Exercise [2], is deemed necessary in view of the global analysis. Consequently, however, propagation of FF is not investigated and propagation models cannot be compared in this aspect. In a local FEM analysis, propagation of FF will play a role. After all, local failure of fibres will lead to a stress redistribution within plies. For the global analysis, fibres are evaluated at ply level and ply

failure is instantaneous. Duly note that for the case at hand, where laminates are ideally subjected to a uniform stress field and without initial defects or stress raisers, this does not hamper accuracy.

Simplification of bilinear softening

The length parameter in the bilinear softening has no physical meaning in this global CLT analysis and is therefore omitted, together with the critical fracture energy, in favour of assumed failure strain to onset strain ratio's. Although this respects the mechanisms of the bilinear softening law, this partially overlooks some of its characteristics in terms of the use of critical fracture energy as a key parameter in damage propagation.

This limitation can be overcome by a fully-fledged FEM analysis where the length parameter features in the areas associated with integration points. Moreover, such an analysis would reflect the mesh independency of this method relative to other damage localization models, such as the sudden MDMs and the Puck model featured herein.

5.2 Analysis results for initiation criteria

Analysis results for initiation criteria are listed hereafter per test case, in the form of failure envelopes accompanied by a discussion thereof. At the end of this section, results are collected and translated into a score for each of the initiation criteria. This score forms a key consideration in the predictive accuracy and computational effort trade-off criteria.

5.2.1 Test case 1

All initiation criteria are in relatively close agreement to experimental results, main discrepancies lying in the transverse compression case, see Figure 5.2. Particularly at the intersection with the τ_{12} axis, results are off for all criteria. This is, however, attributed to a difference in uniaxial strengths used in the analysis. Adapting strengths leads to improved correspondence, see the work by Pinho et al. [15].

Under combined transverse compression and shear, the best correspondence is achieved by the Puck and LaRC04/05 criteria. Notable is that Hashin and Hashin-Rotem criteria, and to a lesser degree the Cuntze criterion, are overly conservative.

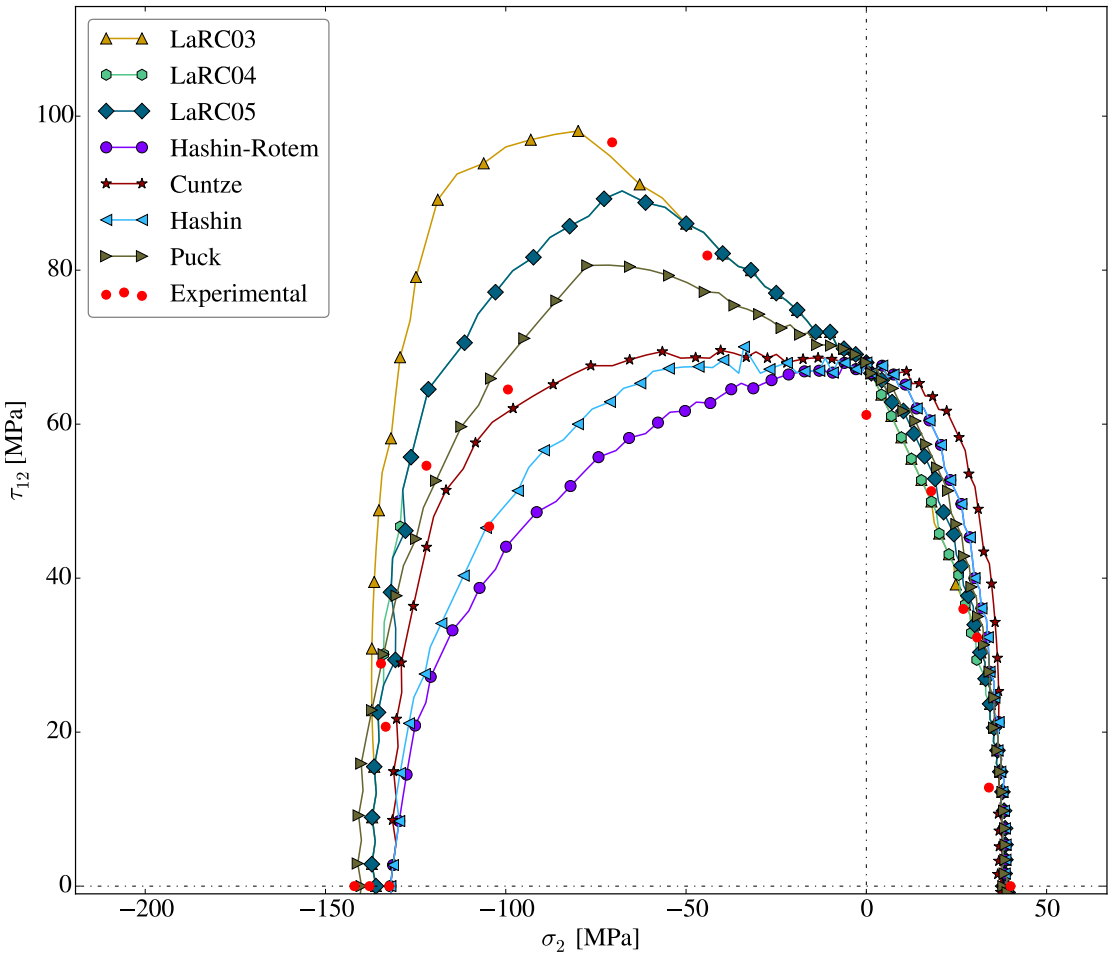

Figure 5.2: Failure envelope (σ_2, τ_{12}) of unidirectional 0° E-Glass/LY-556 lamina (Test case 1)

5.2.2 Test case 2

Disrepancies for this loading case are significant, particularly in the combined longitudinal tension and shear quadrant, see Figure 5.3. Overall, the Cuntze criterion yields the best agreement, particularly in the combined longitudinal compression and shear quadrant. LaRC04/05 criteria are very conservative in this quadrant, whereas the rest of the models gives similar results for the failure envelope.

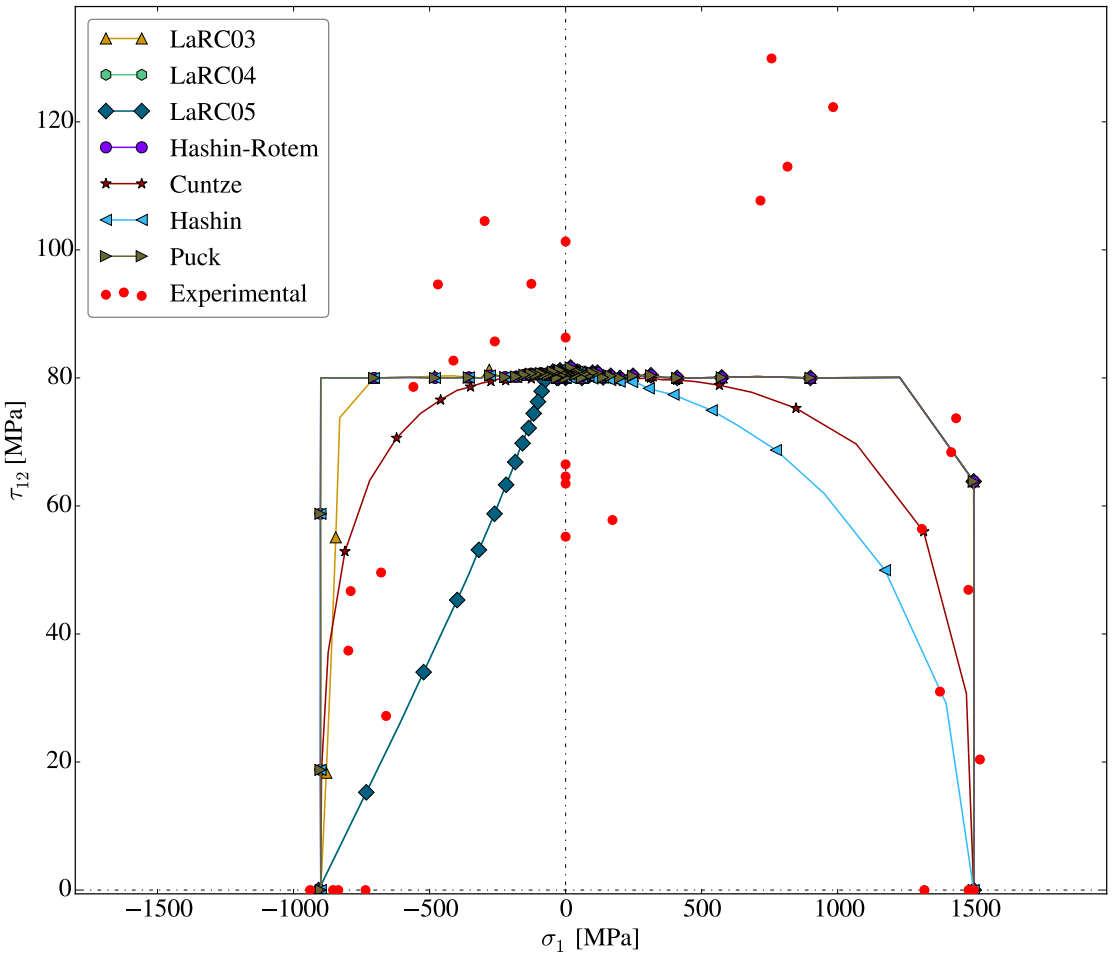

Figure 5.3: Failure envelope (σ_1, τ_{12}) of unidirectional 0° T300/BSL914C lamina (Test case 2)

5.2.3 Test case 3

An overestimation of strength is readily apparent in the combined longitudinal tension and transverse compression region, see Figure 5.4. The least prone to overestimation is the Cuntze criterion, lying closest to experimental results. The remainder of criteria offers comparable results, overall in decent agreement to experimental data. It should be noted that the quantity of experimental data points is limited, particularly for longitudinal compression.

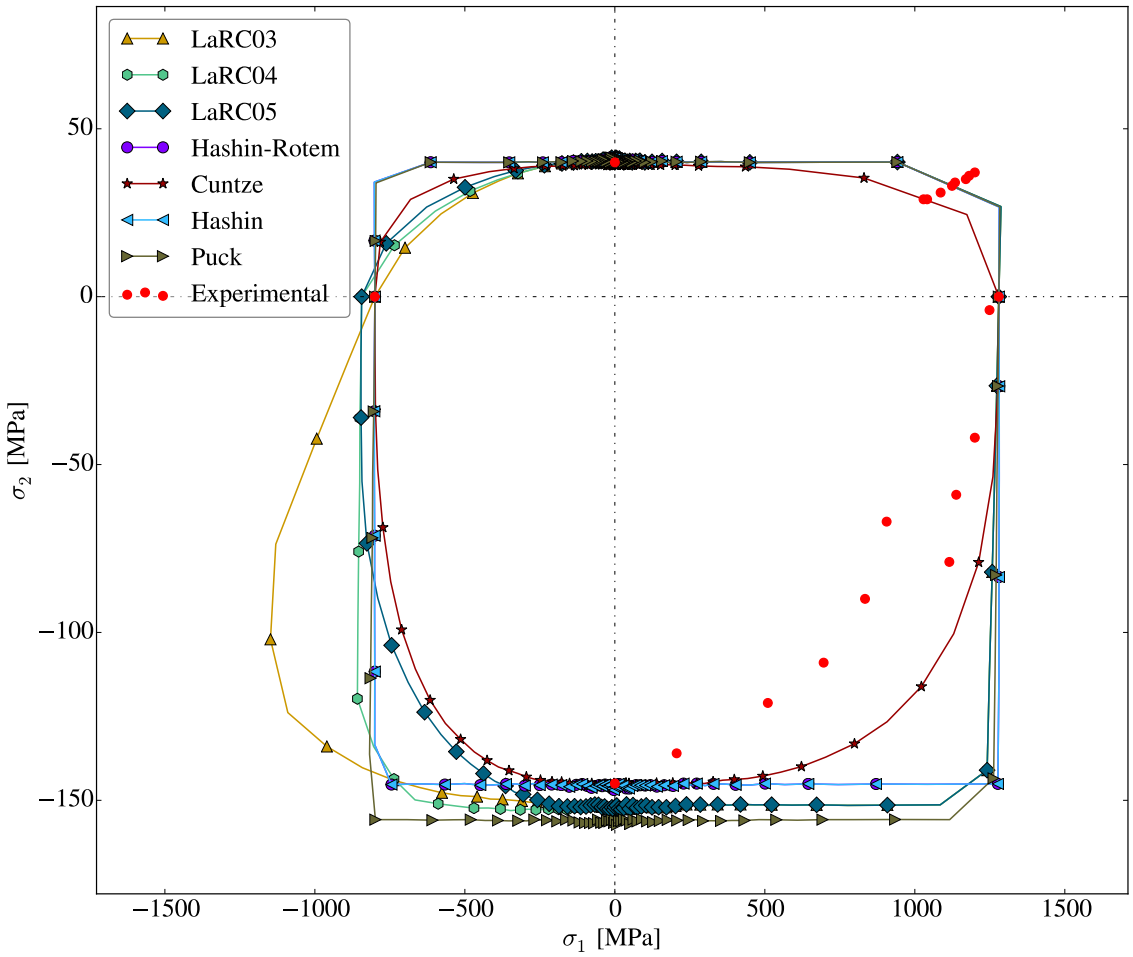

Figure 5.4: Failure envelope (σ_1, σ_2) of unidirectional 0° E-glass/MY750 lamina (Test case 3)

5.2.4 Test case 6

For the multidirectional laminate in this test case, the Cuntze criterion again offers the best agreement to experimental data, see Figure 5.5. The remainder of models is slightly less conservative than the Cuntze criterion. It should be noted that the experimental data is inferred from slope changes in the experimental stress-strain diagram and therefore limited value is to be attached to the exact location of these data points. Moreover, data points are only located in one quadrant.

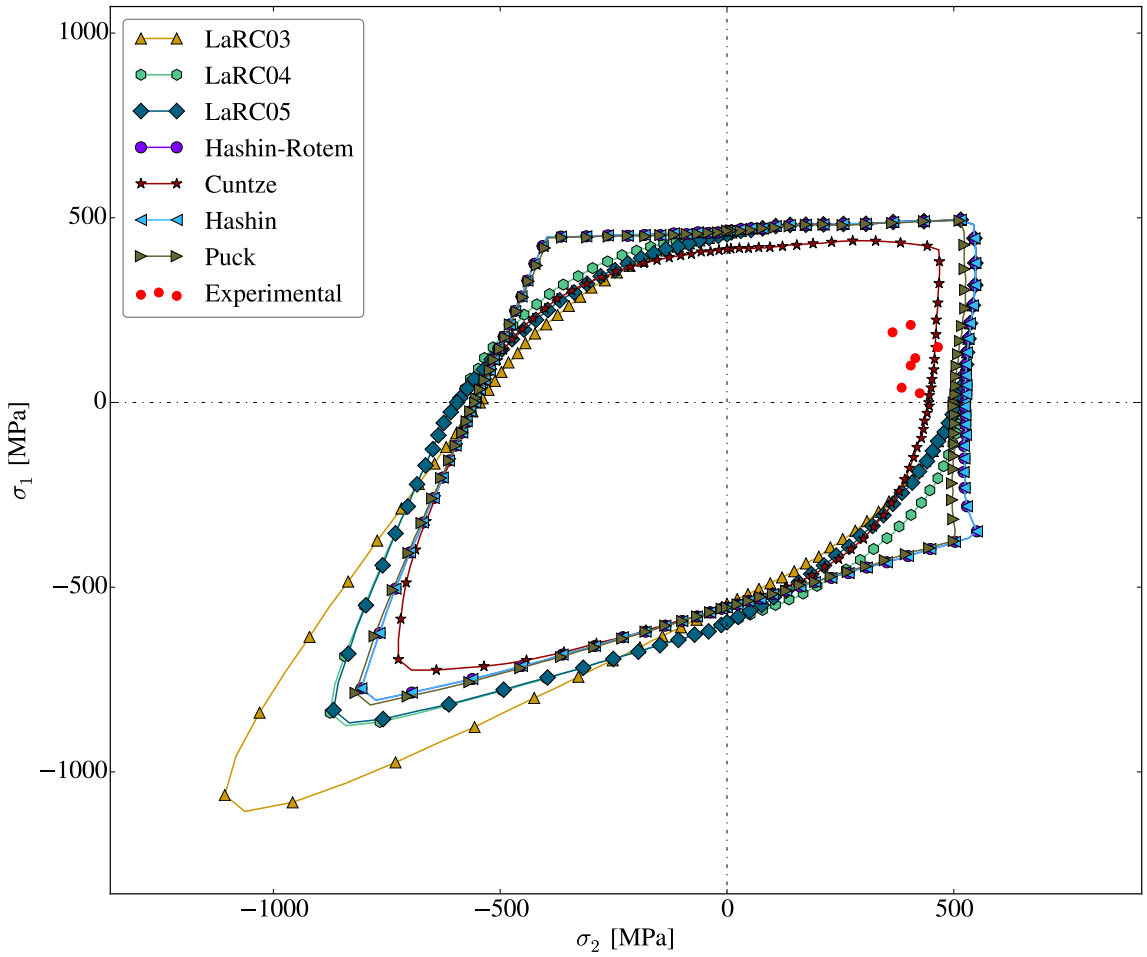

Figure 5.5: Initial failure envelope (σ_2, σ_1) of symmetric $0°/\pm 45°/90°)_s$ AS4/3501−6 laminate (Test case 6)

5.2.5 Test case 9

Notable is the significant discrepancy with respect to experimental data, see Figure 5.6. For the angle ply featured therein, where each ply experiences equal stress exposure, none of the theories performs well. This highlights the deficiencies that even state-of-the-art stress-strain based models feature. Moreover, for the case of equal stress exposure, the proposed mechanism of material degradation (featured in all propagation models) does not work since stress cannot be redistributed by a decrease in stiffness. Consequently, angle plies form a difficult case for the models under evaluation.

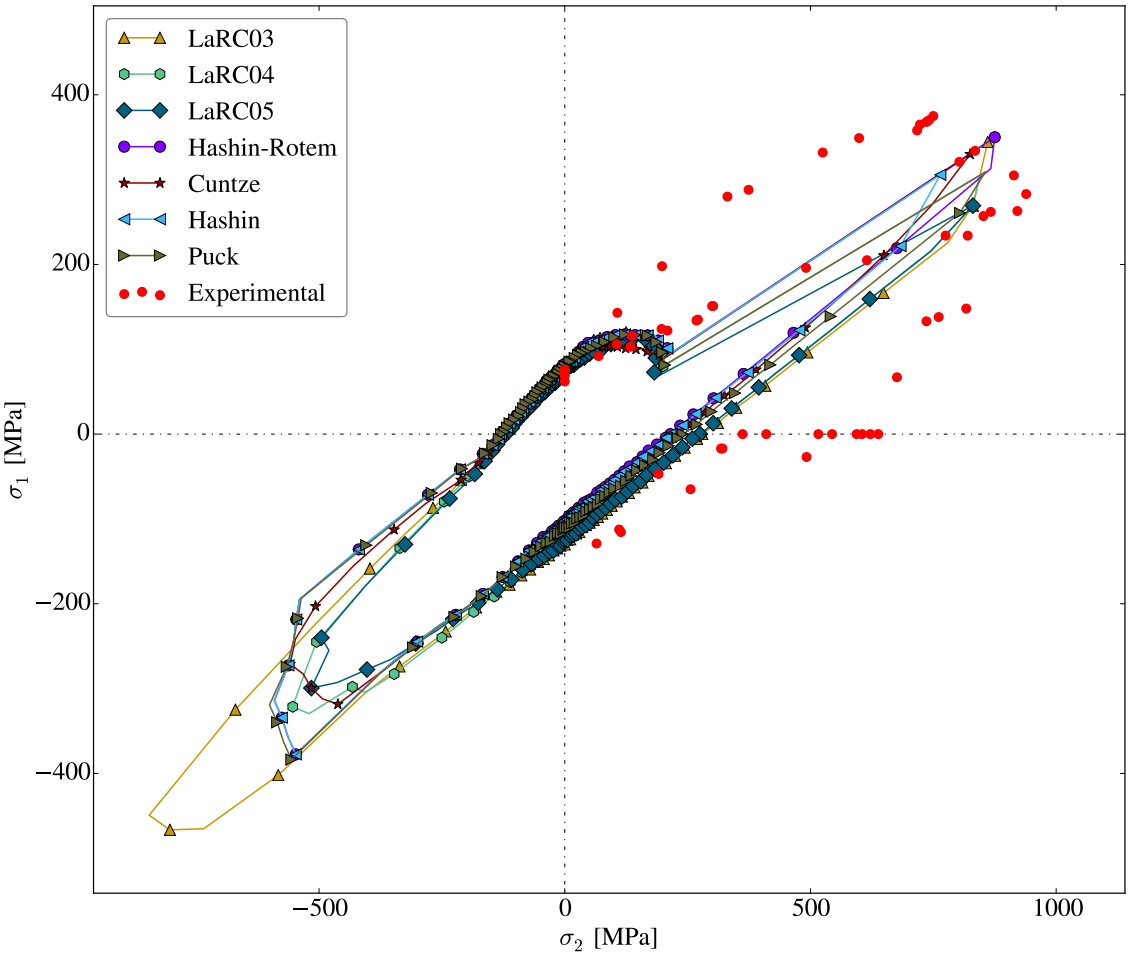

Figure 5.6: Initial failure envelope (σ_2, σ_1) of $\pm 55^\circ$ angle ply E-glass/MY750 laminate (Test case 9)

5.2.6 Total score

The analysis results in terms of predictive accuracy and computational effort are discussed subsequently hereafter. Once these scores are attained, qualitative considerations can be made in the next section in order to make a final judgment on the quality of initiation criteria.

Predictive accuracy

The predictive accuracy as scored in Table 5.1 is obtained for each of the models, both test case specific and average. From these results and the failure envelopes, it can be inferred that relative differences between criteria are not always easily observable. Moreover, the quality of the experimental data can be questioned. Particularly in view of the limited quantity thereof, comparison is a challenge.

From the results, it is readily apparent that the Cuntze model is one of the best-performing criteria when it comes to predictive accuracy, even with the empirical parameters thereof being

estimated in a simplistic manner. Nigh on par are the physically based Puck and LaRC criteria, whereas Hashin and Hashin-Rotem criteria offer significantly less predictive accuracy.

Table 5.1: Initiation model ranking in terms of predictive accuracy (qualitative indications of score: green = good (A-B) ; yellow = intermediate (C) ; red = poor (D-E))

Model	Test case					
	1	2	3	6	9	Average
LaRC03	C	D	C	C	D	C
LaRC04	B	E	C	C	D	C
LaRC05	B	E	C	C	D	C
Hashin-Rotem	E	D	C	C	D	D
Cuntze	D	B	B	B	D	B
Hashin	E	D	C	C	D	D
Puck	B	D	C	C	D	C

Computational effort

In terms of computational effort, see Figure 5.7, simplistic criteria perform better than the more physically advanced criteria. Puck and LaRC criteria take a physical approach and incur significant computational effort, particularly in the iterative determination of the fracture plane angle. In particular, the LaRC04 criterion that requires iterative determination of in-plane and out-of-plane kink angles as well as the misalignment angle incurs a significant amount of computational effort.

5.3 Trade-off initiation criteria

On the basis of the preliminary analysis results and qualitative considerations, the trade-off matrix of Table 5.2 is obtained. For each criterion, theories are listed with a number of theory-specific features that contribute to an overall score on the criterion. In likeness to the preliminary analysis results, scores are qualitative indications based on the relative performance of the various models. The aggregated scores are justified per model firstly. The section is concluded by listing the three top performing models.

5.3.1 Score justification

For each of the models considered, the score is determined by qualitative considerations based on model formulation and reference literature, and the quantitative results obtained previously from the preliminary analysis. A justification of the scores attributed to each criterion is given hereafter.

Hashin-Rotem

The earliest model to distinguish FF and MF, the Hashin-Rotem criteria offer little in terms of physical foundation. Moreover, the model is a two-dimensional formulation and hence can be expected to be of limited worth in three-dimensional loading cases. On the upside it is easily

implementable, does not require any additional parameters and is computationally extremely cheap.

The lack of physical foundation and simplistic basis show through in the results, showing significant discrepancy with respect to experimental data and moreover to other participating theories, other than the Hashin criteria. It is ranked low in terms of predictive accuracy. This is offset by a favourable rank in terms of computational effort, due to its simplicity. While few experimental parameters are required and the criterion is thereby versatile, a lack of three-dimensional capability results in a mediocre rank in terms of versatility. Overall, this implies a poor score for the Hashin-Rotem criteria. The Hashin-Rotem criteria are outperformed (in all aspects) by the similar, but more advanced, Hashin criteria.

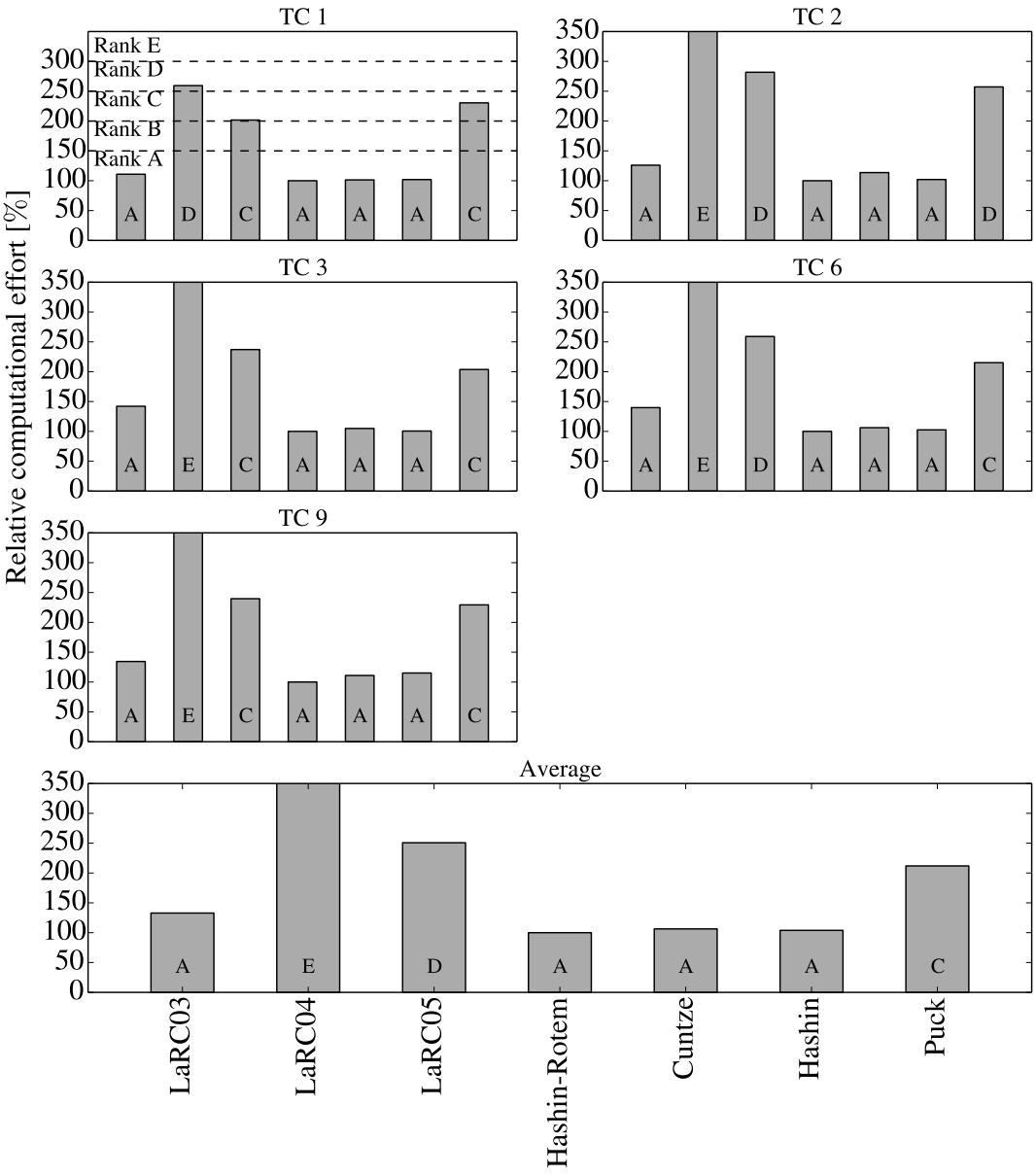

Figure 5.7: Measured relative computational effort for initiation criteria

Hashin

Hashin criteria offer a slightly more physical basis than Hashin-Rotem criteria and additional versatility in view of its three-dimensional formulation. For the rest, it offers much the same advantages and disadvantages as the Hashin-Rotem criteria. Three-dimensional performance offered is deemed decent, after implementations by Camanho and Matthews [53], Tserpes et al. [54] and Makris et al. [63] for three-dimensional loading cases.

When compared to other criteria (excluding Hashin-Rotem criteria), the Hashin criteria distinguish themselves in simplicity while still offering decent agreement to experimental results. These are considered driving forces for its continued use in practice, similar to the application of other simplistic (e.g. maximum stress and strain, Tsai-Hill, Tsai-Wu) criteria [39].

The fact that the Hashin-Rotem criteria are relatively poor in terms of predictive capability, as compared to more advanced criteria, underlies the importance of stepping away from these simplistic criteria towards more advanced criteria. In particular, it should be considered that Cuntze criteria perform significantly better even at comparable computational effort.

Cuntze

Cuntze criteria, based on a semi-empirical approach, are one of the top performing criteria. Whereas Puck and LaRC criteria turn towards a physical treatment of failure mechanisms, Cuntze takes a more empirical approach. A disadvantage thereof is the need for a number of empirical parameters, but even for uniform estimates the results show a good correspondence with experimental data. Moreover, the empirical approach is easily applied and accompanied by relatively little computational effort.

Cuntze offers one of the best performing theories in the preliminary analysis, at the forefront of all models considered - even the more physically based LaRC and Puck criteria. This aligns with results from the second Worldwide Failure Exercise, showing good correspondence in three-dimensional test cases [3]. Computational effort is on the same level of Hashin and Hashin-Rotem criteria. Overall, this leads to a high overall score for the Cuntze criteria, although slightly set back by the need for numerous empirical parameters and a limited physical basis.

Puck

As one of the first initiation criteria with a strong physical basis, Puck criteria offer a step forward from more simplistic Hashin-Rotem and Hashin criteria. Based on phenomenological observations and applications of the Mohr-Coulomb fracture hypothesis, a judicious treatment of MF is included. Drawback of this approach are the requirement of inclination parameters and the iterative determination of the fracture plane angle, resulting in additional computational effort.

The strong physical basis is deemed a sizeable contributor to the relatively good performance of Puck criteria in the preliminary analysis. On a similar basis, the second Worldwide Failure Exercise [3] showed remarkable capability of Puck criteria in predicting failure for three-dimensional cases. Overall, Puck displays good predictive accuracy and versatility without excessive computational effort.

LaRC03

Following up on Puck's work, LaRC criteria continued on the physical basis of the Mohr-Coulomb fracture hypothesis and extended this with a detailed treatment of FFC. The earliest installment, LaRC03, is similar to Puck's criteria and many of the same characteristics apply. It suffers, however, from a flaw in the formulation leading to an overestimation of friction stresses and is moreover limited to two-dimensional application.

Test cases reflect a slightly diminished predictive accuracy as compared to Puck, although computational effort is slightly lower as well. Following installments, particularly LaRC05, perform better and are more versatile.

LaRC04

The extension of LaRC03 to three dimensions and a slightly different approach to FFC brought LaRC04. The adaptations are accompanied by additional computational effort, also in terms of implementation.

Overall predictive capability of the criteria is decent. Computational effort is deemed excessive, however. In all aspect, LaRC05 is an improvement over LaRC04.

LaRC05

The state-of-the-art culmination of LaRC criteria is captured by LaRC05. A strong physical basis underlies its performance, leading to a good predictive capability. In particular, the second Worldwide Failure Exercise [3] showed good predictive capability for three-dimensional cases.

Moreover, computational effort is less than for LaRC04 and lies close to the computational effort for Puck's criteria. Overall, Puck and LaRC05 criteria show a large number of similarities and this shows through in the ranking attributed to these models.

5.3.2 Trade-off outcome

The total outcome, captured in Table 5.2, yields Cuntze, Puck and LaRC05 as top-performing initiation criteria. Overall, these criteria score well in all categories considered. Moreover, the criteria reflect the state-of-the-art well in the sense that advanced empirical criteria, namely Cuntze, are featured as well as advanced physically based criteria, namely Puck and LaRC05.

Still, in spite of these criteria performing relatively the best, discrepancies with respect to experimental data were observed to be appreciable. Even the state-of-the-art models do not capture all experimentally observed phenomena, although it should be noted that experimental data is prone to flaws and any comparison thereto is to be done with caution. Even so, the general conclusions are supported by the Worldwide Failure Exercises [2, 3].

Table 5.2: Trade-off matrix initiation criteria (qualitative indications of score: green = good (A-B) ; yellow = intermediate (C) ; red = poor (D-E)).

Model	Predictive accuracy (50%)	Computational effort (25%)	Versatility (25%)	Aggregated
Hashin-Rotem	(D) Poor performance test cases (D) Limited physical basis	(A) Low computational cost (A) Easy implementation	(A) Few empirical parameters (E) Limited to 2D	(D)
Hashin	(D) Poor performance test cases (C) Reported decent 3D performance (D) Limited physical basis	(A) Low computational cost (A) Easy implementation	(A) Few empirical parameters	(C)
Cuntze	(B) Good performance test cases (A) Reported good 3D performance (D) Limited physical basis	(A) Low computational cost (A) Easy implementation	(C) Numerous empirical parameters	(B)
Puck	(C) Decent performance test cases (A) Reported good 3D performance (B) Strong physical basis	(C) Intermediate computational cost (B) Straightforward implementation	(B) Few empirical parameters	(B)
LaRC03	(C) Decent performance test cases (C) Strong, but partially faulty physical basis	(A) Low computational cost (B) Straightforward implementation	(B) Few empirical parameters (E) Limited to 2D	(C)
LaRC04	(C) Decent performance test cases (B) Strong physical basis	(E) High computational cost (D) Arduous implementation	(B) Few empirical parameters	(C)
LaRC05	(C) Decent performance test cases (A) Reported good 3D performance (B) Strong physical basis	(D) Large computational cost (B) Straightforward implementation	(B) Few empirical parameters	(B)

5.4 Analysis results for propagation models

Analysis results for propagation models are listed subsequently per test case, in the form of failure envelopes accompanied by a discussion. At the end of the section, results are collected and translated into a score for each of the propagation models, both in terms of predictive accuracy and computational effort. Since propagation models form a separate component of the PDA procedure, evaluation for a single initiation model is performed. To this end, the Cuntze criteria (as best performing criteria) are taken and combined with propagation models.

5.4.1 Test case 4

Results from the fourth test case, see Figure 5.8 indicate a decent predictive capability of the models. However, particularly in biaxial compression, results are off. The limited quantity of data therein, as well as the possibility of buckling as is the case for test case 6, complicates any judgment thereon. Sudden MDMs give similar results, as does the Puck criterion, whereas bilinear softening models are more conservative. For the bilinear softening model, a ratio of 4 gives arguably the best correspondence to experimental results.

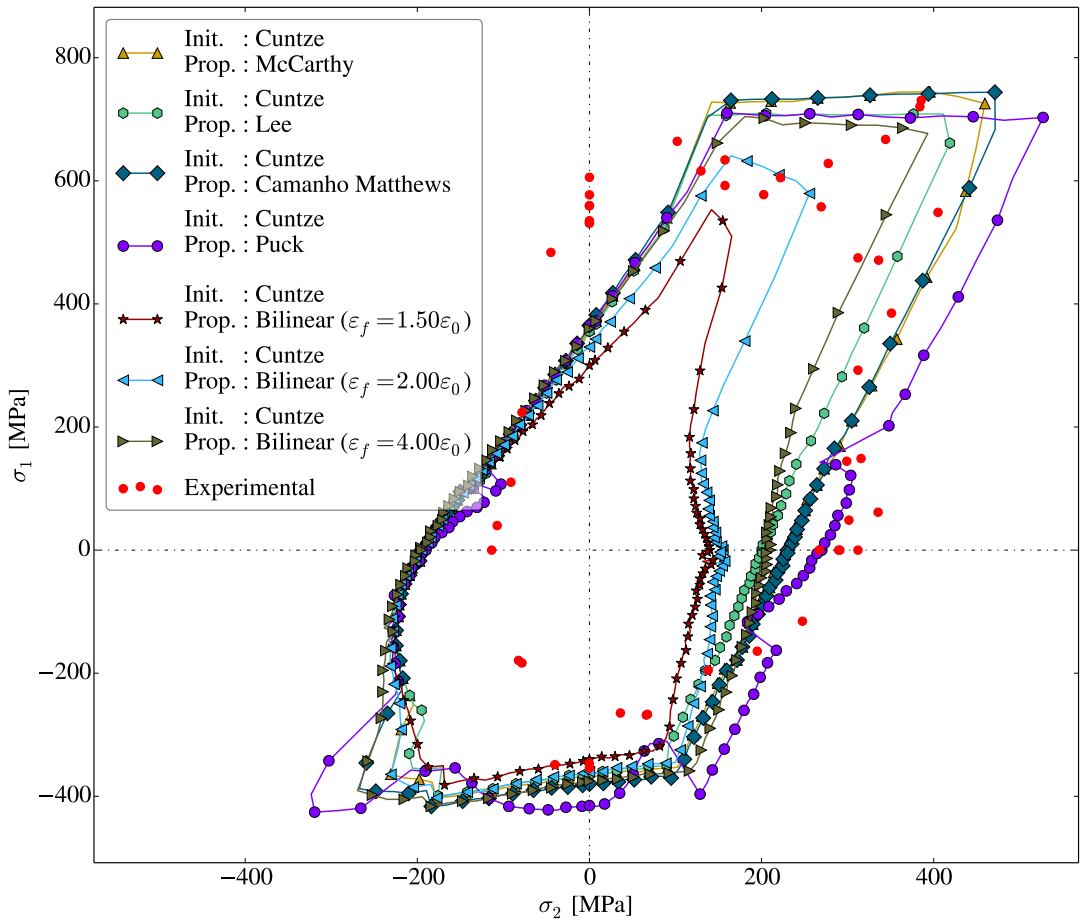

Figure 5.8: Final failure envelope (σ_2, σ_1) of symmetric $(90°/\pm 30°/90°)$ E-Glass/LY556 laminate (Test case 4)

5.4.2 Test case 5

For the fifth test case, see Figure 5.9, correspondence is similarly decent. For combined longitudinal compression and shear, discrepancies are appreciable however. The least conservative is the Camanho Matthews sudden MDM, although it is in decent correspondence to experimental results. Again, the bilinear softening model with the lowest ratio yields the worst correspondence. The remainder of propagation models gives comparable results, as was the case for the fourth test case.

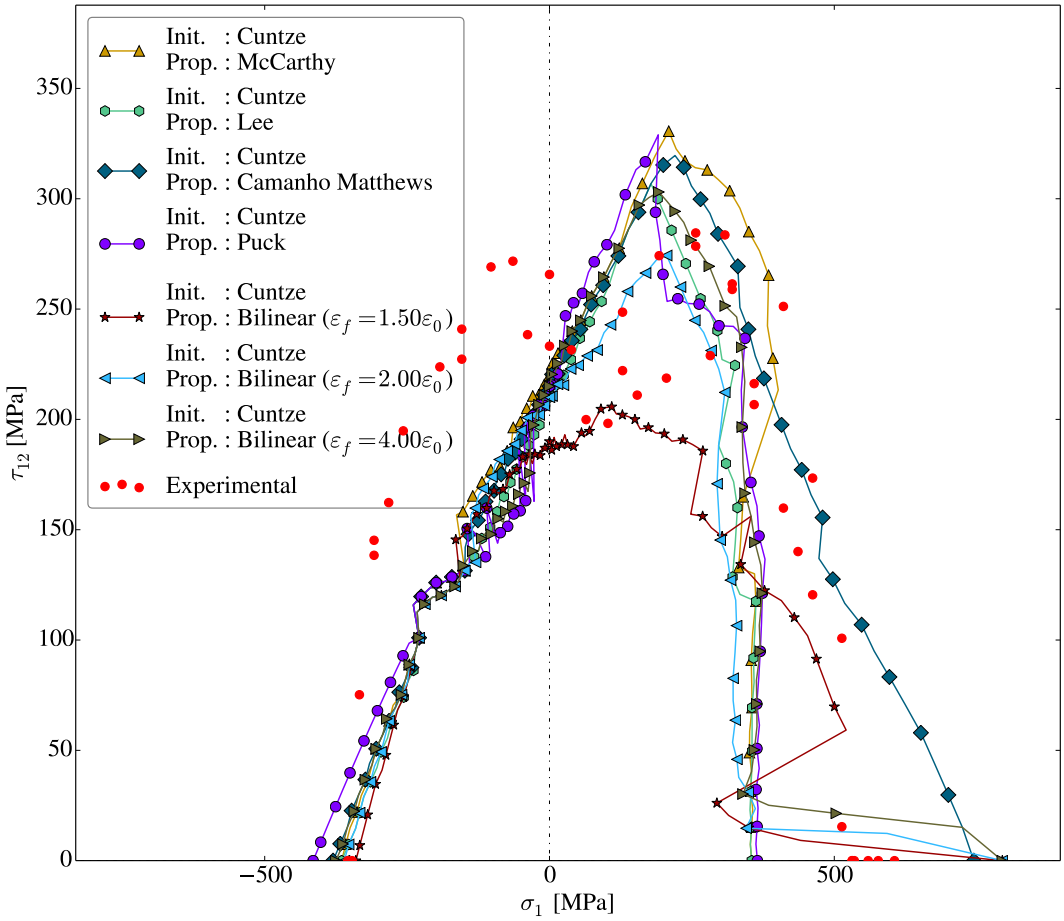

Figure 5.9: Final failure envelope (σ_1, τ_{12}) of symmetric $(90°/\pm 30°/90°)$ E-Glass/LY556 laminate (Test case 5)

5.4.3 Test case 6

Overall good correspondence is achieved, see Figure 5.10. The discrepancy in the biaxial compression region is dedicated to buckling, not considered in any of the failure models. Since initial failure occurs in FFC for most of the envelope, only the biaxial tension quadrant shows differences in propagation models, although these are only pronounced for the bilinear softening model with the highest ratio of failure to onset strain. Comparable results are obtained overall, with few distinguishing features.

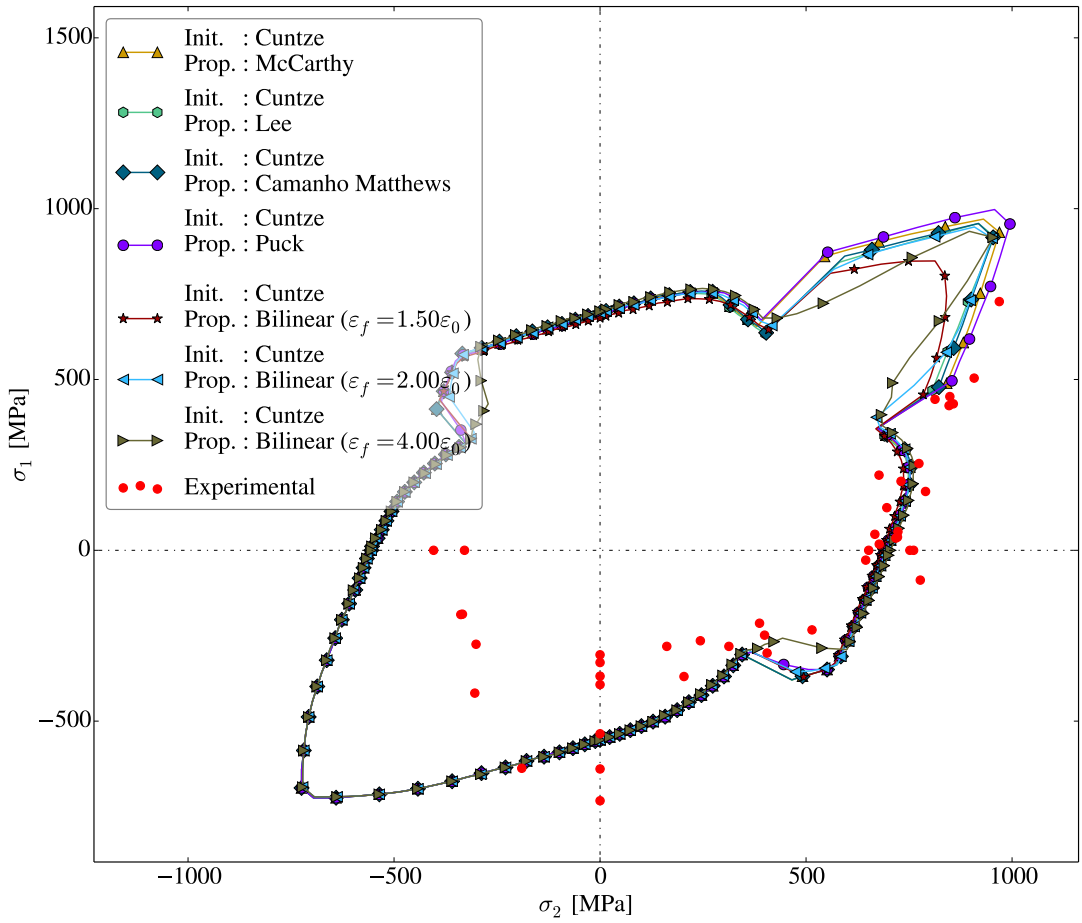

Figure 5.10: Final failure envelope (σ_2, σ_1) of symmetric $0°/\pm 45°/90°)_s$ AS4/3501−6 laminate (Test case 6)

5.4.4 Total score

Total scores for each of the propagation models featured are given hereafter. Firstly, predictive accuracy is discussed. Thereafter, computational effort is evaluated.

Predictive accuracy

Scores for each of the test cases in terms of predictive accuracy, and an overall average score, are given in Table 5.3. Notable is an overall agreement of the various propagation models in all of the test cases considered, offering little basis for distinction in this sense. Underlying explanation can be found in the fact that all models consider propagation as a stiffness degradation and do so in a similar manner, although the precise degradation coefficients differ from model to model. Differences are thus small, however, that differences are altogether not too pronounced. In a local analysis, significantly more damage events occur with ensuing stiffness degradation which will likely lead to larger differences between models.

Table 5.3: Propagation model ranking in terms of predictive accuracy (qualitative indications of score: green = good (A-B) ; yellow = intermediate (C) ; red = poor (D-E))

Model	Test case			
	4	5	6	Average
McCarthy	C	D	B	C
Lee	C	D	B	C
Camanho Matthews	C	C	B	C
Puck	C	D	B	C
Bilinear	C	D	B	C

Computational effort

In terms of computational effort, see Figure 5.11, differences are relatively small. As one would expect, Puck propagation is most computationally expensive since it entails multiple iterations per stress increment in order to degrade properties judiciously as per its formulation.

5.5 Trade-off propagation models

Based on the analysis results and qualitative considerations, Table 5.4 presents the final trade-off matrix. The scores herein are firstly justified in this section, followed upon by a final selection of initiation and propagation models.

5.5.1 Score justification

The score for the various propagation models is justified hereafter. In view of the inconclusiveness of analysis results, the justification is mostly based on qualitative considerations.

Lee

The total ply discount method of Lee poses a simplistic representation of failure mechanisms. The total ply discount is deemed unrealistic in view of residual stiffnesses observed experimentally [13].

A notable deficiency of all sudden MDMs is the potential for numerical instability [64] and mesh dependency [9, 12], since damage is applied instantaneously and locally. Smearing the damage, as in the bilinear softening model, will alleviate the mesh dependency to a certain degree, while a gradual degradation, as for bilinear softening and Puck's model, will reduce numerical instability.

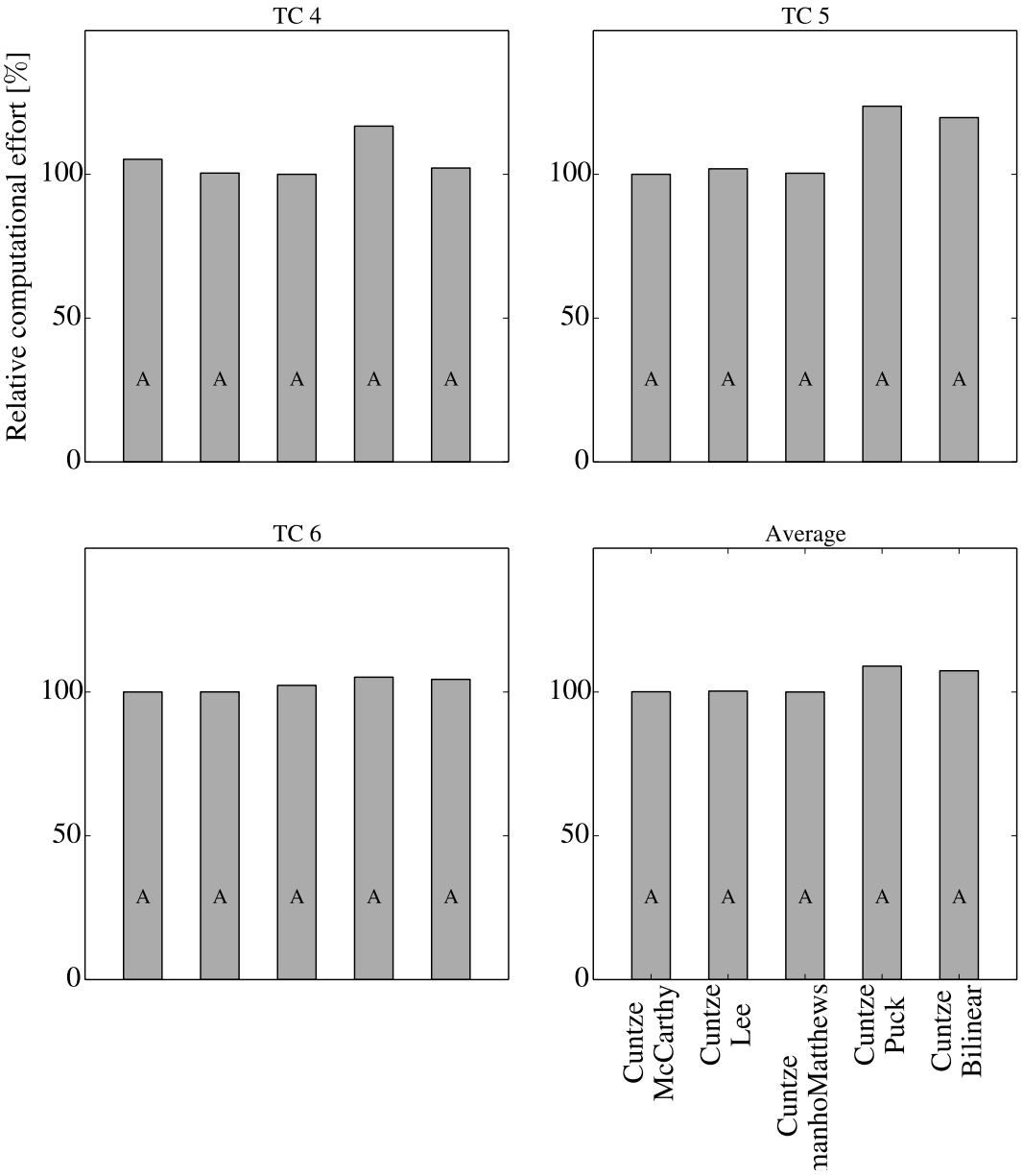

Figure 5.11: Measured relative computational effort for propagation models

McCarthy

Much the same reasoning as for the Lee model applies to the model by McCarthy et al. However, the McCarthy model is less conservative and does not degrade properties to zero, but rather assumes residual stiffnesses (with little of a physical derivation). This is deemed more realistic, but results are still in close correspondence to the Lee model for the test cases evaluated. The absence of G_{12} degradation for MF and FFC is deemed unrealistic. E_1 degradation for MF is not in line with the other models and questionable, since for MF the fibres do not necessarily lose their load-carrying capability.

Camanho Matthews

Again, this model suffers from the shortcomings of sudden MDMs discussed before. The model differs from the other two sudden MDMs in the sense that residual stiffnesses are assumed larger. A shortcoming in the formulation is deemed the absence of any G_{12} and other matrix-related property degradation rules for FF.

Puck

The Puck model degrades properties iteratively. A disadvantage lies in the resulting increased computational effort. While this effort increase is not immediately obvious from analysis results, for FEM the increase in computational effort will be more prohibitive in view of the time taken to calculate the stress state at each stress increment. Moreover, the degradation does not follow from a strong physical basis.

Bilinear softening

The bilinear softening model displayed good correspondence, on par with the other models, for a ratio of failure to onset strain between 2.0 and 4.0. This illustrates that, with a proper selection of fracture toughness for each of the failure modes, good correspondence can be achieved. Moreover, the crack smearing approach alleviates mesh dependency whereas this is unadressed in the other propagation models.

Disadvantageous is the requirement for additional experimental parameters, in this case the fracture energy for each of the failure modes. Although methods are in place for determination thereof [12], these are not standardized.

5.5.2 Trade-off outcome

It is readily apparent from Table 5.4 that the test cases have yielded little preference for any of the models. Rather, differences exist in the formulation of the methods and qualitative considerations based thereupon. In particular, mesh dependency and numerical instability alleviation in the bilinear softening model is a key consideration. The other MDMs offer potential difficulties in mesh dependency and numerical stability and are discounted as such. Although convergence issues can be alleviated to some extent, by for example viscous regularization, this introduces a slight loss of predictive accuracy.

Consequently, there is a clear preference for the bilinear softening model. Insofar as the other models go, the Camanho Matthews and McCarthy models are chosen since these offer a different perspective to sudden degradation, without the implementation and computation effort associated with the Puck degradation. The Lee MDM is seen as overly conservative and thereby not selected for further analysis.

In any case, it is not a straightforward choice and this is inherently complicated by the fact that none of the models show a clear physical basis or realistic representation of failure. Rather, these are tools formulated for practicality in the absence of a more detailed understanding of the underlying failure mechanisms.

5.6 Model selection

Overall, the model selection yields the following:

- Analysis results and qualitative considerations offer a clear preference for Cuntze, Puck and LaRC05 criteria.
- No clear preference can be given to the propagation models, although the bilinear softening law offers good characteristics in terms of numerical instability and mesh dependency. McCarthy and Camanho Matthews offer two different perspectives on sudden MDM without the effort associated with the iterative Puck degradation.
- To review a palette of methods, the similar Puck and LaRC05 initiation criteria are coupled to respectively McCarthy and bilinear softening models. The Cuntze model is applied in conjunction with Camanho Matthews degradation. This yields two strongly differing propagation models for the similar Puck and LaRC05 criteria, yielding a broad array of damage models.

5.7 Conclusions and recommendations

Through a preliminary two-dimensional analysis using CLT on a series of test cases taken from the first Worldwide Failure Exercise, an attempt has been made to objectively compare state-of-the-art initiation criteria and propagation models. Coupled with qualitative considerations on the method formulation, this trade-off has yielded three stress-strain based models.

Well-performing criteria are the Cuntze, Puck and LaRC05 criteria. The latter offer a relatively strong physical basis, whereas the former displays remarkable accuracy using a more empirical approach. Less well-performing are the simpler Hashin and Hashin-Rotem criteria and the LaRC03 and LaRC04 criteria, that are surpassed by their successor LaRC05.

Propagation models are much more difficult to distinguish, since these are mostly simplistic propositions that do not reflect the physical mechanisms in a failure process and perform comparably in the selected test cases. Rather, the choice is guided by numerical considerations. A key consideration is the alleviation of mesh dependency and mitigation of numerical instability for the bilinear softening model as a redeeming feature. From the remainder of the models, McCarthy and Camanho Matthews sudden MDMs are selected.

Overall, this analysis highlights the key difficulties associated with PDA of FRPs using state-of-the-art approaches. Results are highly case-dependent and errors are significant over the entire range of models considered. Any choice between these models is made substantially more difficult by the dependency of composite behaviour on a range of parameters.

The main recommendation in this context is to address trade-off limitations. Primarily, this is to be done by a more varied set of test cases, two- and three-dimensional and an investigation on the local behaviour of composites. Moreover, recent models featured in the third Worldwide Failure Exercise [61] may offer better alternatives when these have been fully developed. This recommendation is partly fulfilled by the ongoing Worldwide Failure Exercise series, forming a valuable learning experience for practicioners of damage modelling of FRPs.

Table 5.4: Trade-off matrix propagation models (qualitative indications of score: green = good (A-B) ; yellow = intermediate (C) ; red = poor (D-E)).

Model	Predictive accuracy (50%)	Computational effort (25%)	Versatility (25%)	Aggregated
Lee	(C) Decent performance test cases (D) Total ply discount unrealistic	(A) Low computational cost (A) Easy implementation	(A) No additional parameters	(C)
McCarthy	(C) Decent performance test cases (C) Absence of G_{12} degradation for MF, FFC (C) E_1 degradation for MF	(A) Low computational cost (A) Easy implementation	(A) No additional parameters	(C)
Camanho Matthews	(C) Decent performance test cases (C) Absence of G_{12} degradation for FF	(A) Low computational cost (A) Easy implementation	(A) No additional parameters	C)
Puck	(C) Decent performance test cases (C) FF seen as catastrophic	(A) Low computational cost (D) Cost disadvantage estimated significantly higher in FEM (C) Challenging implementation	(A) No additional parameters	(C)
Bilinear softening	(C) Decent performance test cases (A) Crack smearing alleviates mesh dependency	(A) Low computational cost (C) Challenging implementation (B) Gradual degradation reduces risk numerical instability	(C) Fracture energies	(B)

Chapter 6

Finite Element implementation of stress-strain based damage modelling

To take full advantage of the predictive capability offered by the theories discussed and selected in the previous chapters, a PDA routine is implemented in Abaqus. FEM implementation offers a versatile and accurate means of analysing structural components, and it is well-established amongst academia and industry alike [7].

This Chapter commences with a brief discussion on the structural definition of FRPs, followed upon by listing a number of numerical considerations specific to PDA of FRPs in FEM. In view of the computational effort associated with the procedure, some efficient modelling approaches are thereafter discussed. Section 6.3 discusses implementation of the PDA routine in an UMAT in ABAQUS. The implementations are assessed by comparison to a number of experimental campaigns and previous modelling approaches from available literature in Section 6.4. Lastly, conclusions and recommendations are given.

Contents

6.1 Structural definition

A structural definition of composites in FEM encompasses both taking into account correctly material heterogeneity and anisotropy and a proper element selection. An overview of the possibilities in a FEM representation of composites is given in Figure 6.1. These are discussed subsequently in ensuing subsections, firstly laminate definitions and secondly element types.

6.1.1 Laminate material definitions

Two laminate material definitions apply to FEM implementations, namely Equivalent Single Layer (ESL) or Layer-wise (LW) approaches [13, 65]. The consequences of each definition extends to the choice of elements and affects accuracy of results significantly [13].

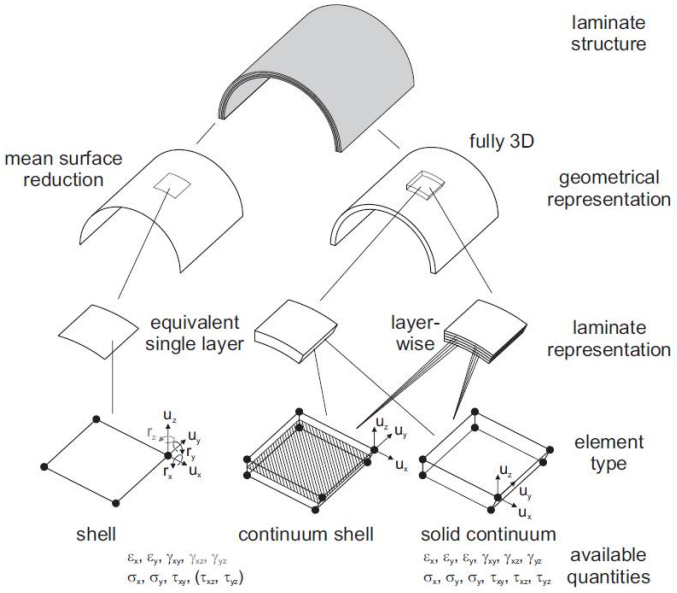

Figure 6.1: Laminate FEM representation possibilities, from [13, p.31]

Selection of a representation is constrained by the discontinuities in stress and displacement fields. Under the assumption of perfect bonding, in-plane displacements and strains are required to be continuous. Stresses can be discontinuous due to varying stiffness. Interlaminar shear stresses will develop which must be continuous, leading to the requirement of a continuous slope of the out-of-plane normal stress [13].

Equivalent single layer

In this approach, a laminate is homogenized into a single material, thereby allowing an entire laminate to be interpreted with one through-thickness element. Consequently, through-thickness behaviour is not accurately represented [13]. Additionally, strain and stress continuity is not satisfied at layer interfaces, particularly problematic in the case of thick laminates [66]. This approach offers low computational effort in view of a limited number of degrees of freedom[13, 66]. Some of the disadvantages of low resolution in out-of-plane direction can be tackled by adopting higher-order shear deformation theories or the addition of integration points in this direction [13]. Examples of application show that decent results can be obtained [8, 34, 52, 54, 67].

Generally, ESL modelling is limited to global laminate responses [13]. For the case of PDA, the ESL approach can be seen as insufficient particularly when considering DLs. These occur interply and thereby it is key to model the interface between layers.

Layer-wise

Contrary to the ESL approach, each ply is modelled separately with a separate displacement field. Strain continuity is enforced by constraint equations at interfaces [66]. Thereby laminate behaviour is geometrically, rather than materially, defined [13]. This explicitly accounts for laminate heterogeneity and allows a more accurate representation of transverse (stress and displacement) components and interlaminar stresses. The LW has therefore found repeated application in especially three-dimensional PDA implementations [9, 11, 13, 15, 46, 53]. In general

the LW approach is more computationally expensive, but offers increased benefits in terms of accuracy [13, 65, 66].

The LW approach is generally more suitable for PDA, since it respects heterogeneity of the laminate cross-section and thereby incorporates ply-by-ply failure and interply failure mechanisms. In addition, it can be tailored to a more accurate through-thickness representation for three-dimensional modelling. Still, the trade-off between accuracy and computational effort for ESL and LW depends on the specific case evaluated.

6.1.2 Element types

A number of element families can be considered, of which the ones most applicable to the representation of composite laminates are discussed. These families offer a differing degree of accuracy and computational effort, thereby making this a key consideration for any FEM implementation of PDA.

Shell elements

For structures with a small thickness relative to in-plane dimensions, shell elements can be applied. The modelling of these structures as two-dimensional planes is beneficial in terms of computational effort, but is limited to the in-plane stress components. As a consequence of the latter, restrictions on strains at the interfaces are not respected by these elements. Implementation of these elements is thereby limited to the ESL approach [13, 65].

Continuum shell elements

Continuum shell elements form an extension of conventional shell elements, allowing them to be stacked in a LW approach [13]. These offer a three-dimensional representation, albeit with lower accuracy than solid continuum elements [13, 65]. Advantageous, with respect to the latter, is a relaxed requirement on the aspect ratio of in-plane dimensions with respect to thickness.

Solid continuum elements

A full three-dimensional implementation is possible by use of solid continuum elements, free of assumptions on field variables and considering out-of-plane stress components. Computational cost is, however, higher, due to the increased number of nodes and associated degrees of freedom [13]. Furthermore, these elements face an issue regarding their aspect ratio. A cubic shape is preferred but in view of relatively small ply thickness, this would require excessively fine meshing. Consequently, adoption of these elements will incur a loss of accuracy due to an overstiffness. A solution to this problem is the use of reduced integration elements, counterbalancing this overstiffness and moreover reducing computational effort [53], albeit with the requirement of an hourglass stiffness and accompanying risk of hourglassing [65].

An additional consideration is a local-global approach, modelling with solid elements only in the vicinity of high-stress regions. This offers improved efficiency as compared to modelling the entire structure using solid elements. This does, however, come with limitations as the boundaries of these regions need to comply with boundary conditions implied by the two-dimensional (shell) global model [65, 68].

6.2 Numerical considerations

This section outlines some complicating factors and counteracting measures for implementation of PDA in FEM. As such, it encompasses a brief synopsis of implicit versus explicit analyses, localization and convergence, symmetry, load stepping and meshing.

6.2.1 Implicit versus explicit

In the present context, PDA is performed by incrementing load quasi-statically over a number of (pseudo) time increments. Within each time increment, damage initiation is checked with damage criteria and propagation is handled by appropriate propagation models. Stepping in time can be done either explicitly or implicitly, in Abaqus handled by respectively Abaqus/Explicit and Abaqus/Standard [64].

An explicit procedure is characterized by the fact that for each time increment, field variables depend solely on the information present at the previous time step. For an implicit procedure, on the other hand, this is not the case and each time increment is handled by an iterative procedure (e.g. Newmark Forward Differencing).

Consequently, a number of differences arise. Whereas implicit analyses are unconditionally stable, explicit analyses are conditionally stable (the critical step size being determined by the largest natural frequency of the structure analysed). To avoid instability, explicit analyses generally require a smaller time step. On the other hand, implicit analyses suffer from convergence problems to a greater extent than explicit analyses. This may require a decrease in time step, overall yielding no preference for either explicit or implicit analyses in this regard [13].

In addition, results for an explicit analysis depend directly on the tangent moduli provided at the start of each increment, used as the sole basis for determination of variables at the next time increment. For an implicit analysis, the quality of the moduli (in the form of the Jacobian) affects the convergence behaviour. Solution quality remains unaffected since equilibrium equations are handled iteratively to alleviate any deficiencies in the moduli. As such, an implicit procedure is less sensitive to errors in the definition of a material [13, 64]. This is particularly relevant for the case at hand, where a user-defined material is introduced.

Overall, each analysis type has its advantages and disadvantages and there is no clear winner. Although choosing an explicit procedure in the case at hand would alleviate convergence difficulties, an implicit procedure is selected for the following reasons. Firstly, it leads to less stringent requirements on the subroutine used to define material constitutive behaviour. Secondly, step size is automatically kept in check in order to ensure convergence. Lastly, in view of blending, extension by XFEM is currently only available in Abaqus/Standard.

In general, the PDA routine can straightforwardly be transferred from an implicit to an explicit definition. This change would merely require a definition of tangential stiffnesses in the user-defined material and an omission of the Jacobian definition for each time increment. The general procedure remains unchanged.

6.2.2 Damage localization

An issue with many of the proposed models, is a mesh dependence due to the localization of damage [57]. A means to counteract this is the crack band method, or crack smearing, to prevent energy dissipation from vanishing for increasingly fine meshing through adapting the local stress-strain behaviour [11]. The method used in practice is almost exclusively that proposed by

Bažant and Oh [56], explained in the context of the bilinear softening model. By introduction of the element characteristic length, damage progression becomes independent of mesh fineness as confirmed by past implementations [9, 11, 12, 34, 57].

The characteristic length in the bilinear softening relation is taken as the square root of the in-plane area associated with an integration point [9], although more advanced measures based specifically on the direction of crack advancement are also envisioned [12]. For solid elements, Abaqus returns a characteristic length estimate as the cubic root of the volume associated with each integration point [55]. Without correction, this would imply a restrictively small characteristic length for elements with a large ratio of in-plane to out-of-plane dimensions. Consequently, degradation would be too lenient. To correct for this, the three-dimensional characteristic length is corrected by the ply thickness as follows

$$L \rightarrow \sqrt{\frac{L^3}{t}} \tag{6.1}$$

since Abaqus returns the characteristic length as

$$L = \sqrt[3]{V} \tag{6.2}$$

for volume V whereas the required characteristic length is

$$L = \sqrt{A} = \sqrt{\frac{V}{t}} \tag{6.3}$$

This mitigates errors induced in the bilinear softening curve by a rough mesh, without requiring any adaptations in input. This issue could be circumvented altogether if displacements were readily available in the subroutine rather than strains, since no length parameter would then be explicitly required in the propagation model.

6.2.3 Convergence issues

Use of an implicit procedure is generally accompanied by convergence issues [64]. These are particularly pronounced for PDA, where damage leads to changes in material constitutive behaviour (i.e. a stiffness reduction). These abrupt changes can cause difficulties in the re-establishment of equilibrium in subsequent timesteps, requiring small time steps to be taken to minimize the size of these discontinuities [11].

To alleviate these convergence issues and thereby avoid having to set time steps excessively small, viscous regularization can be employed [9, 11, 34]. An artificial viscosity η is introduced in the softening behaviour, increasing the energy dissipated with damage evolution. In the form of Duvault and Lions viscosity [9, 34], the evolution of a general damage parameter d (ranging from 0 for a fully pristine material, to 1 for a fully damaged material) is governed by η as [9, 34]

$$\dot{d_v} = \frac{1}{\eta}(d - d_v) \tag{6.4}$$

with d_v the regularized damage variable. This can be worked out in a practical form when stepping from time step i to $i+1$ over time increment Δt as

$$d_{v,i+1} = \frac{\eta}{\eta + \Delta t} d_{v,i} + \frac{\Delta t}{\eta + \Delta t} d_{i+1} \tag{6.5}$$

To illustrate, the evolution of a damage parameter from 0 to 1 is shown in Figure 6.2 for a number of viscosities and time steps. It is readily apparent that an increasing viscosity effects a more gradual transition in damage variable, which will benefit convergence.

A disadvantage of this approach is that the viscosity is artificial, leading to an artificial increase in energy dissipated. To this end, it is generally recommended to keep the viscosity parameter as small as possible to retain solution quality [9]. While this is definitely true for physically based degradation, this holds to a lesser extent for particularly the sudden MDMs. Since these are not physically based and an instantaneous degradation is irrealistic, the introduction of artificial viscosity poses less of an issue. This is particularly important considering that these MDMs are likely to need the highest artificial viscosity to cope with the steep degradation of properties.

An alternative to viscous regularization would be a gradient method [69], although these have not been applied to PDA due to the large effort and fine mesh associated with implementation [57]. As noted before, use of an explicit method would obviate the need for these methods altogether (at the expense of other factors).

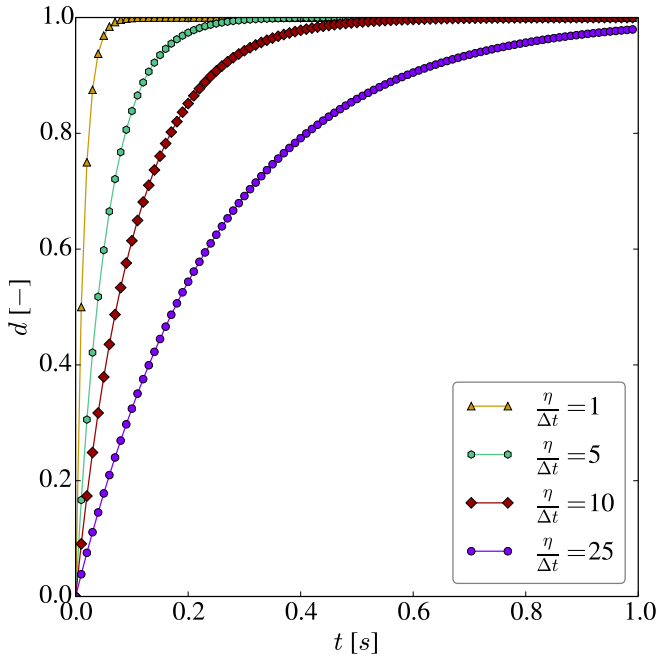

Figure 6.2: Illustration of the effect of Duvault and Lions viscosity on the evolution of a damage variable ($\Delta t = 10^{-2}$ [s])

6.2.4 Symmetry

Symmetry allows a reduction in the number of integration points and equations to be solved. Proper use entails taking into account symmetry of material, loading and geometry. All specimens featured are rectangular plates including a centered hole, loaded symmetrically at the ends. In terms of geometry and loading, this allows modelling only a quarter of the in-plane dimensions to represent the full specimen.

However, when plies are at an angle (perpendicular nor parallel to the main loading direction), this symmetry does not extend to the material. Applying symmetry in such a case would imply

mirroring the ply angles about the symmetry axis. The discontinuity in fiber orientation at the symmetry plane would then incur additional stress concentrations.

Therefore, only a quarter of the in-plane dimensions can be modelled when there are no such plies in the laminate or when the prospective symmetry axis is not critical in damage. In all cases, with a symmetric lay-up and uniformly applied loading, through-thickness symmetry can be used.

6.2.5 Load stepping

For accurate prediction of damage, a small time step is necessary to propagate damage to adjacent elements. This only applies, however, to the portion of loading beyond initial failure. Before initial failure, key interest lies in obtaining a good stress representation for which a much larger time step is acceptable.

To this end, a variable amplitude loading is implemented that rapidly applies the loading up to initial failure (which is estimated from a trial run) and thereafter is applied more gradually, such that for the entire sequence the same small time step can be used. Using this methodology, an excessively large number of steps before initial failure can be omitted and computational effort is significantly lowered.

To illustrate, Figure 6.3 shows the variable amplitude loading. For a uniform time step, it is readily apparent that the steep initial portion up to initial failure can now be evaluated much less expensively. Duly note that, for the cases at hand, the first portion is significantly steeper than depicted in Figure 6.3 to take maximum advantage of this consideration.

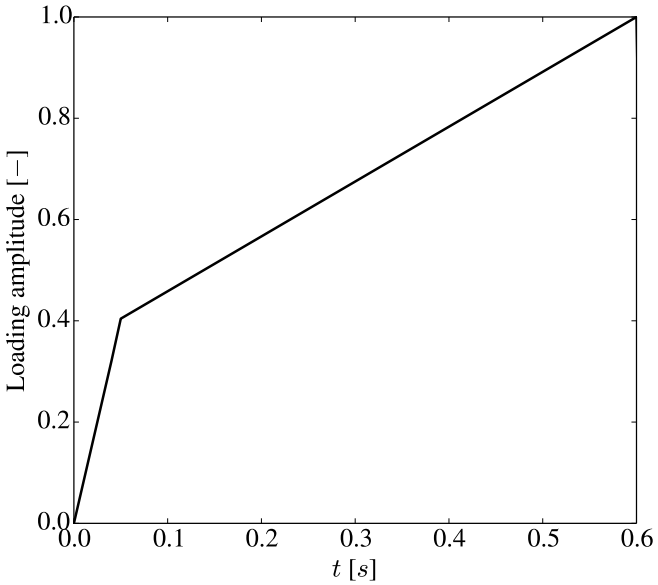

Figure 6.3: Illustration of variable amplitude loading

6.2.6 Meshing

In all cases, the area around the hole is meshed finely whereas areas further away can be meshed more coarsely. After all, near the hole is where stress concentrations arise and damage initiation

sites exist, whereas further away from the hole the mesh only needs to be regular and coarse enough to yield a good global stress representation.

6.3 Implementation in UMAT

The PDA routine is integrated in a UMAT subroutine, called at every integration point at every time increment. This subroutine is chosen since it allows:

- A full definition of constitutive behaviour in terms of the material stiffness matrix (Jacobian)
- Retrieval of the local stress and strain state for evaluation of damage criteria
- Degradation of properties to include the effects of damage directly in the Jacobian definition
- Seamless integration in existing FEM models, without requiring adaptations
- Obviating the need to submit a new analysis for each load increment (e.g. by Python scripting) and circumventing the significant computational effort associated therewith

At the end of each increment, the local variables are passed onto the UMAT. In the UMAT, the following actions take place subsequently:

1. The local stresses and strains are retrieved and subsequently used to evaluate failure criteria. Material properties required are read in from an external input file, containing a library of materials.
2. When damage is detected, damage variables are updated and - if viscous regularization is adopted - gradually increased.
3. The damage variables act as flags to indicate whether property degradation is to take place. Property degradation follows as a direct reduction in material stiffness parameters, passed into the Jacobian.
4. The updated, damaged, stiffness matrix or Jacobian is used to update the stress tensor after incrementing the strain. The updated stress and strain tensor form the basis for the following iteration, passed into the main routine along with the defined Jacobian.

These steps are illustrated schematically in Figure 6.4.

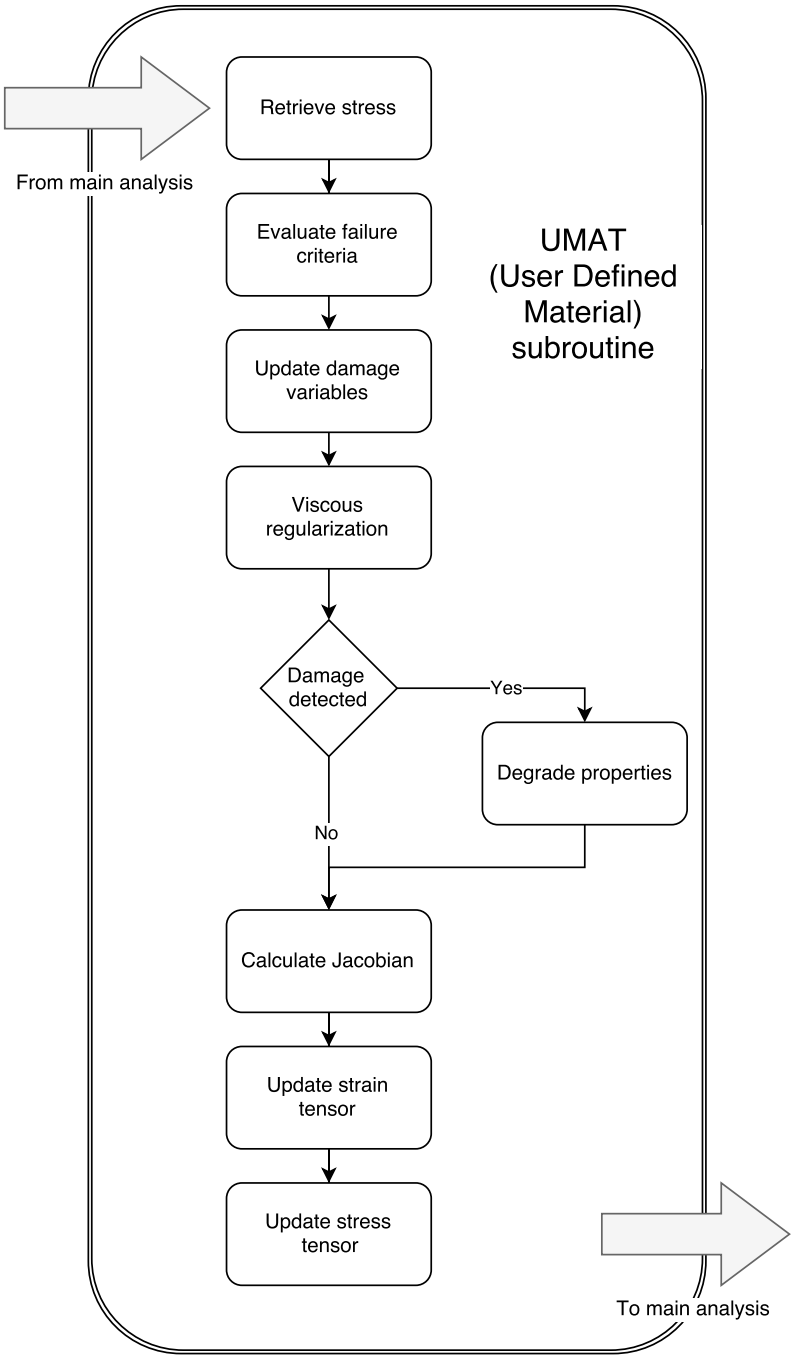

Figure 6.4: Overview of UMAT structure

6.4 Comparison with test cases

A number of cases are selected from open literature and implemented in conjunction with the PDA routine. This serves to:

- Verify the implementation
- Benchmark the implementation against past implementations of PDA in FEM
- Identify the effect of model parameters (mesh fineness, increment size, shear non-linearity, viscosity, fracture energies)

- Compare the three selected stress-strain based approaches
- Identify potential shortcomings and pitfalls of stress-strain based PDA in FEM

Previous remarks hold as to the limited quantity of test cases. Ideally, test cases should cover a wide range of loading conditions, material and laminate configurations. Practical reasons limit the quantity of test cases used and thereby, in a strict sense, limit the generality of any conclusions reached.

A trio of test cases are selected, two evaluating an OHT CFRP specimen and one an OHT GLARE specimen. These test cases are included for their past evaluation, numerically and experimentally, that allow benchmarking to the state-of-the-art and an objective comparison to experimental observations. The cases cover a diversity of materials and lay-ups.

In the following test cases, models are designated as given in Table 6.1. This designation is used throughout the entire section.

Table 6.1: Stress-strain based model designation test cases

Model	Initiation criteria	Propagation model
DM1	Puck	McCarthy et al.
DM2	Cuntze	Camanho and Matthews
DM3	LaRC05	Bilinear softening

6.4.1 CFRP Open-Hole Tension Chang and Chang

A CFRP OHT specimen is evaluated, in the wake of work by Chang and Chang [67], Tan [70] and Maimí et al. [10, 34]. Since experimental data on the failure stress is available, this test case allows a comparison of model predictions versus experimental data, albeit to a limited degree. Moreover, since the open hole induces stress concentrations there is a clear site for damage initiation. A sensitivity study is conducted on the mesh size, time increment size, fracture energies, shear non-linearity and viscosity to investigate the effect thereof on solution quality.

Test case description and modelling

The test case considers a specimen clamped on one end and with a uniform axial displacement applied to the other end, see Figure 6.5. The specimen consists of a total of 20 layers of T300/1034-C carbon/epoxy, in a $[0°/(\pm 45°)_3/90°_3]_S$ lay-up. Properties are taken from Maimí et al. [10, 34], including in-situ strengths as per the theory by Camanho et al. [29] that was already adopted for the preliminary analysis. Properties are summarized in Appendix E..

Shear non-linearity is modelled by means of a Hahn-Tsai fit with fit parameter $\beta = 2.98 \cdot 10^{-8}$ MPa^{-3}, made compatible with the formulation of the stiffness matrix in the UMAT by forward differencing at step i to obtain

$$\tau_{12,i+1} = \frac{1}{\frac{1}{G_{12}} + 3\beta\tau_{12,i}^2} \tag{6.6}$$

This does necessitate a sufficiently small time step to mitigate errors induced by the approximation. In view of the small timestep required for convergence this does not pose an issue. With the initial large displacement steps, care must be taken. However, in view of the limited non-linearity at low strains this is not very problematic.

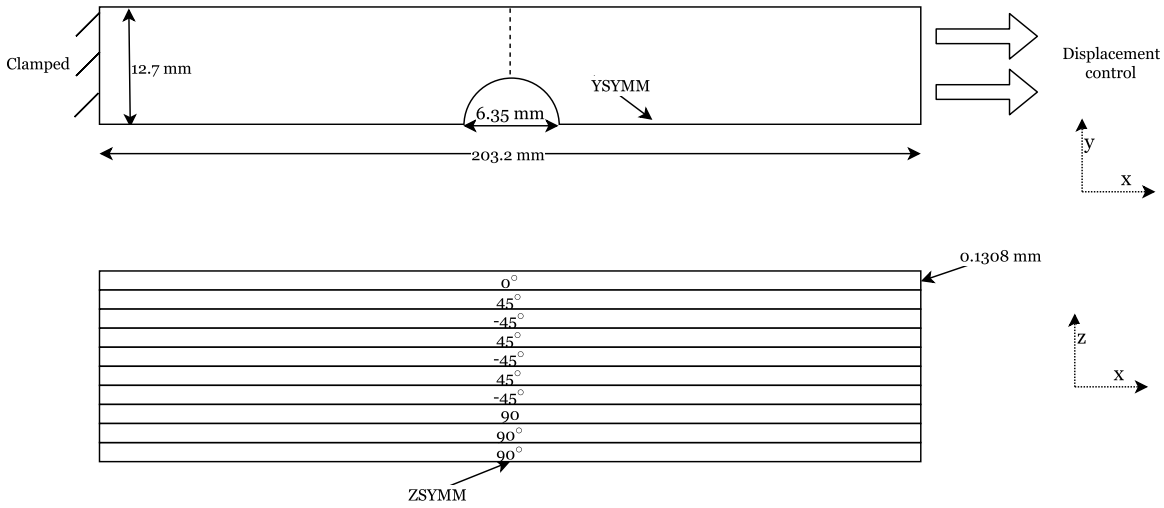

Figure 6.5: Schematic overview of CFRP OHT test case model

One fourth of the specimen is modelled, cut through the mid-plane with symmetry in through-thickness direction to take advantage of laminate symmetry. The $\pm 45°$ layers prevent an accurate representation by modelling one-eighth of the model. On the long axis, this poses less of a problem since failure does not occur there in this case.

Plies are modelled by one layer of (solid continuum) C3D8 elements each. Although additional layers per ply would be beneficial in terms of accuracy for through-thickness field representation, this would mean additional computational effort. The mesh is (relatively) fine near the hole and increasingly coarse moving away from the hole. Damage is expected near the hole [34, 46, 59, 67, 71, 72], hence the region further away needs to be only modelled fine enough to yield a good global representation.

Predicted load-displacement relations

Load-displacement relations obtained by the models are shown in Figure 6.6. All model predictions are relatively close. The first portion of the load-displacement is identical since no damage occurs and all models employ the same constitutive model.

Final failure loads, at which the laminate stiffness matrix is no longer positive definite, are given in Table 6.2 for the implemented models. These are compared to the experimental final failure stress of 235.8 MPa obtained by Chang [67], as well as to predictions by Chang and Chang [67], Tan [70] and Maimí et al. [10, 34]. Global behaviour is relatively well predicted by all models implemented, although DM1 displays a significantly larger discrepancy than DM2 and DM3.

It should be noted that, while the results by Tan conform closely to the experimental result, agreement is less good for different lay-ups, dimensions and materials [70]. On the contrary, of the test cases featured by Maimí et al., the discrepancy for this test case is largest [34]. Therefore any judgment on model predictive capability should be made only tentatively.

Moreover, Tan truncates the results up to the point where FF has occurred along the net section in the $0°$ ply. Whereas for DM2 and DM3 ultimate failure coincides with this point, DM1 displays the defined final failure only at a displacement of 1.67 mm whereas FF has propagated along the entire net section already at 1.5 mm displacement. Adopting this definition of final failure would thereby yield a slightly lower discrepancy. This is not performed, however, since

such a definition can not generally be made for more complex test cases. In addition, the predicted ability to handle sustained loading after net section FF is deemed a feature inherent to DM1 and should as such be preserved.

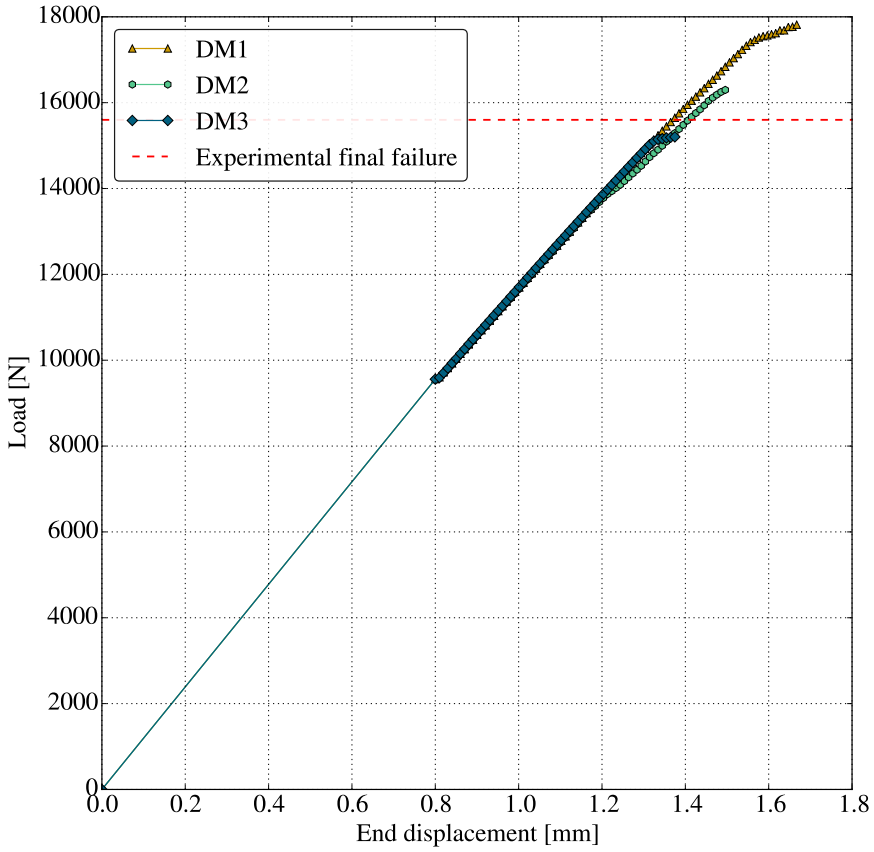

Figure 6.6: Predicted load-displacement relation CFRP OHT test case, along with experimental failure load from Chang and Chang [67]

Table 6.2: Predicted and measured final failure stress for OHT test case

Model	Predicted [MPa]	Discrepancy	
		[MPa]	[%]
DM1	268.1	33.5	14.2
DM2	245.3	10.5	4.46
DM3	228.8	-5.98	-2.55
Maimí et al.	263.1	27.3	11.6
Tan	248.2	12.4	5.26
Chang and Chang	180.0	-55.8	-23.7

Damage patterns

To fully investigate the performance of the implemented models, it is essential to investigate local behaviour. For the case at hand, the main failure mechanism is the FF in the 0° plies, final failure occurring for all cases when the net section in this ply has failed. In addition, secondary failure in the form of MF in all plies, along the same band, governs the failure process.

Figure 6.7 shows the progression of FF for various displacements, for the 0° ply. All models yield the same failure pattern. For DM3, however, near final failure the FF proceeds along a line at 45° with respect to the loading direction, as opposed to perpendicular to the loading direction, until the entire net section has failed in FF, see Figure 6.8.

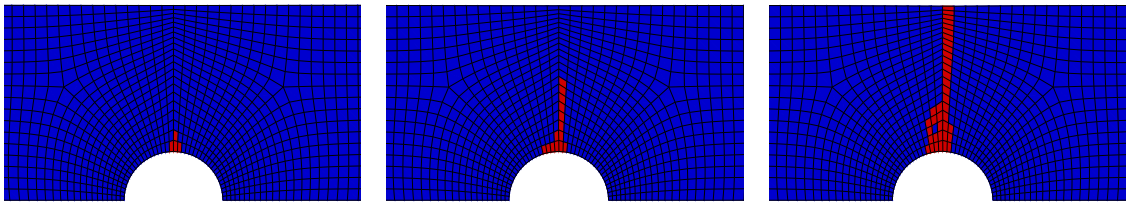

(a) 0.8 mm **(b)** 1.2mm **(c)** 1.4 mm

Figure 6.7: Progression of FFT in 0° ply for OHT test case per applied displacement, DM2 (red and blue denote respectively damaged and undamaged elements)

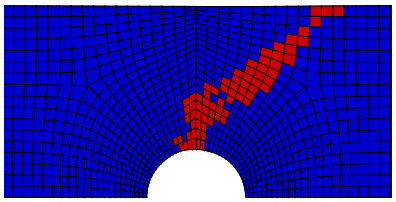

Figure 6.8: Final failure pattern of FFT in 0° ply for OHT test case, DM3 (red and blue denote respectively damaged and undamaged elements)

The outermost of each orientation for the $\pm 45^\circ$ and 90° ply blocks is selected for visualization, results being comparable for the other plies within these blocks - although generally less severe since the ply discontinuity induces additional stress concentrations in the outermost plies of each ply block. Models predict the same failure pattern in these layers, although the rate of damage growth does differ between models, as elaborated upon in the next subsection on damage density evolution.

Figures 6.9, 6.10 and 6.11 show that MF occurs in 45°, 0° and 90° plies along the same failure band. This occurs in close relation to FF in the 0° ply, each failure causing a redistribution of stresses to other plies. The difference in failure modes is due to the $\pm 45^\circ$ and 90° plies being loaded primarily in shear, as opposed to the 0° plies loaded significantly in tension.

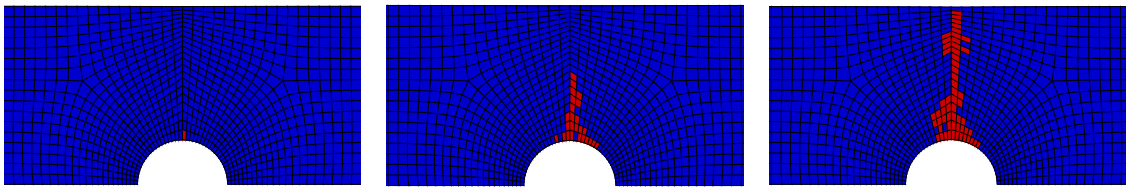

(a) 0.8 mm **(b)** 1.2 mm **(c)** 1.4 mm

Figure 6.9: Progression of MFT in outermost 45° ply for OHT test case per applied displacement, DM2 (red and blue denote respectively damaged and undamaged elements)

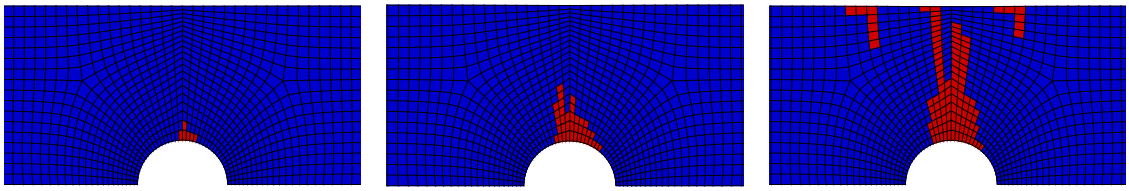

(a) 0.8 mm **(b)** 1.2 mm **(c)** 1.4 mm

Figure 6.10: Progression of MFT in outermost 90° ply for OHT test case per applied displacement, DM2 (red and blue denote respectively damaged and undamaged elements)

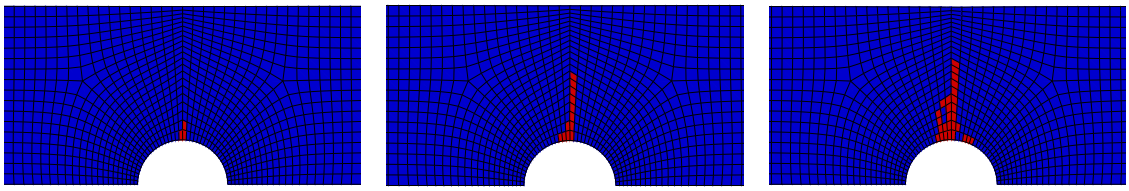

(a) 0.8 mm **(b)** 1.2 mm **(c)** 1.4 mm

Figure 6.11: Progression of MFT in 0° ply for OHT test case per applied displacement, DM2 (red and blue denote respectively damaged and undamaged elements)

This damage pattern correlates with the findings of Chang and Chang [67], Tan [70] and Maimí et al. [10, 34]. However, in the absence of detailed experimental observations on the failure sequence and mechanisms, further comparison to experimental data is warranted.

After all, all of these models are inherently stress-strain based continuum damage models. As such, these suffer from the same flaw that Van der Meer pointed out, namely that heterogeneity if not fully respected by evaluation on a mesoscale [11]. Consequently, in reality this heterogeneity may well cause a different failure pattern than the one predicted.

A glaring deficiency related to the latter is the growth of matrix cracks through the fibers, see Figures 6.9-6.11, whereas experimental evidence suggests that matrix cracks are constrained to grow along the fibers [11, 59, 73, 74]. This is common to all purely stress-strain based damage models. Particularly in view of promising developments for predicting MF using XFEM [11, 59], fracture mechanics based modelling provides a more physically correct perspective.

Damage density evolution

A different perspective on damage evolution is offered by considering crack density, monotonically increasing during the loading process. Damage density provides a simple indication of the severity of damage. It is a useful concept for translating the extensive local damage mapping into a simple scalar, although a significant portion of information is lost in this translation.

For the case at hand, FF and MF density through the entire laminate are plotted for each of the models in Figure 6.12. Overall, Figure 6.12 shows that growth occurs rapidly after approximately 1.2 mm displacement for all of the models considered. All models display roughly similar initiation stages for FF, up to a displacement of 1.2 mm. Moreover, these plots show that FF and MF develop earliest for DM2, on one hand attributed to the interaction in the Cuntze criteria and on the other hand attributed to the Camanho and Matthews MDM.

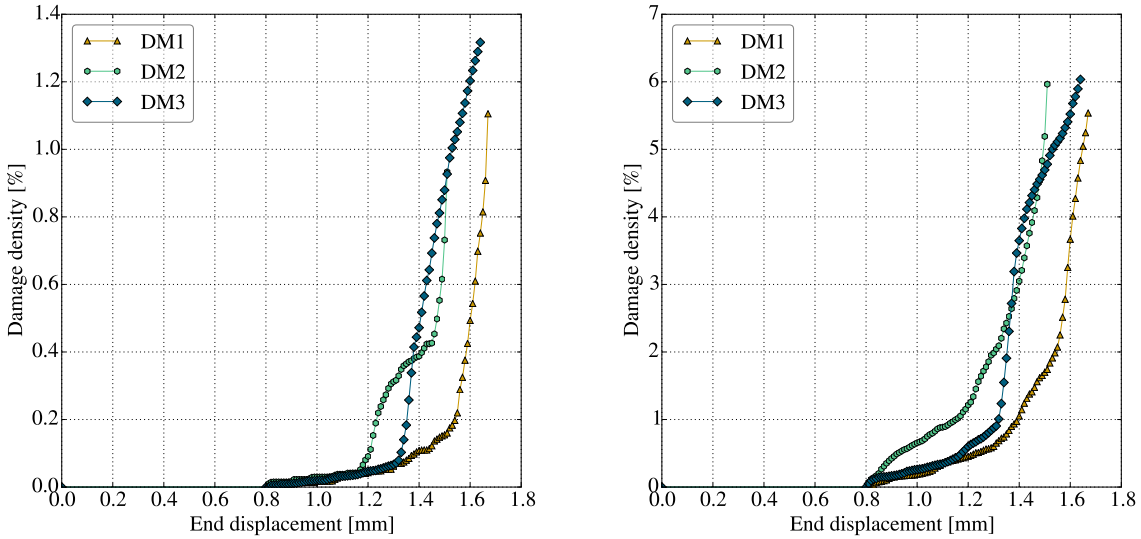

(a) FF **(b)** MF

Figure 6.12: Predicted damage evolution OHT test case

Qualitative effects of parameters

A qualitative study is conducted on the effect of a number of input parameters. This study serves to describe the effect various considerations have on the prediction accuracy of results. Of key interest are shear non-linearity, mesh size, viscosity and fracture energies. Ideally, this study is conducted on a number of cases and models but practicality limits the evaluation. In all cases, damage patterns are equivalent for the considered variations in model parameters. A subset of the models is selected for visualization to highlight the key features, since the effects have been observed to be qualitatively the same for all models.

Shear non-linearity Shear non-linearity is found to increase correspondence to the experimental failure load, see Table 6.3. The amount of $(\pm 45°)$ layers in the laminate effects a large influence of shear non-linearity in this case. It is readily apparent that adopting shear non-linearity yields better agreement to the experimental final failure load. Moreover, this is in line with the general observation that shear non-linearity is essential to take into account [12, 18].

Table 6.3: Effect of shear non-linearity DM1 predictions for OHT test case

	Model	Predicted [MPa]	Discrepancy [MPa]	Discrepancy [%]
DM1	Nonlinear shear	268.1	33.5	14.2
	Linear shear	305.6	70.8	30.2

Viscosity For the analyses conducted, the viscosity parameter is chosen to be small enough to still yield a converged solution at $5 \cdot 10^{-6}$ [s]. Adopting a larger viscosity, for illustrative purposes a significantly larger viscosity in this case (at $5 \cdot 10^{-3}$ [s]), yields an overestimation of the failure load by 31.4 % for DM1, see Table 6.4. This corresponds to general conclusions on the effect of the viscosity parameter [9, 11] and speaks in favour of adopting a small viscosity parameter. Overall, however, the sensitivity to the viscosity parameter is not very strong [9].

Table 6.4: Effect of viscosity DM1 predictions for OHT test case

	Model	Predicted [MPa]	Discrepancy [MPa]	Discrepancy [%]
DM1	$\mu = 5 \cdot 10^{-6}$ [s]	268.1	33.5	14.2
	$\mu = 5 \cdot 10^{-3}$ [s]	310.0	74.2	31.4

Fracture energies The effect of the fracture energy correction is significant for DM3. Not taking the correction into account increases the prediction error significantly, see Table 6.5. This effect is much the same as adopting a higher viscosity, since a fracture energy that is too high will cause insufficient degradation in likeness to a viscosity that is too high. Correcting for the mesh aspect ratio yields much better agreement.

Table 6.5: Effect of fracture energy correction DM3 predictions for OHT test case

	Model	Predicted [MPa]	Discrepancy [MPa]	Discrepancy [%]
DM3	uncorrected	268.9	34.1	14.5
	corrected	228.8	-5.98	-2.55

Mesh size The effect of the mesh size is relatively small. For a significantly rougher mesh, with one third of the elements of the finer mesh, the final failure load is predicted only slightly differently, see Table 6.6. Even with the crack band model used in DM3, a slight mesh dependence is visible. The slightness of the variation with the significantly rougher mesh is reassuring, although it should be noted that a different mesh orientation has an effect as well.

6.4.2 GLARE Open-Hole Tension

To investigate the predictive capabilities beyond FRP laminates, a Fibre Metal Laminate (FML) is evaluated in the form of a GLass REinforced Aluminum (GLARE) 3 3/2-0.3 OHT laminate. Pre-

Table 6.6: Effect of mesh DM1 and DM3 predictions for OHT test case

	Model	Predicted [MPa]	Discrepancy [MPa]	Discrepancy [%]
DM1	fine mesh	268.1	33.5	14.2
	rough mesh	261.4	26.6	11.3
DM3	fine mesh	228.8	-5.98	-2.55
	rough mesh	237.4	2.60	1.11

dictions are compared to experimental observations by De Vries [75] and numerical modelling by Lapczyk and Hurtado [9].

Test case description and modelling

A GLARE 3 3/2-0.3 laminate with a central hole is evaluated, consisting of three aluminum layers with 0° and 90° GFRP plies in between, see Figure 6.13. A uniform tensile displacement is applied at one end, while the other end is clamped.

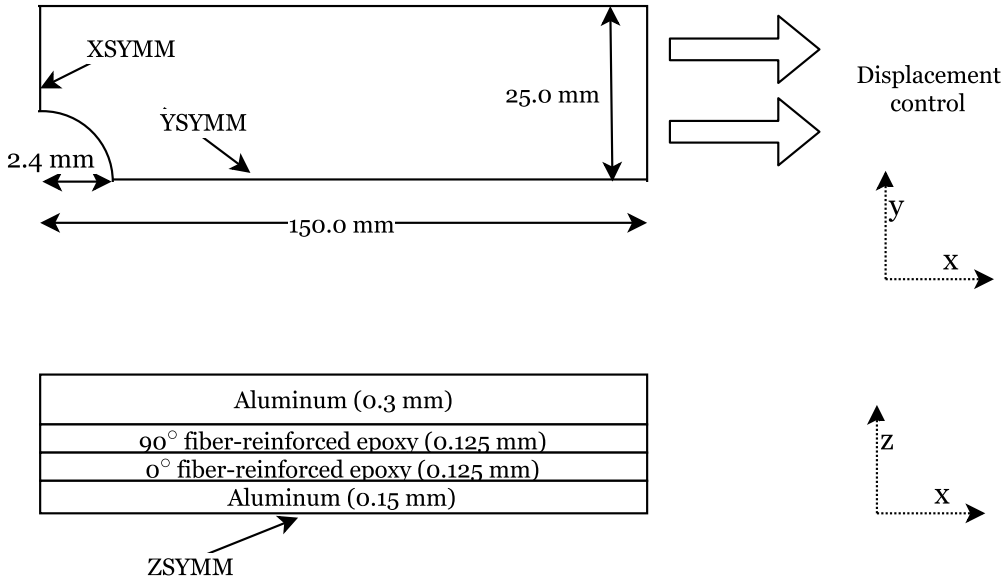

Figure 6.13: Schematic overview of GLARE test case model

In view of loading, material and geometrical symmetry, one eighth of the plate is modelled. Similar mesh considerations apply as before, with a fine mesh near the hole and an increasingly coarse mesh for the rest of the specimen.

Input values are as reported by Lapczyk and Hurtado [9], see Appendix E. Fracture energies are corrected to take into account the mesh aspect ratio, as discussed for the previous test case. For this case, however, the correction is not particularly influential for the results in view of the small value of the fracture energies.

Aluminum layer behaviour is modelled by isotropic hardening, conform the model by Lapczyk and Hurtado [9]. No failure of aluminum layers and DL are taken into account.

Predicted load-displacement relations

The predicted load-displacement relation is shown in Figure 6.14 for the three models considered, along with the experimental failure load extracted from the net blunt notch strength of 446.2 MPa reported by De Vries [75] and specimen dimensions.

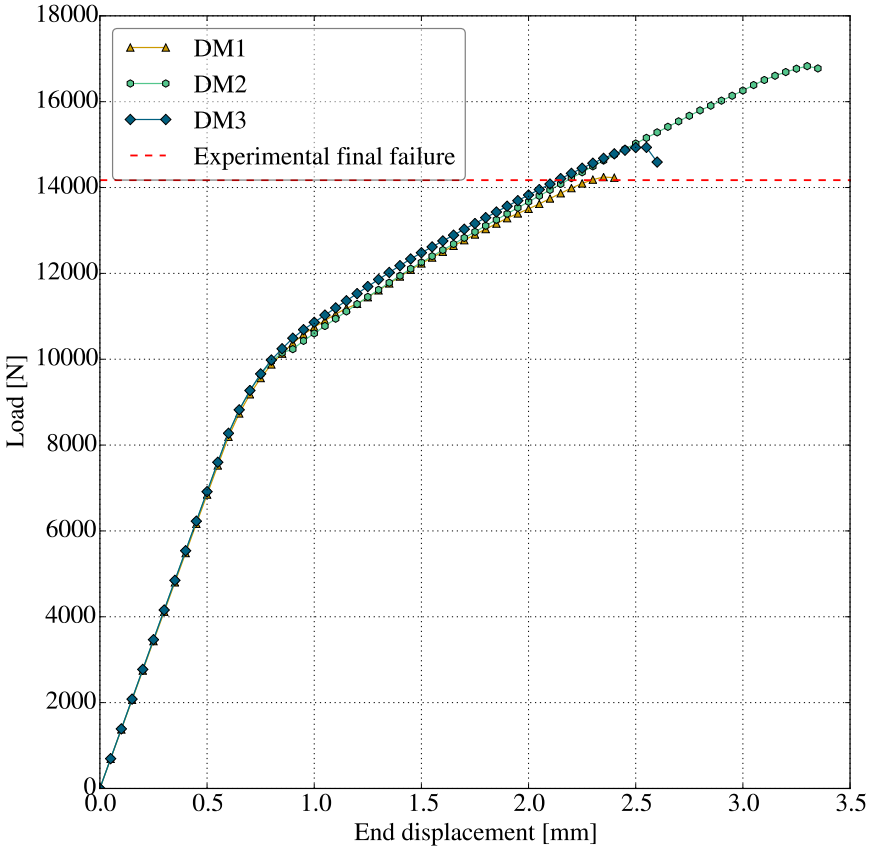

Figure 6.14: Predicted load-displacement relation GLARE test case, along with experimental failure load from De Vries [75]

The initial portion of the curve shows the elastic portion of the aluminum layers, at a displacement of 0.8 mm transitioning into plastic behaviour. The slope remains relatively constant until a critical portion of FF is reached in the 0° ply, after which no additional load can be sustained.

The net blunt notch strength is compared to the experimental value of 446.2 MPa [75], and the implementation by Lapczyk and Hurtado [9], in Table 6.7. DM1 predicts the strength to within a small margin, as does DM3, whereas DM3 overestimates the strength greatly. Compared to Lapczyk and Hurtado's implementation, DM1 and DM3 perform comparatively well even though DLs are not taken into account. The significant discrepancy in the prediction by DM2 lies in the degradation, discussed at greater length in the context of damage evolution.

Table 6.7: Predicted and measured net blunt notch strength for GLARE test case

Model	Predicted [MPa]	Discrepancy [MPa]	Discrepancy [%]
DM1	448.3	2.29	0.51
DM2	529.7	83.6	18.7
DM3	470.0	24.1	5.39
Lapczyk and Hurtado	453.2	7.20	1.61

Damage pattern

All models predict the same damage patttern. Damage is initiated in the 90° ply in the form of MFT, as shown in Figure 6.15, progressing from the hole edge where a stress concentration exists. Thereafter, FFT and MFT originate at the hole edge in the 0° ply, see Figures 6.17 and 6.16. FFT is the critical failure mode and the laminate fails when FFT has propagated along a critical length on the net section.

These observations are in close agreement with results by Lapczyk and Hurtado [9], and generally with experimental observations [75]. For DM3, the similarity is reassuring in view of the similar basis that DM3 and the implementation of Lapczyk and Hurtado share.

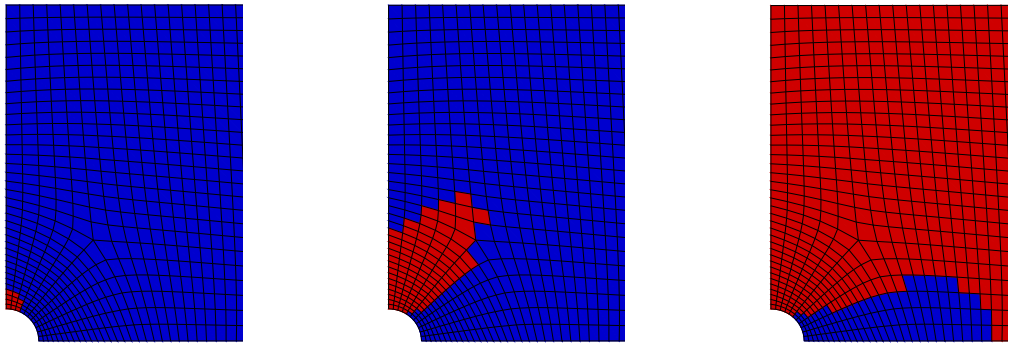

(a) 0.5 mm **(b)** 0.75 mm **(c)** 1 mm

Figure 6.15: Progression of MF in 90° ply for GLARE test case per applied displacement, DM3 (red and blue denote respectively damaged and undamaged elements)

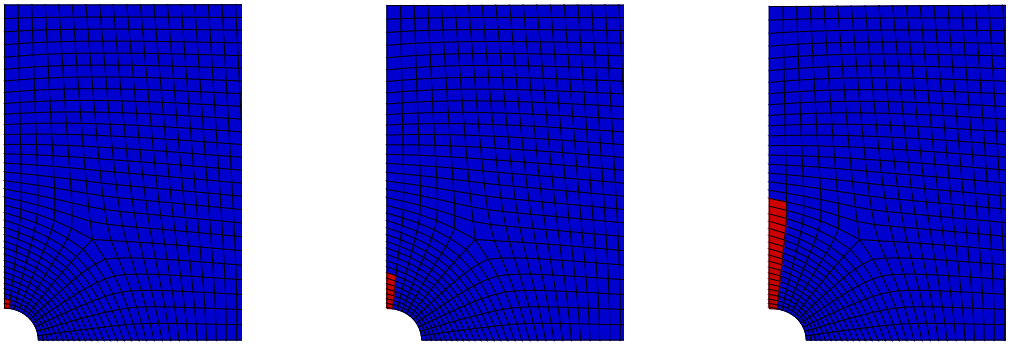

(a) 1.5 mm **(b)** 2 mm **(c)** 2.5 mm

Figure 6.16: Progression of FF in 0° ply for GLARE test case per applied displacement, DM3 (red and blue denote respectively damaged and undamaged elements)

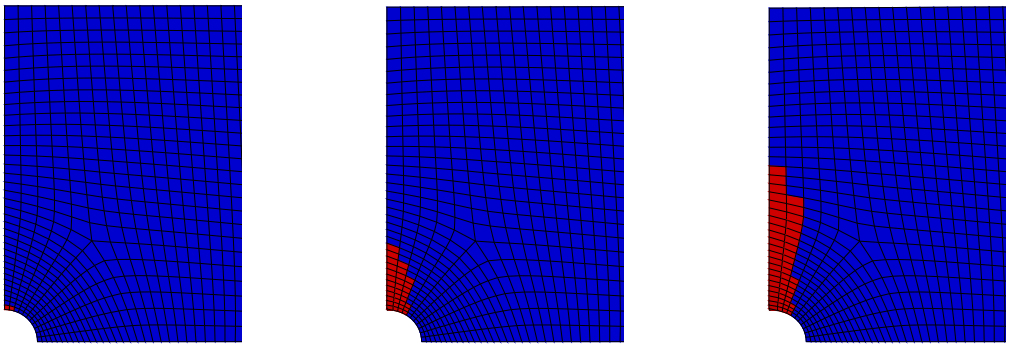

(a) 0.75 mm **(b)** 2 mm **(c)** 2.5 mm

Figure 6.17: Progression of MF in 0° ply for GLARE test case per applied displacement, DM3 (red and blue denote respectively damaged and undamaged elements)

Damage density evolution

Looking at the evolution of damage in the form of damage density provides another perspective on the failure process and highlights key differences between the methods implemented. Figure 6.18 shows the predicted crack density, estimated as the percentage of damaged elements in the two GFRP layers, for each of the models considered.

Figure 6.18a shows that DM1 develops FF significantly earlier than the other models. This is due to the degradation of E_1 in the McCarthy degradation due to MF, which the other models do not consider. Adjacent to the FF initiation site, MF precedes FF and in the case of DM1 signficantly degrades E_1 such that stresses are redistributed and FF develops earlier.

A key difference between DM2 and the other models is the relatively slow progression of FF along the net section for the former, due to insufficient degradation of properties in the Camanho MDM. Absence of Poisson's ratio and shear degradation for FF is a possible cause, more so than any deficiency in MF for this case since FF initiates at roughly the same displacement after the 90° ply is fully damaged by MF.

Moreover, from Figure 6.18a it is readily apparent that DM3 sustains noticeably less FF than the other models. This is attributed to the severe degradation of properties in the DM3 model due to FF.

Figure 6.18b shows that MF develops slowly at first, after which it rapidly spreads throughout nearly the entire $90°$ ply (see Figure 6.15). Simultaneously, MF starts developing in the $0°$ ply (see Figure 6.17).

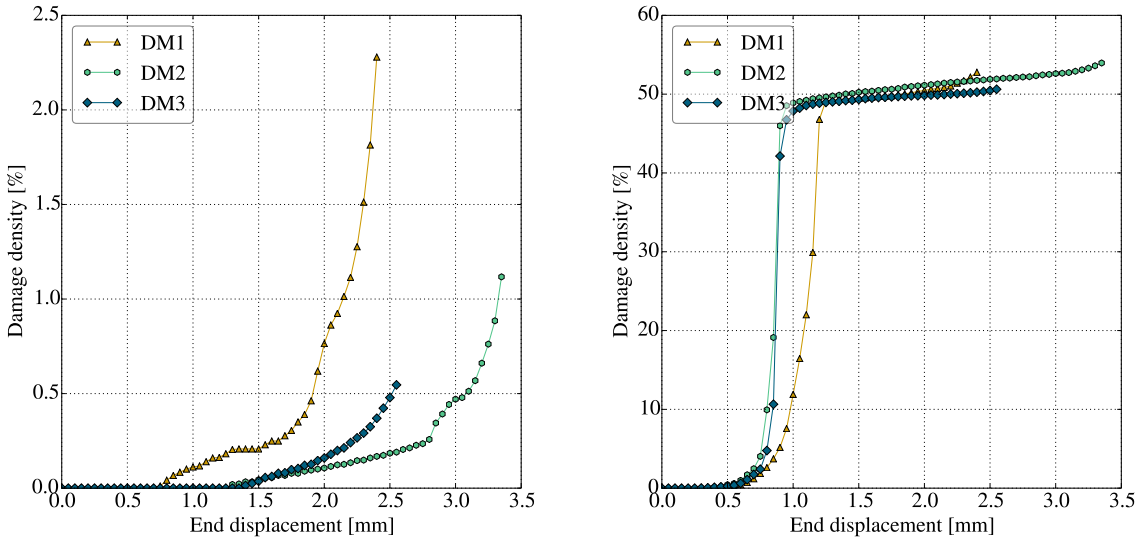

(a) FF **(b)** MF

Figure 6.18: Predicted damage evolution GLARE test case

6.4.3 CFRP Open-Hole Tension Nixon-Pearson et al.

This case study is based on experimental campaigning by Nixon-Pearson et al. [73, 74]. It serves to validate the localization of damage based on X-ray Computed Tomography (CT) scans. It is primarily intended as an illustrative case, highlighting some of the key deficiencies that are often overlooked or omitted in publications on state-of-the-art stress-strain based models.

Test case description and modelling

An OHT specimen in analogy to the previously discussed CFRP OHT case is analysed, loaded uniaxially in tension with a central hole of 3.175 mm diameter, see Figure 6.19 [73]. A $[45° \ / \ 90° \ / \ -45° \ / \ 0°]_{2s}$ lay-up is considered. Material properties for IM7-8552 CFRP are taken from Camanho et al. [71], and model-specific parameters identical as for the previous CFRP OHT case, see Appendix E.

Plies are modelled by one layer of C3D8 elements each. Contrary to previous cases, symmetry is only used in through-thickness direction in view of laminate symmetry.

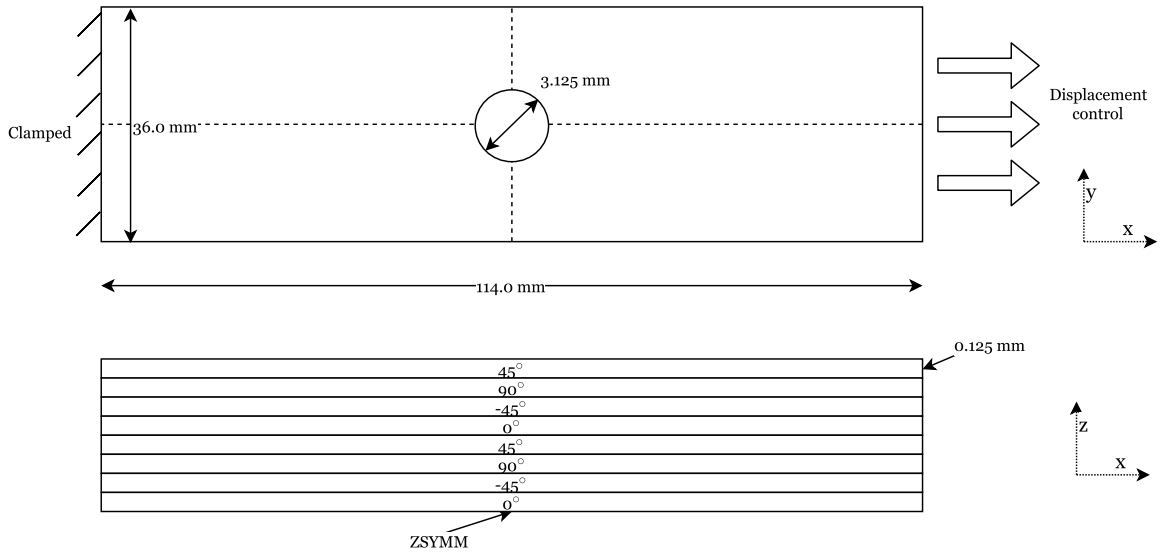

Figure 6.19: Schematic overview of second CFRP OHT test case model

Predicted load-displacement relations

Load-displacement predictions are compared to results by Nixon-Pearson et al. [74], who tested a trio of batches of 5, 4 and 6 specimens. Within each batch, variations in final failure are limited, but between batches results differ significantly. Model predictions, along with the batch average final failure loads and an experimental load-displacement curve, are given in Figure 6.20. Predictions are compared in Table 6.8.

The large batch-to-batch differences cast some doubt on the reliability of the experimental results. The single experimental load displacement curve is moreover not ideal for comparison, in view of these batch differences and the variability in load-displacement - in terms of both apparent stiffness and failure occurrence - illustrated in an earlier, similar study by Nixon-Pearson et al. [73]. The comparison is thereby mostly for qualitative purposes.

Model predictions are conservative. DM3 performs remarkably well, as for the previous study cases. DM2 performs notably worse than both DM1 and DM3. One possible cause for the conservativeness is the lack of DL modelling, since DLs may cause a favourable redistribution of stresses.

Table 6.8: Predicted and measured failure strength for second CFRP OHT test case, compared to experimental failure strengths from Nixon-Pearson et al. [74]

Model	Predicted [MPa]	Discrepancy (batch 1 | batch 2 | batch 3) [MPa]	[%]
DM1	484.8	-96.2 | -47.2 | -15.2	-16.6 | -8.87 | -3.04
DM2	433.0	-148 | -99.0 | -67.0	-25.5 | -18.6 | -13.4
DM3	500.4	-80.6 | -31.6 | -0.37	-13.9 | -5.94 | -0.07

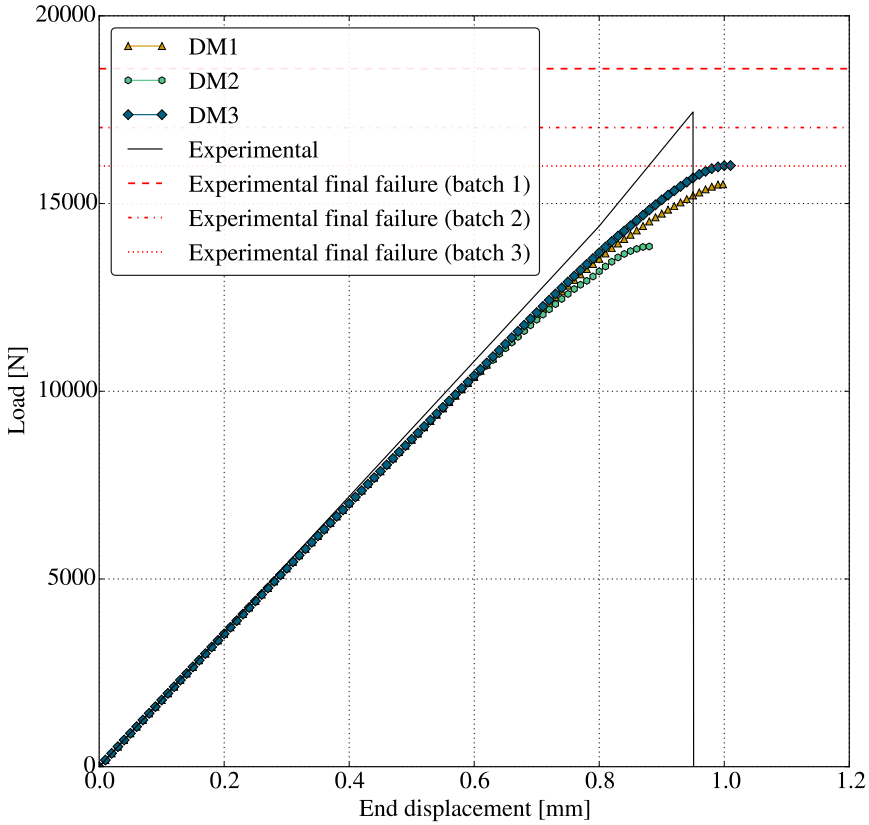

Figure 6.20: Predicted load-displacement relation Nixon-Pearson et al. CFRP OHT test case, along with experimental data [74]

Damage mapping

X-ray CT scans by Nixon-Pearson et al. [74] are compared to model predictions in Figures 6.21-6.28. Scans show predominantly matrix splits. Damage maps are given at 85 % of the predicted failure load, as opposed to the experimental failure load, to assess the patterns qualitatively at a comparable damage state rather than at a comparable stress state, since the focus lies primarily on the orientation and localization of matrix cracks.

These results show decent correlation between damage patterns predicted by DM3 and CT scans, in the sense that MF is predicted to grow mostly parallel to the fibers, at the same locations as experimentally observed. This can be observed throughout all plies.

DM1 and DM2, on the other hand, predict crack orientations relatively poorly. Contrary to DM3, damage is predicted for all layers to be concentrated along the net section. This is in clear disagreement with CT scans, particularly for $0°$ and $\pm 45°$ plies, where MF is predicted to grow through the fibers. Overall, these results speak in favour of the bilinear softening model. Still, all stress-strain models show extensive, unrealistic smearing, and, moreover, the fact that the bilinear propagation model gives a good representation for this case does not mean that this will generally be true - as illustrated extensively in the next chapter.

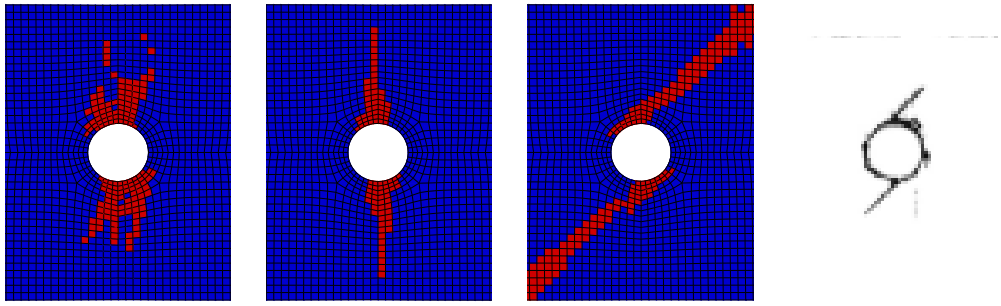

(a) DM1 **(b)** DM2 **(c)** DM3 **(d)** CT [74, p.270]

Figure 6.21: Progression of MF in surface $45°$ ply for Nixon-Pearson et al. OHT test case at 85 % of failure load (red and blue denote respectively damaged and undamaged elements)

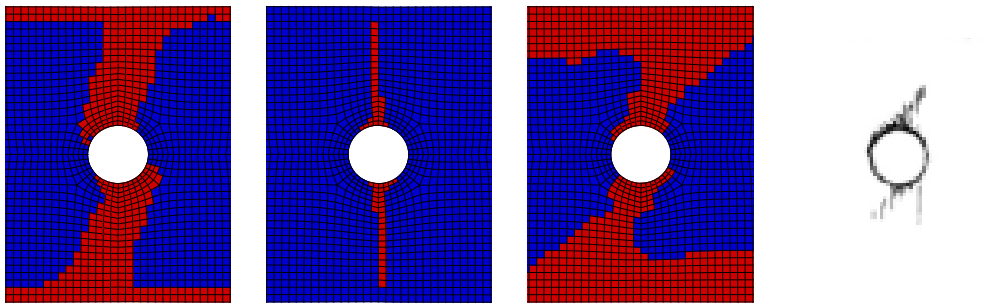

(a) DM1 **(b)** DM2 **(c)** DM3 **(d)** CT [74, p.270]

Figure 6.22: Progression of MF in surface $90°$ ply for Nixon-Pearson et al. OHT test case at 85 % of failure load (red and blue denote respectively damaged and undamaged elements)

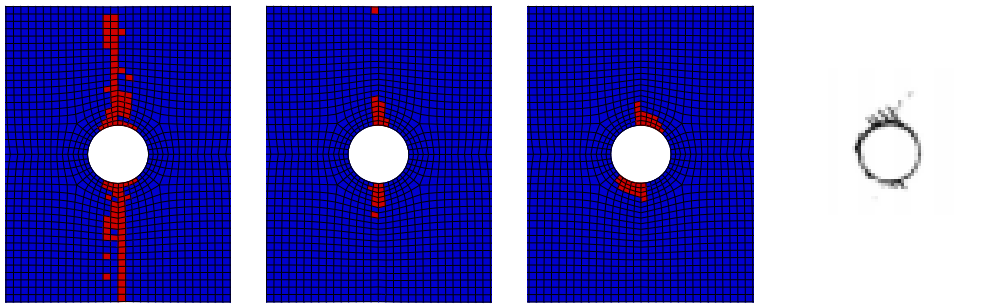

(a) DM1 **(b)** DM2 **(c)** DM3 **(d)** CT [74, p.270]

Figure 6.23: Progression of MF in surface $-45°$ ply for Nixon-Pearson et al. OHT test case at 85 % of failure load (red and blue denote respectively damaged and undamaged elements)

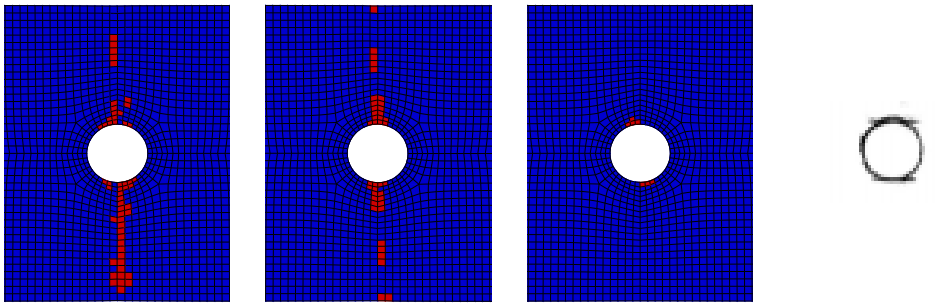

(a) DM1 **(b)** DM2 **(c)** DM3 **(d)** CT [74, p.270]

Figure 6.24: Progression of MF in surface $0°$ ply for Nixon-Pearson et al. OHT test case at 85 % of failure load (red and blue denote respectively damaged and undamaged elements)

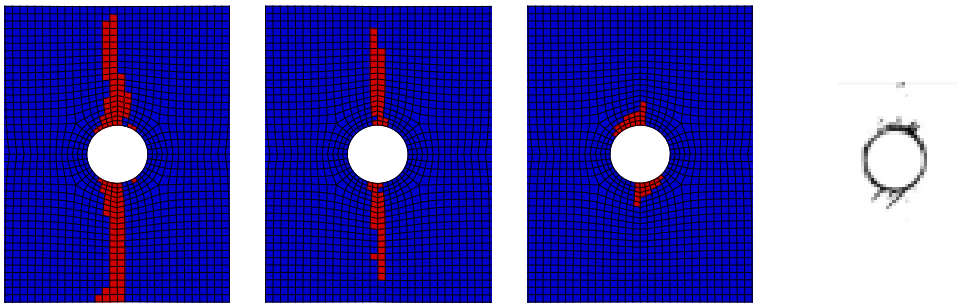

(a) DM1 **(b)** DM2 **(c)** DM3 **(d)** CT [74, p.270]

Figure 6.25: Progression of MF in center $45°$ ply for Nixon-Pearson et al. OHT test case at 85 % of failure load (red and blue denote respectively damaged and undamaged elements)

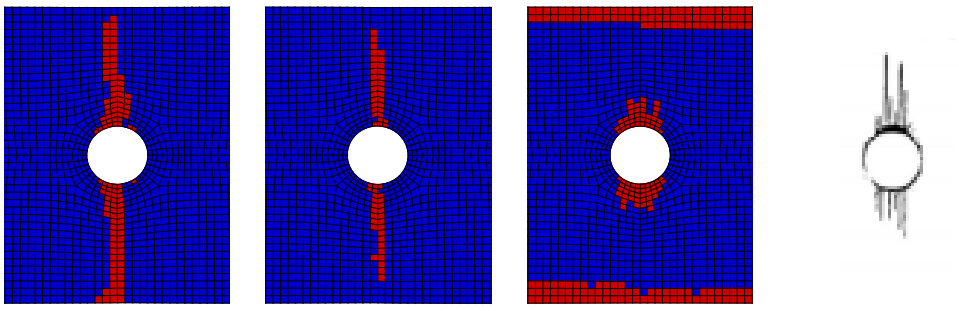

(a) DM1 **(b)** DM2 **(c)** DM3 **(d)** CT [74, p.270]

Figure 6.26: Progression of MF in center $90°$ ply for Nixon-Pearson et al. OHT test case at 85 % of failure load (red and blue denote respectively damaged and undamaged elements)

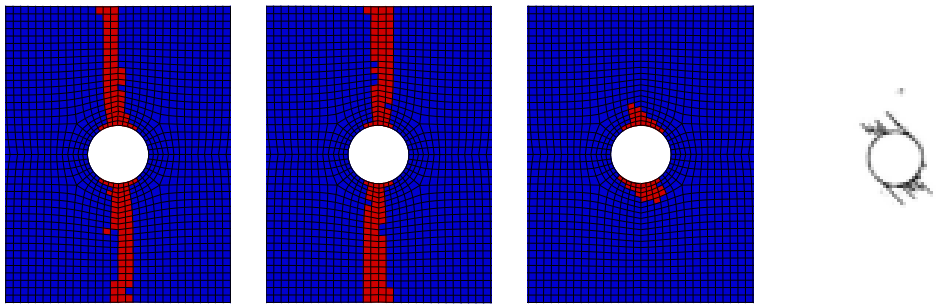

(a) DM1 **(b)** DM2 **(c)** DM3 **(d)** CT [74, p.270]

Figure 6.27: Progression of MF in center $-45°$ ply for Nixon-Pearson et al. OHT test case at 85 % of failure load (red and blue denote respectively damaged and undamaged elements)

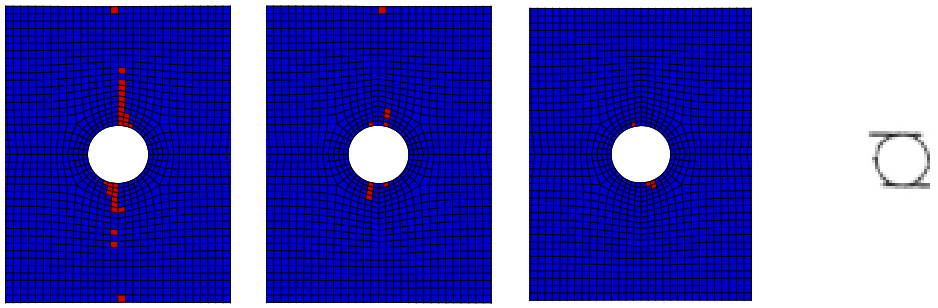

(a) DM1 **(b)** DM2 **(c)** DM3 **(d)** CT [74, p.270]

Figure 6.28: Progression of MF in center $0°$ ply for Nixon-Pearson et al. OHT test case at 85 % of failure load (red and blue denote respectively damaged and undamaged elements)

Damage density evolution

In likeness to the previous cases, damage density can be considered. FF and MF density through the entire laminate are plotted for each of the models in Figure 6.29. Due to the large amount of MF, evidenced by the high damage density thereof, particularly Figure 6.29b is of interest. These results show that DM2 develops damage most rapidly, as was observed for the first OHT test case. DM1 and DM3 do not show the same trend of damage evolution for the former test cases, underlining the complexity of failure prediction and the limited validity of conclusions reached on the basis of a limited number of test cases.

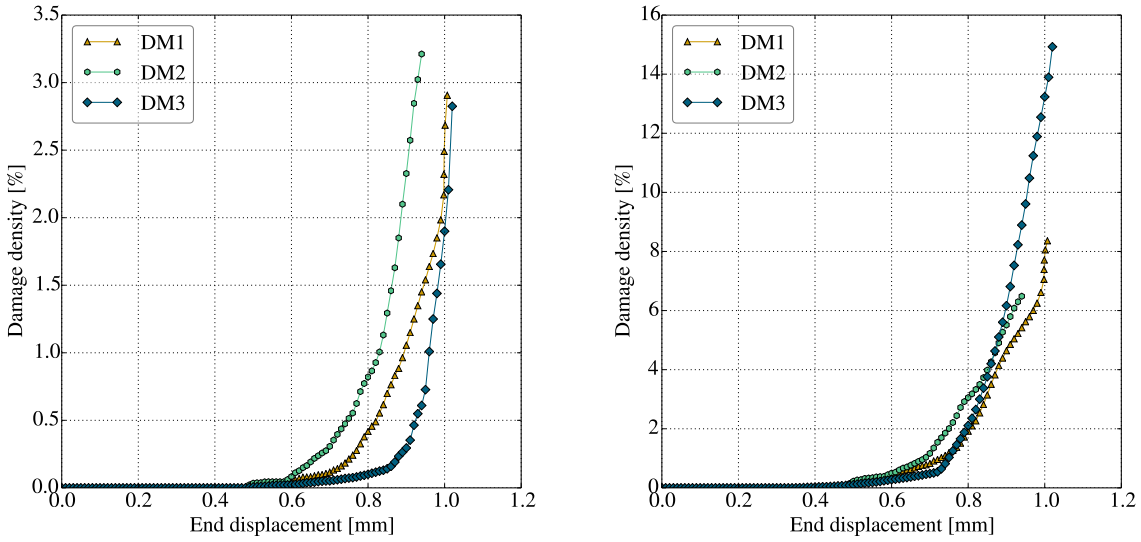

(a) FF **(b)** MF

Figure 6.29: Predicted damage evolution OHT test case Nixon-Pearson et al.

6.5 Conclusions and recommendations

Three stress-strain based models for PDA of FRPs have been implemented in Abaqus, by means of a UMAT subroutine. The UMAT fully defines the constitutive behavior, including shear non-linearity, and initiates and propagates damage in the form of MFT, MFC, FFT and FFC. DLs are not modelled, since there is no adequate model for propagating DLs using stress-strain based arguments.

A fully three-dimensional analysis was conducted on a number of test cases, evaluating two OHT CFRP specimens and an OHT FML specimen, from which the following conclusions are reached:

- Good agreement is achieved to experimental final failure data, for cases where DLs are not the driving failure mechanism. Predictions are remarkably close to experimental values, on par to past implementations. LaRC05 and bilinear softening provide the most consistent performance throughout the evaluation, discrepancies to experimental data lying within 5.4 %. The other two models, Puck initiation coupled to McCarthy et al. degradation and Cuntze initiation coupled to Camanho and Matthews degradation, show less consistency. This is mainly attributed to the propagation models, since the preliminary analysis showed the initiation criteria to perform comparably.
- On a local scale, validation is more difficult in the absence of detailed experimental data on failure modes. Compared to X-ray CT scans for an OHT CFRP specimen, the McCarthy et al. and Camanho and Matthews sudden MDMs were found to display large discrepancies. MF was predicted to grow through the fibres, whereas experimental evidence suggests that this is not the case [59, 74]. This points to the common deficiency of stress-strain based models that fiber-matrix microstructure is not fully respected [11]. The bilinear softening model, on the other hand, showed better agreement to the experimentally observed failure patterns. Still, none of the models pertain to a strong physical basis and damage is excessively smeared in all cases.

- Convergence can be problematic for the implicit schemes, although viscous regularization partly relieves this. Choosing the viscous regularization too large has a detrimental effect on accuracy, by delaying the failure sequence.
- To take correctly into account the characteristic length for the bilinear softening model, a correction for element three-dimensionality is key. The proposed correction is shown to yield consistently accurate predictions.

These conclusions, especially on model performance, should be made with caution. Similar as for the preliminary analysis, remarks hold as to the limited validity of a case-by-case evaluation.

Nonetheless, the conducted analyses show that the implemented stress-strain based models offer a pragmatic and convenient approach to predicting PDA of FRPs with remarkable accuracy when it comes to predicting final failure, particularly on a global scale. Through UMAT implementation, the models can be easily integrated in existing FEM applications with minimal adaptations required.

First and foremost recommendation is to cover a broader spectrum of loading, material and lay-up configurations. In particular, this is to be complemented by detailed experimental campaigning. Without comprehensive data on the localization of damage modes, it is difficult to reach definite conclusions on model predictive capability.

Secondly, the cases highlight the limitation of stress-strain based models when it comes to respecting fiber-matrix microstructure. Addressing this limitation requires a discontinuous approach to damage modelling, for which one solution is a fracture mechanics based perspective in the form of XFEM [11, 59]. Alternatively, micromechanics based models offer a comprehensive way of taking into account the local microstructure and failure on a microscale.

Chapter 7

Blend with fracture mechanics based damage modelling

Traditionally, stress-strain and fracture mechanics approaches to damage modelling have been applied in isolation. Continued practice thereof, however, overlooks many of the advantages that a blended approach has to offer. In particular, stress-strain models offer no satisfying methodology for predicting DL growth and disrespect matrix crack growth directions. Fracture mechanics models, on the other hand, have a strong basis for predicting DLs through CZMs [25, 60] and the recent advance of XFEM offers possibilities for modelling matrix cracking taking into account fiber-matrix microstructure [11, 59].

This chapter commences with a brief motivation for a blend with fracture mechanics. Thereafter, blend methodology is discussed. Performance of the blend is evaluated in detail by means of an extensive case study from literature and lastly validated with respect to an experimental campaign that has been conducted.

Contents

7.1 Motivation

Key motivation for the blend is to:

- Include DLs as a driving failure mechanism, including their strong interaction with matrix cracks [11];
- Predict MF in better correspondence to reality, obviating the heuristic stiffness degradation and enforcing crack growth along fibers.

For the former, stress-strain approaches are lacking particularly in terms of propagation, as argued previously in Chapter 4. The absence of DL modelling incurs grave errors in cases where DLs are the driving failure mechanism, as explored in a case study in section 7.3. Consequently, blending in DL using fracture mechanics will extend model applicability.

Moreover, stress-strain approaches fall short in terms of the heuristic stiffness degradation and arbitrary crack orientation. As illustrated by the case studies of the previous chapter, damage is excessively smeared and experimental damage patterns are poorly reproduced. Moreover, interaction between MF and DLs is poorly modelled using stress-strain methods, as illustrated in the case study of section 7.3. A judicious blend, where matrix crack propagation is handled through fracture mechanics, alleviates these shortcomings to predict and describe damage patterns more realistically.

7.2 Blending methodology

Fracture mechanics based arguments are blended into the proposed stress-strain framework in two areas: DL modelling and matrix crack growth. For the former, CZMs supplement the stress-strain models. For the latter, XFEM replaces the MF degradation proposed in the MDMs. Motivation and methodology for these blends is discussed hereafter. Due to the consistent performance of the LaRC05 and bilinear softening damage model (DM3), this model is used for blending.

An overview of the blending implementation is given in Figure 7.1. Elaborated upon hereafter, this Figure presents the stress-strain based model DM3, an intermediate blend DM4 and the fully blended model DM5 in relation to the model components.

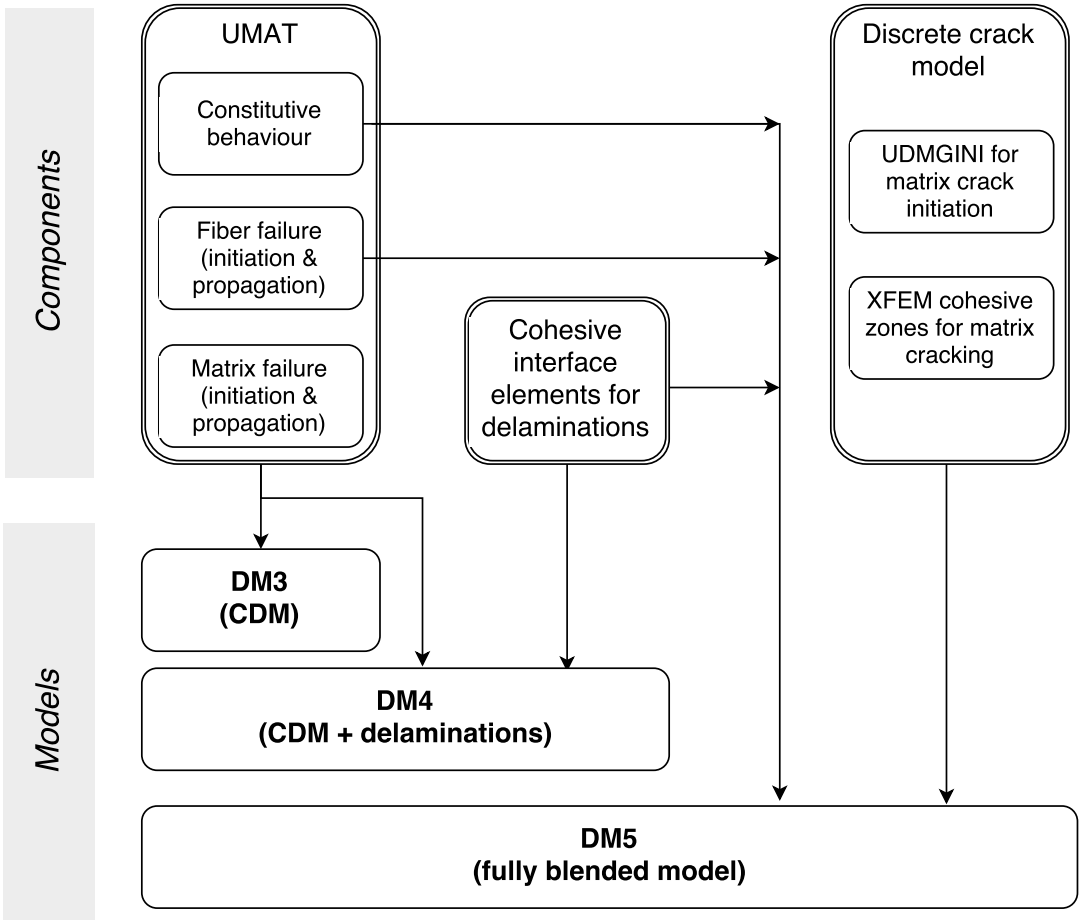

Figure 7.1: Schematic overview of blended model synthesis

7.2.1 Delamination modelling

DLs are modelled using CZMs, according to the motivation provided hereafter. Implementation follows on the basis of a study conducted in parallel on the use of fracture mechanics for damage prediction [6].

Method selection

Stress-strain based methods for predicting DL growth are severly lacking, whereas fracture mechanics based arguments have found numerous application in DL modelling [5, 11, 25, 60, 76–79]. In particular, CZMs offer a versatile means for predicting DLs. Advantageous of CZMs with respect to the main alternative, in the form of Virtual Crack Closure Technique (VCCT) [80], are the following aspects [5, 81, 82]:

- No remeshing during crack advancement is required to model the crack front, as for VCCT;
- No pre-crack is required, as for VCCT, which allows modelling structures where initiation sites are unknown;
- Obviates the oscillatory behaviour and numerical instability displayed by VCCT;
- Crack joining poses an issue in VCCT since cracks are presupposed to grow into undamaged regions, due to the self-similar shape assumption inherent to VCCT.

Still, there are many disadvantages of CZMs, foremost among which are:

- A lack of strong physical foundation [5]. In fact, recent experimental evidence suggests that interfacial damage is not confined to the interface and the interfaces follow a trapezoidal traction-separation law [83], contrary to what CZMs assume [9, 11, 25, 60, 77–79];
- The large number of parameters involved, not always measurable or with a physical meaning;
- Fine meshing required to ensure an appropriate number of elements in the process length [78], as well as the additional computational cost of adding interface elements;
- Convergence problems that are often encountered with the use of CZMs [6, 11].

No clear alternative is, however, available that parallels the versatility of CZMs for modelling DLs. Moreover, CZMs have been used widely with good correspondence to experimental results [11, 25, 60, 77–79]. Prerequisite for the latter, however, is a proper determination of the many parameters in CZMs. This is particularly arduous in view of the lack of a clear physical or measurable meaning behind some of these parameters.

A number of parameters are inherent to CZMs and influential for accuracy and convergence. These parameters are the following [60, 78]:

- Interaction coefficient to describe mode interaction;
- Interface strength to describe allowable tractions on the interface;
- Interface stiffness to describe load-bearing capability of the interface;
- Viscosity to improve convergence behaviour through more gradual stiffness reduction in the softening part of the traction-separation law. This is purely artifical and ideally kept as small as possible.

The effect of these parameters has to a large extent been investigated [6, 25, 60, 78]. A detailed treatment of CZMs is left out in favour of referencing to [6], as it is outside of the scope of the current study and moreover a well-established topic [11, 25, 60, 77, 78].

Implementation

The previously developed UMAT operates largely independently of the cohesive zones for DL modelling, linked only by the local stress and strain state of integration points. When a DL occurs, a discontinuity in stress and strain is initiated at the interface. This affects the local stress and strain state used in the UMAT due to a redistribution of stresses. Vice versa, intralaminar failure (in the form of FFT, FFC, MFT or MFC) translates to a local stiffness reduction that causes stress redistribution to affect tractions and separations at the interface.

Cohesive zones are inserted in between each layer as solid brick elements with relatively small thickness (0.5 % of ply thickness [6]) and specified in terms of initiation criteria and a damage evolution law. Opening modes are related by an interaction law, in the form of the Benzeggagh-Kenane criterion [84], found to display good overall correspondence for a judiciously chosen interaction coefficient based on experimental data [77]. Other interaction laws, such as the power law, are similar but lack the ability to represent mode interaction accurately for all cases. None of the interaction laws is truly physically based [5]. A linear traction-separation relation is implemented in the wake of past implementations [9, 11, 25, 60, 77–79], but other shapes (e.g. exponential softening) could be considered as long as the fracture energy is retained [77].

Artificial viscosity is implemented to improve the rate of convergence. Duly note that this should be kept as small as possible to prevent adding excessive artificial damping that compromises solution accuracy.

7.2.2 Matrix crack modelling

Matrix cracks, both compressive and tensile, are modelled through XFEM in conjunction with cohesive elements. Analogous to the previous subsection, motivation and implementation are discussed subsequently.

Method selection

A discontinuous approach to MF alleviates one of the key flaws observed in stress-strain based methods, namely that crack growth direction is not necessarily respected. The local stress and strain state guides crack growth in these models, disregarding the effect of fiber-matrix microstructure that cause cracks to grow along the fibers, as evidenced by experimental observations [11, 59, 73, 74, 79, 85].

Discontinuous modelling of matrix cracks requires placement of interface elements within each ply. In principle, to account for MF at any location, these should be placed throughout the entire model to allow modelling of local cracking. It is intuitively obvious that this would become prohibitively expensive. Although one way to address this is by placing interface elements selectively at locations where MF is expected, this suffers from the key limitation that these locations must be accurately known in advance. For cases where these damage patterns are known, this technique has proven to be decently capable of an accurate representation of the failure process [79]. Still, this would require extensive campaigning that partially invalidates the point of simulation-based predictions.

Consequently, a much more effective solution is adopting XFEM to locally enrich regions if damage initiation criteria are met, and insert an interface in these regions. This allows accurate crack modelling in a versatile and efficient manner, with little mesh dependence, and has been adopted to yield good predictions previously [11, 59]. Moreover, since an actual crack is modelled there is a much stronger physical basis to propagation than the mostly heuristical MDMs considered in stress-strain formulations.

Implementation

XFEM crack growth is allowed in all elements, evaluated at the centroid of each element by means of a user-defined UDMGINI subroutine. Within this subroutine, the Puck MF criterion defines damage initiation. Fracture angles in plies are limited to planes parallel to the local fibre orientation, as per experimental evidence [11, 59, 73, 74]. Stiffness degradation for MF in the UMAT subroutine is set to inactive, replaced by the stress redistribution that occurs at the crack location.

Upon damage initiation, elements are enriched [86] and cracks inserted, governed by a linear traction-separation law in likeness to the previously discussed CZM for DLs. Due to the similarity between MF and DL in the sense that both concern local cracking in the matrix, governing parameters are taken the same for both processes. Still, it should be noted that these are different processes and the similarity is adopted only since it is the best available estimate in absence of experimental data.

7.3 Ply-blocked laminate

A case study is ran on a ply-blocked laminate, in the wake of experimental campaigning by Green et al. [85], Nixon-Pearson et al. [73, 74], experimental campaigning and modelling by Hallett et al. [79] and by Van der Meer [11]. Established experimental data, in the form of X-ray observations, and the damage process of this case make this an excellent illustrative case to highlight the deficiencies of stress-strain based modelling, even with CZMs blended in for DLs.

Henceforth, the stress-strain based model on the basis of LaRC05 and bilinear softening in combination with CZMs for DLs is referred to as DM4. The full blend with DLs modelled through CZMs and MF through XFEM is referred to as DM5.

7.3.1 Test case description and modelling

A CFRP OHT specimen is considered, similar to that evaluated in subsection 6.4.3, see Figure 7.2. Contrary to that case, where layer orientations were dispersed throughout the laminate, plies are blocked in a $[45^\circ_n, 90^\circ_n, -45^\circ_n, 0^\circ_n]_s$ ($n = 1, 2, 4, 8$) lay-up of 0.125 mm thick IM7-8552 plies. Ply blocking effects DLs as the driving failure mechanism, interacting strongly with MF as evidenced by experimental findings [11, 73, 74, 79].

In line with the approach taken by Van der Meer, ply blocks are simulated as one ply with thickness $0.125n$ mm. Minimal loss in accuracy is expected, since DLs are expected between rather than within ply blocks [11]. This relieves computational effort and allows for more efficient modelling.

Ply material properties are taken from Camanho et al. [71]. Model-specific parameters are identical to the previously considered case (see subsection 6.4.3), see Appendix E.

In-situ strengths are taken from Camanho et al. [71], although their applicability is less straightforward for fracture mechanics based methods [11], which requires investigation outside of the scope of this study. In particular, after DLs plies are not constrained and the intralaminar strength can be expected to decrease. Results show that using non in-situ strengths already yields significant damage due to thermal cracking leading to rapid failure thereafter, and moreover a failure pattern that corresponds less well to experimental observations. Consequently, the use of in-situ strengths is deemed more warranted.

Cohesive zone parameters, for DLs and MF modelling, are given in Appendix E (taken from [11, 79]). According to the methodology prescribed by Turon et al. [78], interlaminar strengths are reduced in order to alleviate mesh requirements. Strengths are reduced such that six elements are in the cohesive process zone. To aid convergence, G_{Ic} for matrix cracks is increased to 0.3 and G_{IIc} by the same factor to preserve the mixed-mode ratio.

Thermal effects are taken into account, a requisite due to the fact that the thermal energy is transferred into DLs. Due to the heavily DL-driven failure for these cases, the effect is significantly larger than for previously evaluated test cases. Orthotropic thermal expansion is assumed, with $\alpha_1 = 0.0\ °C^{-1}$ and $\alpha_2 = 3.0 \cdot 10^{-5}\ °C^{-1}$ for $\Delta T = -160\ °C$ [11].

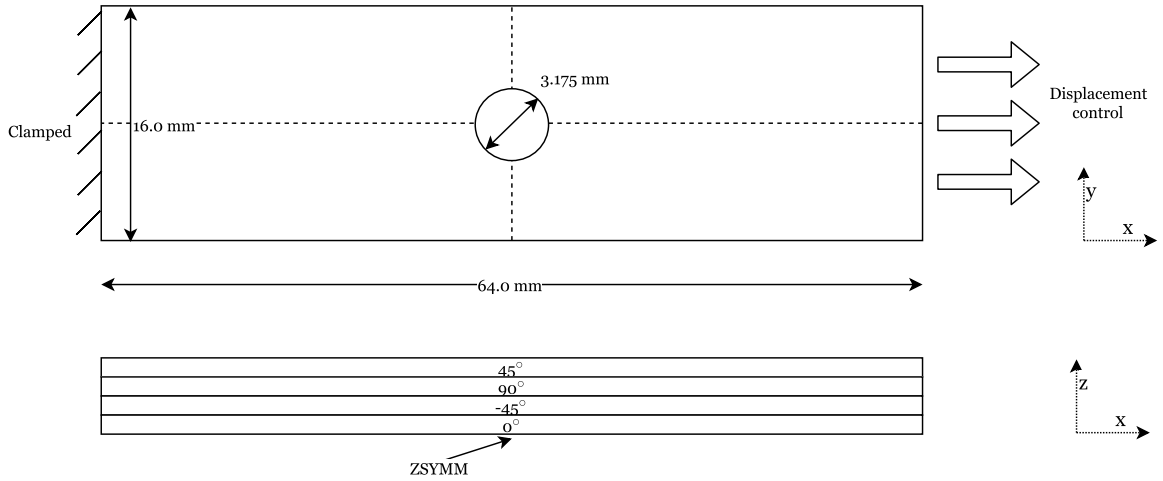

Figure 7.2: Schematic overview of ply-blocked CFRP OHT test case model

7.3.2 Final failure and size effect predictions

Failure predictions are compared to results by Green et al. [85], obtained for four different batches with $n = 1, 2, 4, 8$. Increasing n effects an increase in stiffness discontinuities between ply blocks, leading to more severe DLs and consequently earlier failure. Figure 7.3 shows the varying degree to which models are able to capture this size effect. Failure is in this case defined as the first load drop, attributed to DLs [73, 74, 85].

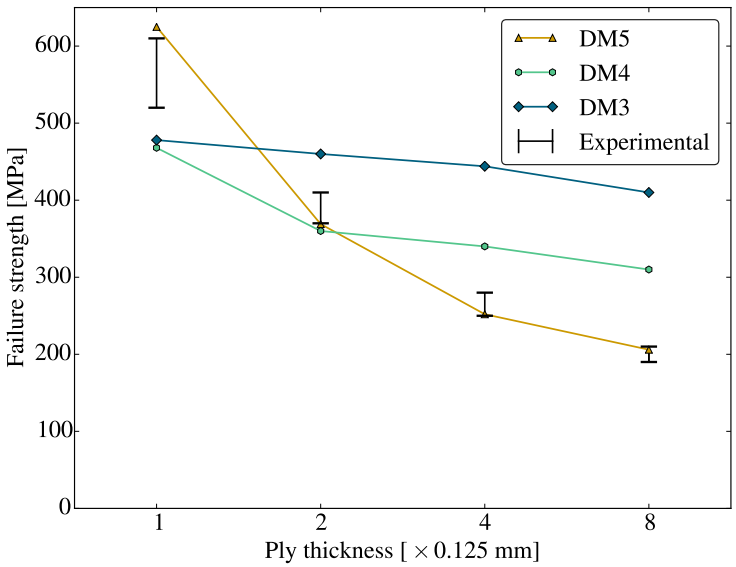

Figure 7.3: Predicted failure strength for ply-blocked OHT test case, along with experimental failure strength from Green et al. [85]

Only DM5 is able to capture the size effect well, DM3 and DM4 proving incapable of fully modelling MF-DL interaction and the effect of ply thickness thereon. This conforms to expectations, since DM3 does not take into account any DLs at all, whereas DM4 features little MF-DL interaction that dominates the failure process for this case [73, 74]. DM3 only captures a slight variation due to variation of in-situ strength with thickness. Consequently, only part of the size effect is captured using DM4 and DM3.

This underlines the redeeming features of not only modelling DLs by a CZM, but in addition modelling MF using XFEM to better model MF-DL interaction. Failing to do so leads to overestimation of laminate strength, errors growing with increasing ply blocking (hence DL presence). For cases where DLs are more limited, foremostly $n = 1$, DM3 and DM4 yield reasonably accurate predictions. These observations are generally in line with those of Van der Meer [11].

7.3.3 Damage mapping

As previous results indicate (see subsection 6.4.3 and section 7.1), global accuracy does not imply local accuracy. Discrepancies in damage patterns are inherent to stress-strain based models and even more apparent for this case with strong MF-DL interaction [11]. Damage maps are shown for $n = 2$, since detailed experimental data is available for $n = 2$. For increasing n, DLs become more prominent.

Figures 7.4-7.7 show the predicted development of MF alongside X-ray CT scans from Nixon-Pearson et al. [74]. From these figures, it is apparent that only DM5 is capable of modelling the correct crack orientation. DM3 and DM4 both show noticeable discrepancies with respect to CT scans, and it is notable that the inclusion of DLs in DM4 does not offer an improvement over DM3 when it comes to predicting damage patterns.

In all layers, DM5 predicts matrix cracking relatively well, although secondary matrix cracks in the $90°$ and $-45°$ ply are not predicted until the point of final failure. In particular, this causes a discrepancy in the overall crack pattern in the $90°$ ply. Crack predictions lag behind

experimental crack observations, at least in part attributed to the use of strengths that are too high. This is particularly noticeable in the $90°$ and $0°$ plies.

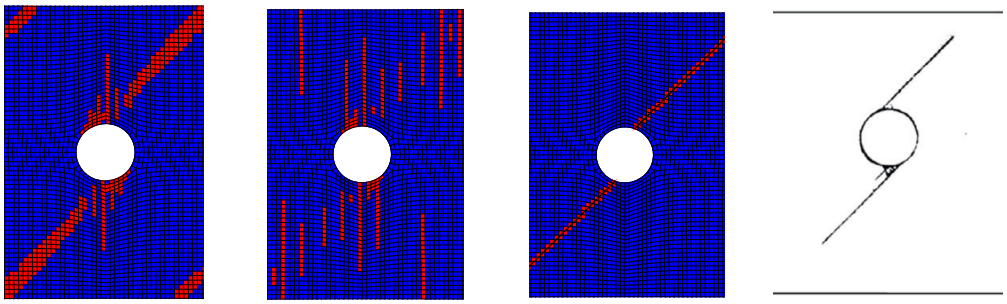

(a) DM3 **(b)** DM4 **(c)** DM5 **(d)** CT [73, p.886]

Figure 7.4: Progression of MF in $45°$ ply for $n = 2$ ply-blocked OHT test case at 80% of failure load (red and blue denote respectively damaged and undamaged elements)

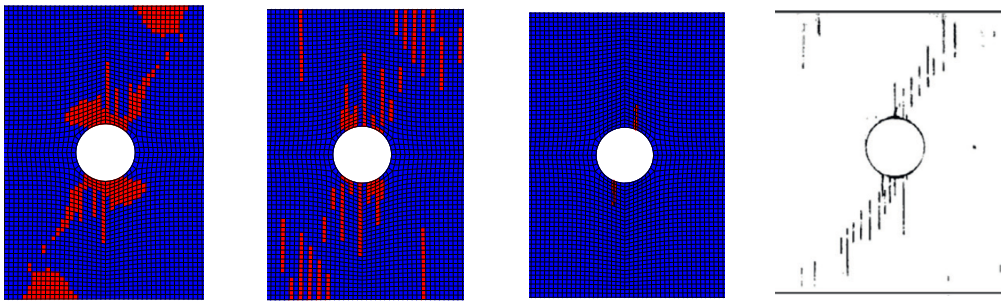

(a) DM3 **(b)** DM4 **(c)** DM5 **(d)** CT [73, p.886]

Figure 7.5: Progression of MF in $90°$ ply for $n = 2$ ply-blocked OHT test case at 80% of failure load (red and blue denote respectively damaged and undamaged elements)

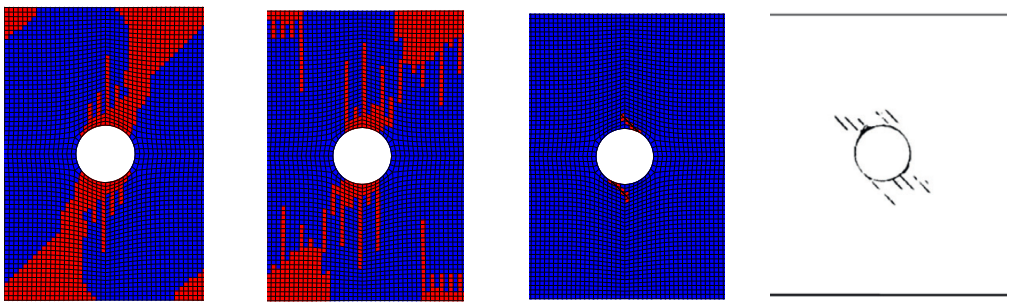

(a) DM3 **(b)** DM4 **(c)** DM5 **(d)** CT [73, p.886]

Figure 7.6: Progression of MF in $-45°$ ply for $n = 2$ ply-blocked OHT test case at 80% of failure load (red and blue denote respectively damaged and undamaged elements)

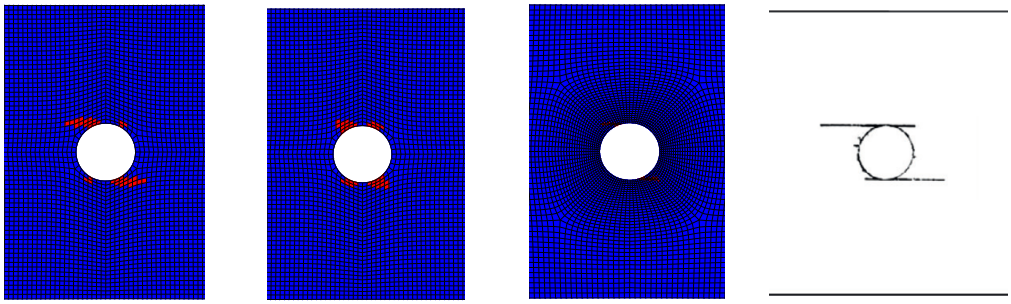

(a) DM3 **(b)** DM4 **(c)** DM5 **(d)** CT [73, p.886]

Figure 7.7: Progression of MF in $0°$ ply for $n = 2$ ply-blocked OHT test case at 80% of failure load (red and blue denote respectively damaged and undamaged elements)

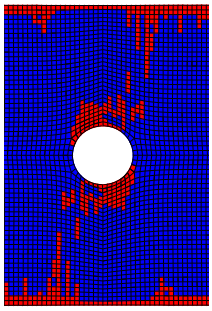

(a) DM4 **(b)** DM5

Figure 7.8: Progression of DL at $45°/90°$ interface for $n = 2$ ply-blocked OHT test case at 80% of failure load (red and blue denote respectively damaged and undamaged elements)

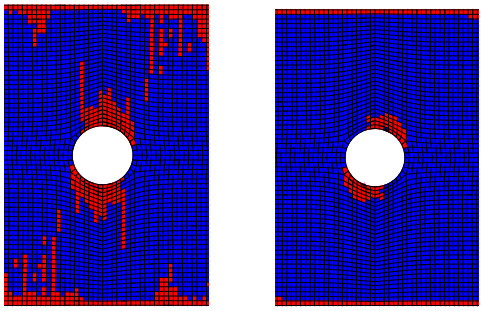

(a) DM4 **(b)** DM5

Figure 7.9: Progression of DL at $90°/-45°$ interface for $n = 2$ ply-blocked OHT test case at 80% of failure load (red and blue denote respectively damaged and undamaged elements)

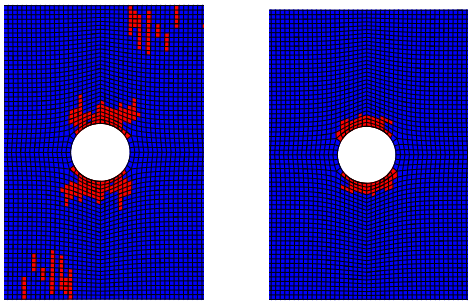

(a) DM4 **(b)** DM5

Figure 7.10: Progression of DL at $-45°/0°$ interface for $n = 2$ ply-blocked OHT test case at 80% of failure load (red and blue denote respectively damaged and undamaged elements)

Figures 7.8-7.10 show DL patterns for DM4 and DM5. Compared to the triangular pattern reported by Nixon-Pearson et al. [74], Van der Meer [11], Hallett et al. [79] and Green et al. [85], the pattern predicted by DM5 conforms decently. The $-45°/0°$ DLs are deemed relatively underpredicted for the $n = 2$ case. DM4 predictions are off, attributed to the fact that the specific DL pattern is the result of strong MF-DL interaction which is not captured well by the stress-strain based approach to MF.

To illustrate the effect of increasing ply thickness, Figure 7.11 shows DLs predicted by DM5 for the $n = 8$ case. The triangular DL patterns and extensive DLs reported by multiple authors [11, 74, 79, 85] are highly visible for this case. DM4 observations have been omitted since these are much the same as for the $n = 2$ case.

Overall, DM5, with a fracture mechanics based approach to MF and DLs, is capable of predicting local damage patterns decently. Damage patterns are reproduced to a much better extent than by DM3 and DM4, particularly concerning DLs. Still, crack predictions lag behind experimental observations, and damage patterns are not ideally reproduced.

The importance of evaluating multiple test cases has previously been shown. Strong conclusions should be based on a wide set of test cases, where experimental observations are key. In this light, there is a way to go when it comes to judging predictive capability.

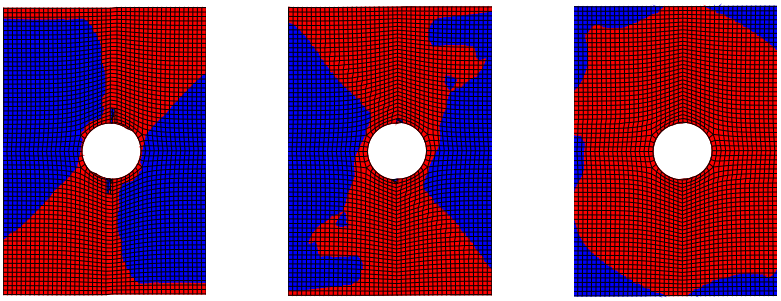

(a) $45° \ / \ 90°$ **(b)** $90° \ / \ -45°$ **(c)** $-45° \ / \ 0°$

Figure 7.11: Progression of DL for $n = 8$ ply-blocked OHT test case at failure, as predicted by DM5 (red and blue denote respectively damaged and undamaged elements)

7.3.4 Sensitivity study

A sensitivity study is conducted in order to substantiate the chosen parameters and illustrate the effect of choosing these differently for DM5. Sensitivity is conducted in the artificial or numerical components of the analysis, being mesh size, interface viscosity and interface stiffness. The sensitivity study is conducted on the case $n = 2$.

Mesh dependence

Figure 7.12 shows the failure strength for $n = 2$ for three mesh refinement ratios (50, 75 and 100 % the number of elements normalized with respect to the finest mesh) governing the mesh density in the finely meshed region of the hole. Variations are slight.

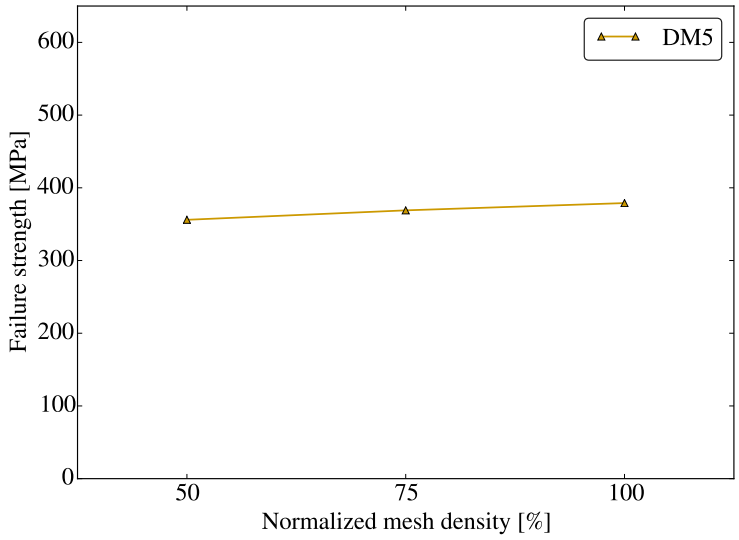

Figure 7.12: Predicted failure strength for $n = 2$ ply-blocked OHT test case, for various mesh densities

Interface viscosity

Increasing the artificial viscosity term leads to a delay in the failure process and is thereby ideally kept as small as possible. Figure 7.13 supports this conclusion, showing that results are less conservative for a higher viscosity, in line with general conclusions on artificial viscosity [9, 78]. A higher viscosity significantly relieves computational effort, expressed in Figure 7.13 in terms of the required number of increments to final failure (for the lowest viscosity 690 increments). It is readily apparent that a higher viscosity offers significantly improved computational efficiency, at comparable accuracy.

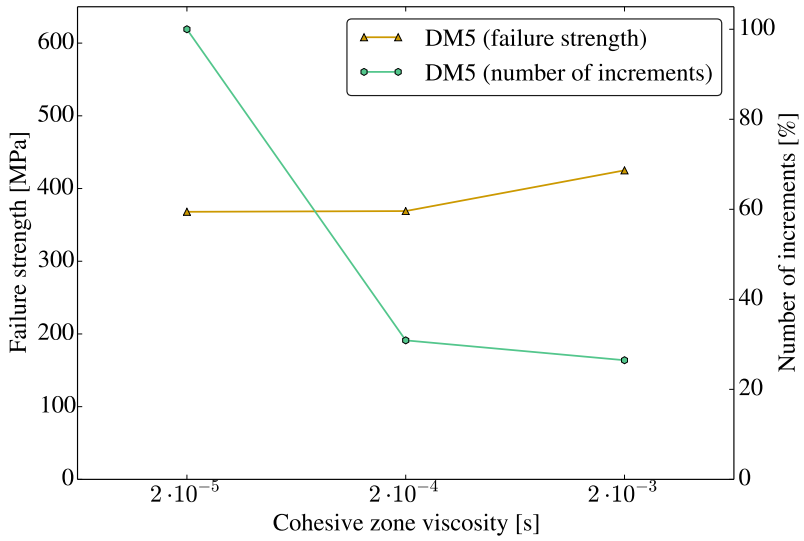

Figure 7.13: Predicted failure strength and required number of increments for $n = 2$ ply-blocked OHT test case, for various viscosity parameters (for both MF and DL modelling)

Interface stiffness

Past implementations of CZMs have shown that as long as the stiffness is high enough, the analysis is relatively insensitive to changes in interface stiffness. This is confirmed by running the analysis with a significantly smaller stiffness and a significantly larger stiffness, yielding variations in failure strength of less than 5 MPa and yielding identical failure patterns.

7.3.5 Convergence issues

In particular DM5 displays appreciable convergence issues. On one hand this is attributed to the CZM for DLs, and on the other hand to XFEM for MF modelling. The former is supported by the fact that DM4 displays overall consistent convergence difficulties throughout the analysis due to expansion of the DL region. Convergence issues for XFEM, on the other hand, occur less consistently throughout the analysis but can be severe enough to prematurely cause abrupt termination. These issues were particularly notable when layers were fully cracked and started developing secondary cracks.

For cases $n = 2$ and $n = 4$, the load drop at failure was not captured due to these issues. Still, predictions are deemed close to final failure in view of extensive damage visible particularly for $n = 2$. For $n = 4$, however, damage was not fully developed at the termination of the analysis.

Introducing artificial viscosity provides a powerful tool to mitigate convergence issues, although even with a large viscosity parameter the load drop at failure is difficult to capture consistently well. One option moving forward is the adoption of an explicit scheme, although drawbacks thereof have already been discussed in section 6.2.1, but development of a more robust convergence framework is proferred as a key recommendation.

7.4 Experimental validation with open-hole tensile tests

An experimental campaign has been conducted to validate the methodologies developed on a set of CFRP OHT specimens. Key motivation for this campaign is the need to compare to experimentally observed damage observations and failure loads.

This section commences with a description of the experimental campaign and proceeds with the modelling thereof. Thereafter, results are compared and discussed in relation to both global and local predictions.

7.4.1 Experimental campaign

The experimental campaign was conducted as follows, briefly outlined in terms of specimen manufacturing, testing, monitoring and general results. AE and DIC results are discussed in the subsequent section for a direct comparison to model predictions.

Specimen manufacturing

Six specimens have been manufactured from AS4/8552 unidirectional prepreg plies of 0.17 mm nominal thickness. Laminates were autoclave cured according to the cure cycle recommended by Hexcel [87]. Specimens have a total thickness of 2.7 mm, consisting of 16 plies in a [45° /

$-45° \ / \ 0° \ / \ 90°]_{2s}$ lay-up. Specimen dimensions are a length of 250 mm, a width of 25 mm and a hole diameter of 6.35 mm. Specimens were cut to size using a diamond cutting blade and holes were drilled using carbide drill bits. Specimens were labelled S01 to S08.

Testing procedure

Specimens were tested on a 60 kN MTS test bench, see Figure 7.14, loaded at a displacement rate of 1 mm/min. Six specimens were tested up to final failure.

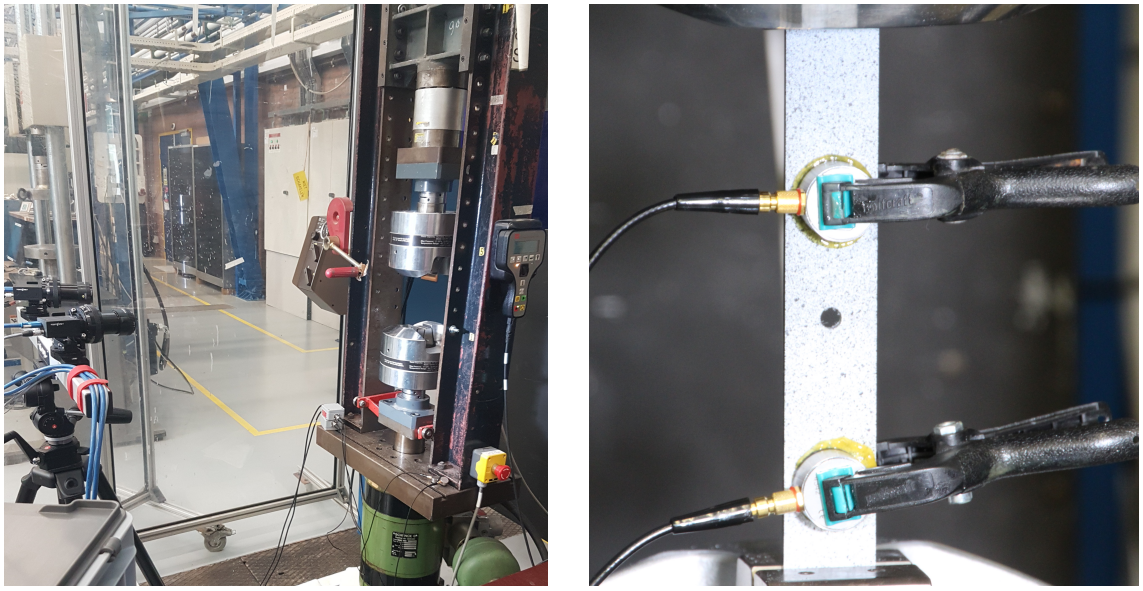

(a) DIC and test set-up **(b)** Specimen and AE sensor placement

Figure 7.14: Experimental set-up

Inspection procedure

In order to provide a complete assessment of the specimen state during loading, multiple inspection techniques have been employed. These are the following, discussed briefly.

Load-displacement monitoring Displacement was recorded directly from the test bench. Load was measured using a load cell, passed into DIC and AE systems to correlate measurements to the applied loading.

Digital Image Correlation Full-field strains were acquired using three-dimensional Digital Image Correlation (DIC). A Vic-3D Digital Image Correlation Measurement System was calibrated and used to capture deformation fields at the center of the specimen, in the vicinity of the hole, where damage is concentrated. Specimens were painted with a black-and-white speckle pattern to improve correlation quality. The set-up is shown in Figure 7.14a, consisting of dual camera's mounted and calibrated for a full-field image of the specimen near the hole.

Acoustic Emission Acoustic Emission (AE) was used to determine the number and severity of damage events during loading through amplified acoustic signals. AE is perfectly suited for

determining failure locations and damage processes during the entire loading sequence [88], whereas DIC only captures the displacement field and visible surface damage.

Two VS900-M piezoelectric sensors were placed on each specimen, greased for good attachment and conduction, see Figure 7.14b. Sensors were placed asymmetrically for the purpose of damage localization. Noise was filtered out by imposing a 60 dB threshold, determined as the signal strength without any loading. Sensor signals were preamplified and processed by a Vallen AMSY-6 instrument.

Experimental results

Experimental results are described hereafter. Firstly, load-displacement measurements and failure loads are presented. Secondly, damage observations are briefly discussed. A full overview of AE, CT and DIC observations is given in relation to the model predictions in section 7.4.3.

Load-displacement Final failure loads obtained for the six specimens tested up to failure are given in Table 7.1, including the Coefficient of Variation (CV). The results show limited scatter, reflected by the low coefficient of variation, around an average of 26.2 kN. Low variation indicates a consistent specimen and testing quality, in light of which the modelling assumption of initially undamaged specimens is deemed warranted.

Failure loads are extracted from load-displacement diagrams acquired from bench displacement and load cell measurements. Load-displacement relations are given in Figure 7.15.

Table 7.1: Experimental results for final failure

Specimen	Failure load [kN]	Failure stress [MPa]	CV [%]
1	26.06	386.1	
2	25.0	370.3	
3	26.27	389.1	
4	27.32	404.7	
5	27.04	400.6	
6	25.44	376.9	
Average	26.2	387.9	3.4

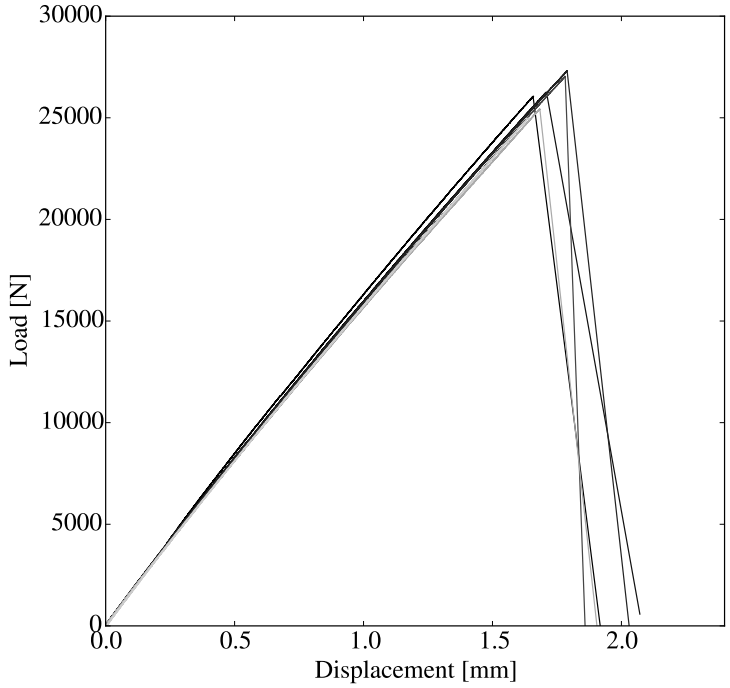

Figure 7.15: Experimental load-displacement curves

Damage observations The typical failure pattern is as depicted in Figure 7.16. All specimens exhibit exclusively this damage pattern, characterized by:

- Pull-out type failure. Fiber breakage at the ultimate load with extensive matrix cracking and DLs visible. FF is visible in the 0° plies along the net section.
- Significant matrix cracking along the fibers, from the hole edge spanning the width of the specimen. In particular, extensive matrix cracking can be observed in the outer $\pm 45^\circ$ plies.
- Fiber fracture in the 0° plies, from the hole edge spanning the width of the specimen, effecting a full separation of these plies.
- DLs, from the hole edge spanning the width of the specimen, in most of the layers.

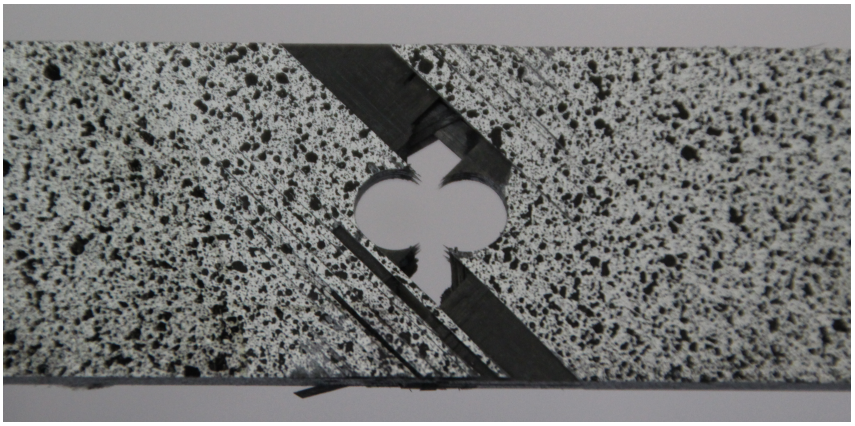

(a) Top view

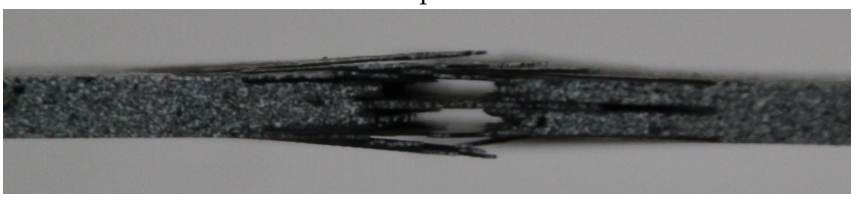

(b) Side view

Figure 7.16: Specimen failure pattern after ultimate (pull-out) failure

7.4.2 Test case modelling

A $[45°, -45°, 0°, 90°]_{2s}$ lay-up is modelled as eight layers of C3D8 elements, one per ply, with cohesive zones interspersed. Symmetry is only used in through-thickness direction in view of laminate symmetry. The laminate is clamped at one end, and a uniform axial displacement is applied at the other end, see Figure 7.17.

Material properties and model-specific parameters are given in Appendix E, along with the cohesive parameters. Orthotropic thermal expansion is assumed, with $\alpha_1 = 0.0\ °C^{-1}$ and $\alpha_2 = 3.0 \cdot 10^{-5}\ °C^{-1}$ [89] and $\Delta T = 160\ °C$ [87].

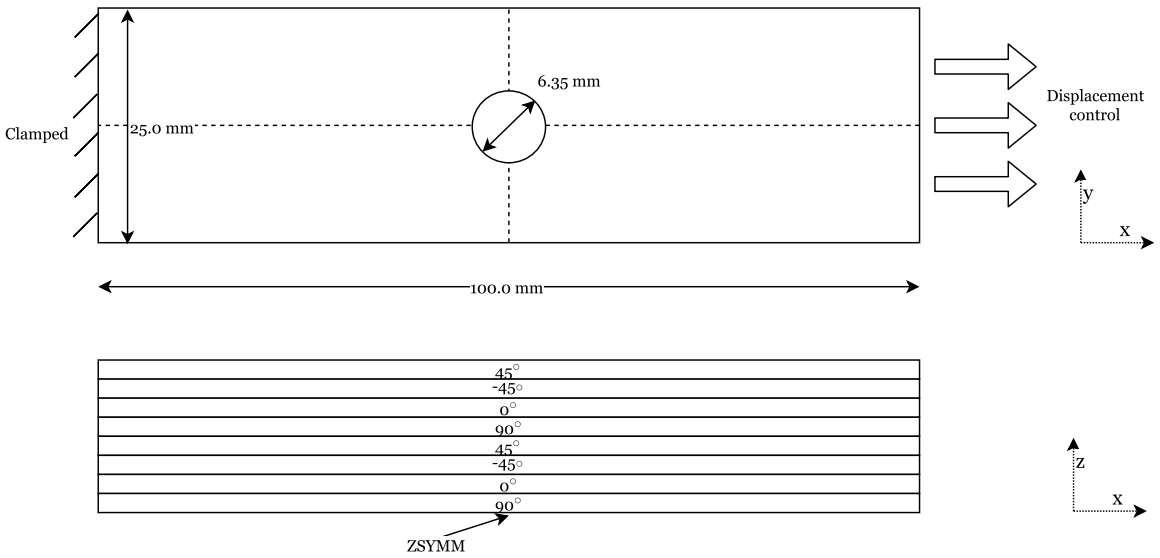

Figure 7.17: Schematic overview of experimental campaign CRFP OHT model

7.4.3 Results and discussion

As extensively argued before, both local and global damage assessments should be part of any well-formed conclusion on model predictive capability. To this end, this section commences with an evaluation of final failure loads, followed upon by validation of strain fields using DIC data, investigation of local damage patterns and finally a discussion on damage growth in relation to AE observations.

Final failure

Model predictions are compared to the experimental failure stress in Table 7.2 and to experimental load-displacement measurements in Figure 7.18, for DM3, DM4 and DM5. All models achieve good correspondence to the average experimental faillure load of 26.2 kN, corresponding to a failure stress of 388 MPa, errors to within 10 %. DM4 achieves slightly poorer correspondence than DM3 and DM5, attributed to a discrepancy in failure patterns particularly in terms of DLs.

These results support the tentative conclusions formulated earlier, namely firstly that DM3 is capable of achieving good correspondence for cases with limited DLs and secondly that DM5 offers a perspective on local failure more closely corresponding to reality that leads to overall good failure predictions.

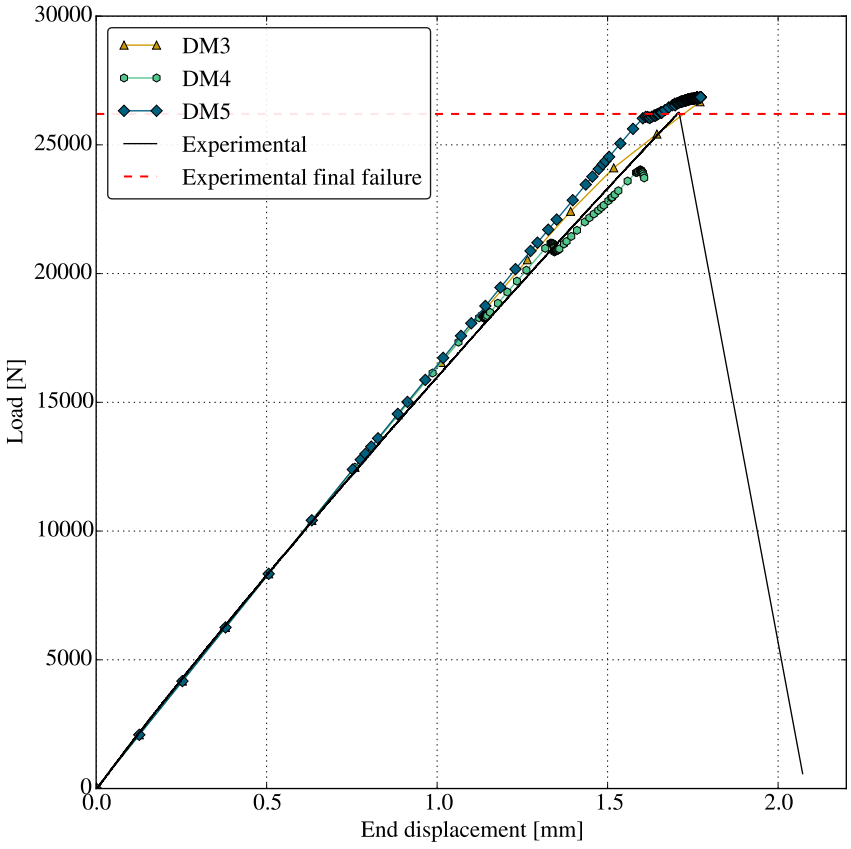

Figure 7.18: Predicted and typical experimental load-displacement curves

Table 7.2: Predicted and measured final failure stress for experimental case

Model	Predicted [MPa]	Discrepancy [MPa]	Discrepancy [%]
DM3	399.8	11.8	3.1
DM4	355.6	-32.4	-8.3
DM5	394.1	0.45	1.6

Strain field

Experimental observations are compared to model predictions in terms of strain maps at various percentages of the experimental failure load in Figures 7.19-7.21. DIC images show unchanging strain and displacement patterns for increasing loading, highly similar for each of the specimens tested. From this, it can be inferred that the strain distribution in the top layer is not noticeably altered by the presence of damage.

The scale is matched to DIC observations and values outside this range are marked in grey, to the end of clearly showing discrepancies and to provide a high contrast color map of the strains for both DIC observations and predictions. Duly note that all predictions have a grey region around the hole, since DIC is not able to determine strains directly at the hole edge (due to the absence of correlation points there).

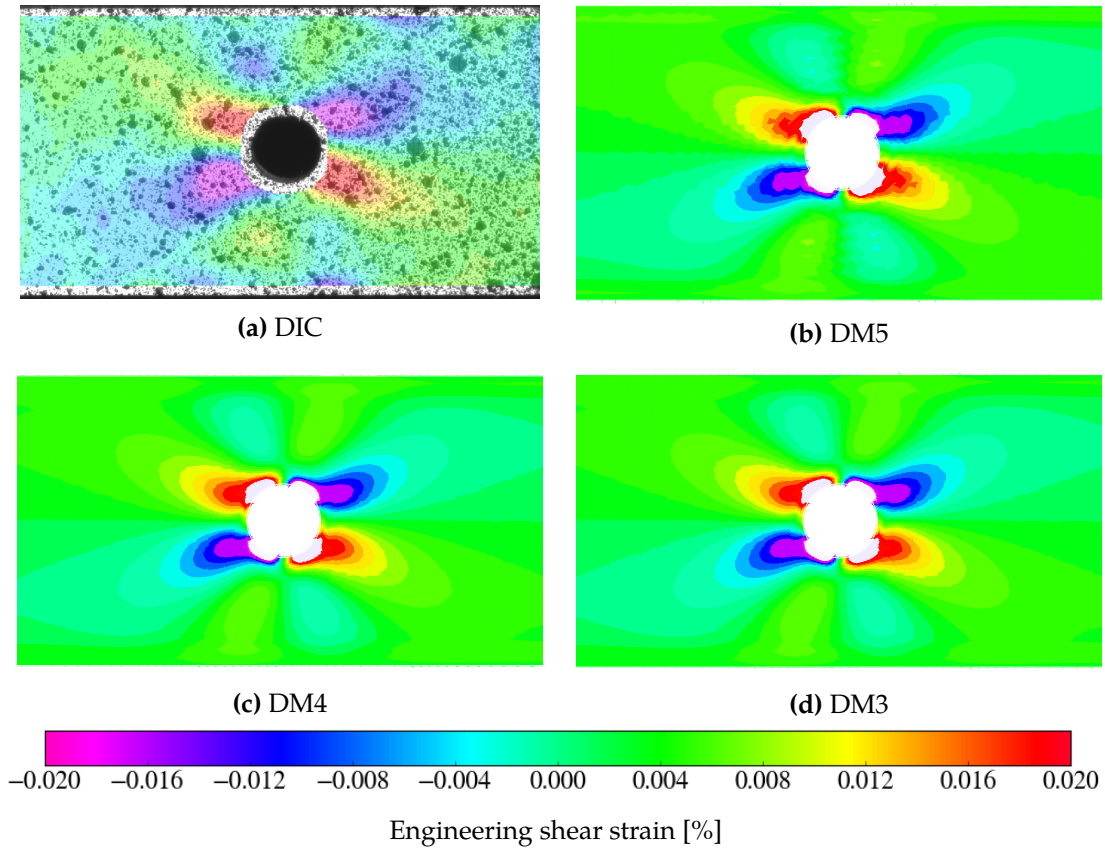

(a) DIC **(b)** DM5 **(c)** DM4 **(d)** DM3

Figure 7.19: Comparison of measured and predicted strain field at 10 % of failure load

Figure 7.19 shows the in-plane shear strain map at 10 % of the failure load as measured by DIC

and predicted by DM3, DM4 and DM5. It is readily apparent that the strain field in undamaged specimens is very well predicted, through the constitutive behaviour defined in the UMAT subroutine.

For increasing loads and thereby increasing damage, agreement becomes less good for DM3 and DM4. At 80 % of the failure load, DM3 and DM4 overpredict local strains, evidenced by the grey regions in Figure 7.20. DM5, on the other hand, is in good correspondence to the DIC image.

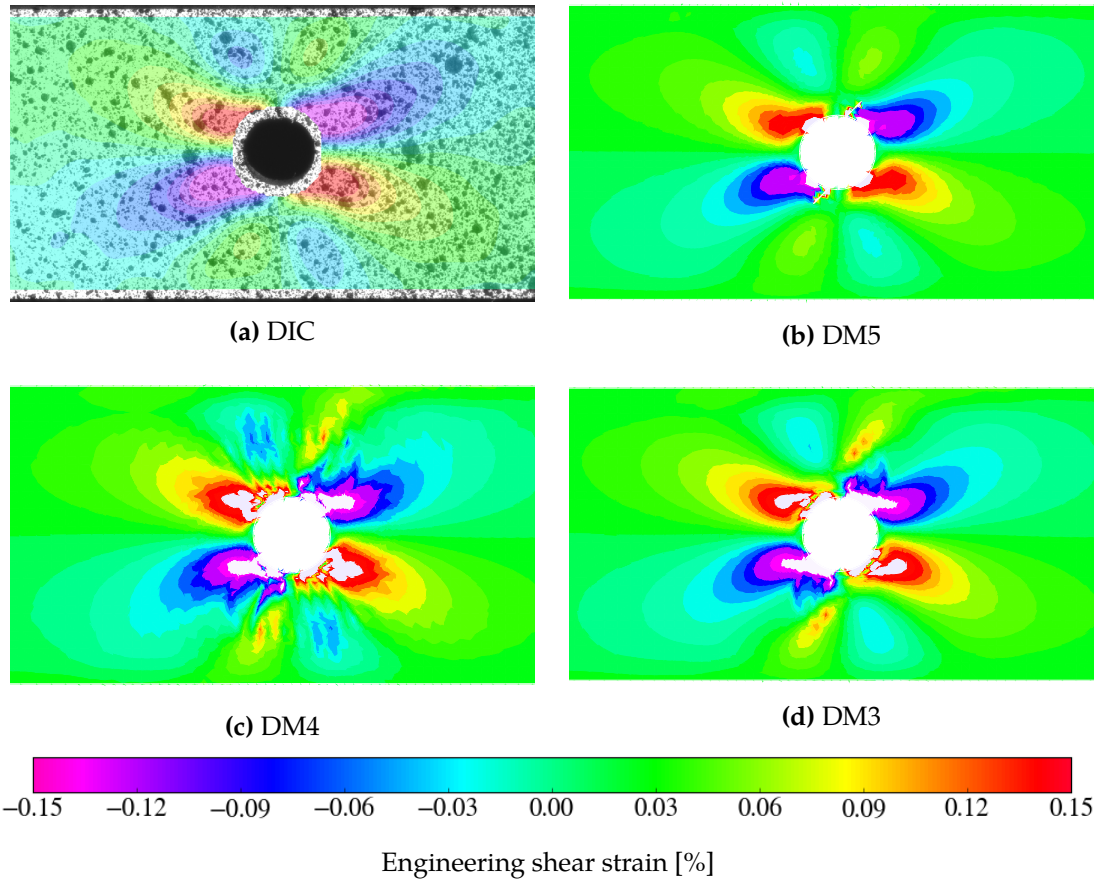

Figure 7.20: Comparison of measured and predicted strain field at 80 % of failure load

Close to final failure, Figure 7.21 shows that all models display discrepancies with respect to the DIC observations. For DM3 and DM4, this is most apparent as strains are predicted significantly higher. Strains are relatively well predicted by DM5. Still, the localization of strains at the crack developing in DM5 is not visible in the DIC image.

These are key observations, in particularly concerning DM3 and DM4. The unphysical nature of the smeared stiffness degradation inherent to stress-strain based models for PDA effects an altered strain field. This is not observed in DIC images, not even close to final failure where the specimen is significantly damaged. Contrary to these models, the discrete cracking in DM5 produces a strain field much more in line with DIC observations.

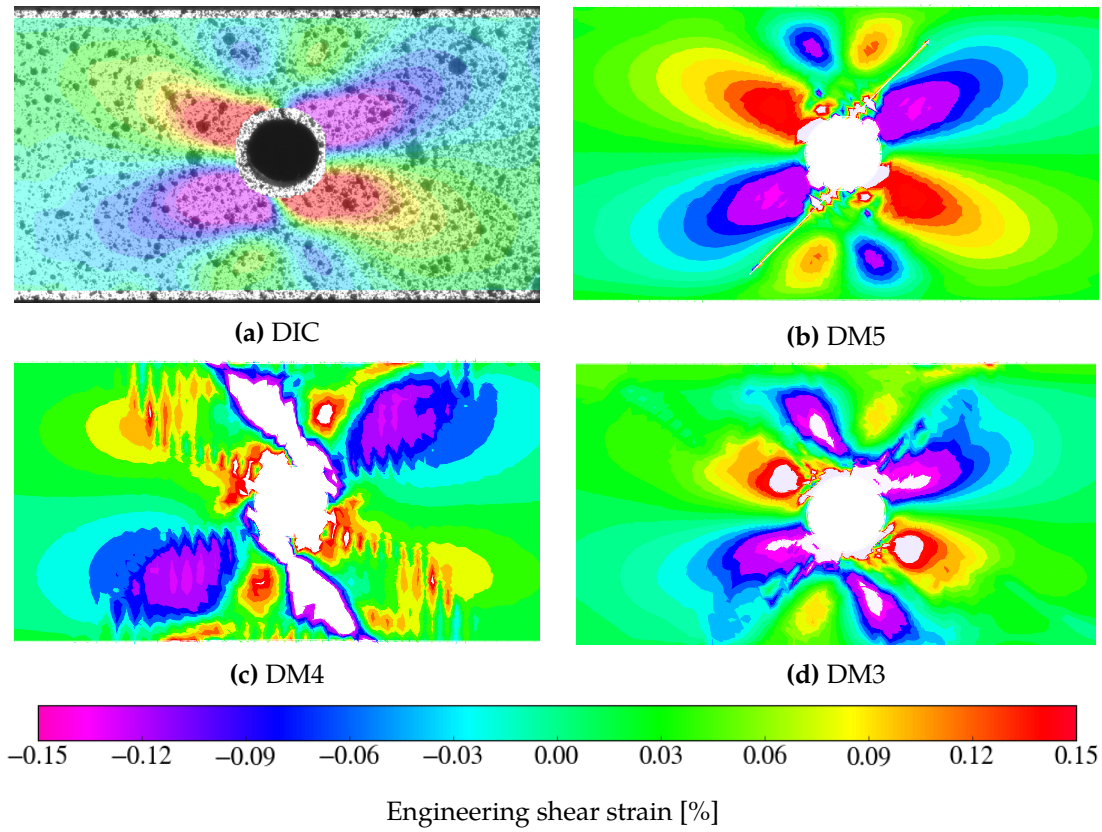

Figure 7.21: Comparison of measured and predicted strain field at 95 % of failure load

Damage patterns

Damage patterns are given in Figures 7.22-7.25 in terms of MF, and in Figures 7.26-7.29 in terms of DLs, at 90 % of the predicted failure load (in likeness to the previous study cases). Only the outer four plies and their interfaces are depicted, since the center plies show highly similar damage patterns. FF is only prevalent in the $0°$ plies, shown in Figure 7.30.

Figures 7.22-7.25 support previous observations, namely that both DM3 and DM4 do not always respect matrix crack orientation. This is particularly notable in the $-45°$ plies. Compared to these models, DM5 initially predicts lower crack advancement. Close to failure, contrary to the widespread damage predicted by DM3 and DM4, DM5 predicts rapid growth of cracks.

Figure 7.30 shows that FF grows in a narrow band from the hole towards the edges of the specimen, for all models considered. This is in line with the visual observations, identifying pull-out failure characterized by eventual FF in the $0°$ ply.

Figures 7.26-7.29 show that DLs progress from the hole edge. As loading increases, these form a roughly triangular DL pattern for DM5 as observed visually. For DM4, DLs originate much earlier and in a seemingly unrealistic pattern. This is attributed to the DL-MF interaction that is incorrectly modelled through the stiffness reduction, moreover yielding MF patterns that are off.

Overall, these observations underline that DM5 is the only model capable of correctly modelling crack orientation, although a precise judgment on the extent of damage predicted is difficult to make, particularly in the absence of detailed X-ray CT scans. Still, the failure patterns produced ostensibly conform to the observed damaged specimen state after ultimate failure.

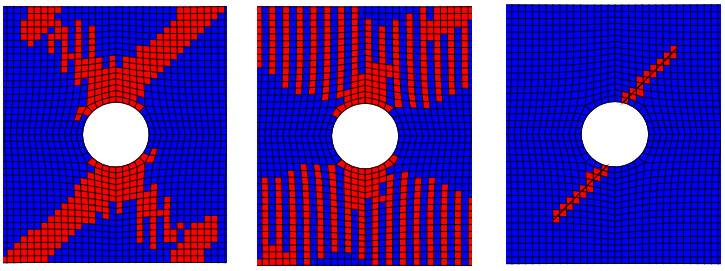

(a) DM3 **(b)** DM4 **(c)** DM5

Figure 7.22: Progression of MF in outer $45°$ ply for experimental test case at 90% of failure load (red and blue denote respectively damaged and undamaged elements)

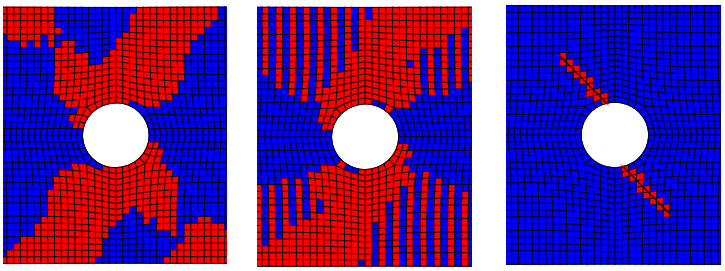

(a) DM3 **(b)** DM4 **(c)** DM5

Figure 7.23: Progression of MF in outer $-45°$ ply for experimental test case at 90% of failure load (red and blue denote respectively damaged and undamaged elements)

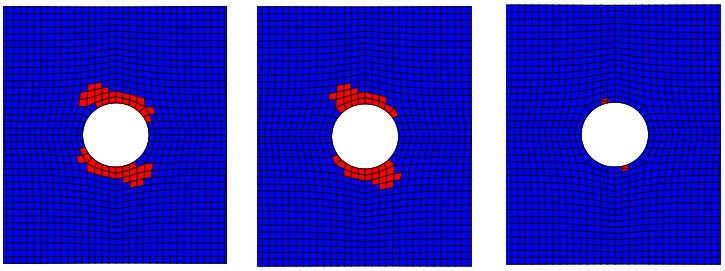

(a) DM3 **(b)** DM4 **(c)** DM5

Figure 7.24: Progression of MF in outer $0°$ ply for experimental test case at 90% of failure load (red and blue denote respectively damaged and undamaged elements)

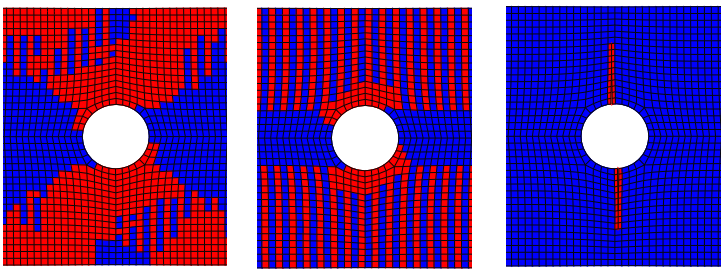

(a) DM3 **(b)** DM4 **(c)** DM5

Figure 7.25: Progression of MF in outer $90°$ ply for experimental test case at 90% of failure load (red and blue denote respectively damaged and undamaged elements)

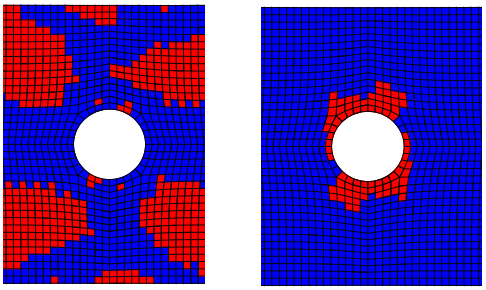

(a) DM4 **(b)** DM5

Figure 7.26: Progression of DL in outer $45°/-45°$ interface for experimental test case at 90% of failure load (red and blue denote respectively damaged and undamaged elements)

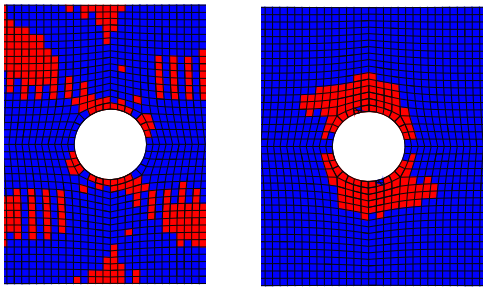

(a) DM4 **(b)** DM5

Figure 7.27: Progression of DL in outer $-45°/0°$ interface for experimental test case at 90% of failure load (red and blue denote respectively damaged and undamaged elements)

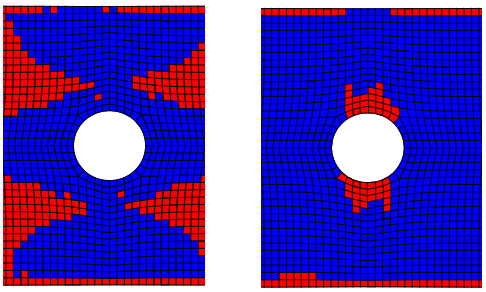

(a) DM4 **(b)** DM5

Figure 7.28: Progression of DL in outer $0°/90°$ interface for experimental test case at 90% of failure load (red and blue denote respectively damaged and undamaged elements)

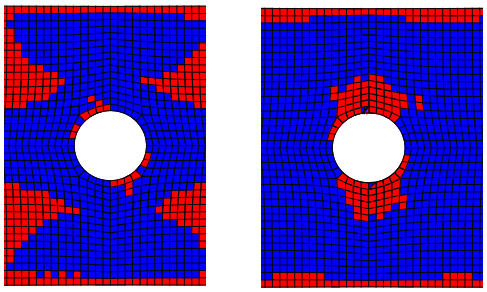

(a) DM4 **(b)** DM5

Figure 7.29: Progression of DL in outer $90°/45°$ interface for experimental test case at 90% of failure load (red and blue denote respectively damaged and undamaged elements)

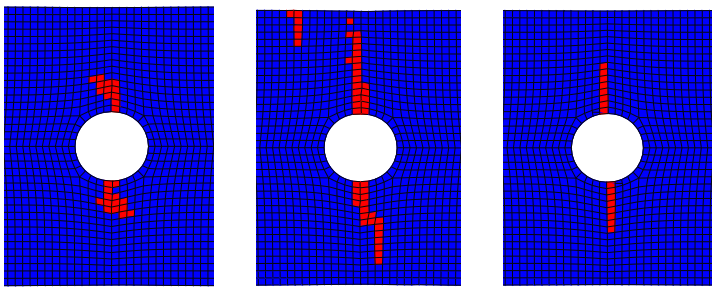

(a) DM3 **(b)** DM4 **(c)** DM5

Figure 7.30: Progression of FF in outer $0°$ ply for experimental test case at final failure (red and blue denote respectively damaged and undamaged elements)

Damage growth

Predictions can be compared qualitatively to AE observations, although any conclusions are only made tentatively on the general trend of damage evolution. Quantitative comparison is substantially more difficult, due to the noise received by AE and the additional requirement of translation of element damage to energy release. Figure 7.31a shows that energy release starts at roughly 40 % of the failure load, developing initially at a relatively slow pace but at an increasingly high pace. This energy release is - to an extent - representative of the number of damage events, inferred from the strength of incoming signals. High energy signals are measured close to final failure, likely due to fiber fracture.

Model predictions are outlined in Figure 7.31b-7.31d, showing the percentage of damaged elements per damage mode. These are normalized, in order to highlight the rapidity of the damage growth (rather than the extent of damage), resulting in the damage patterns discussed previously. Any distinction between failure modes in the comparison to AE data is hardly justifiable, hence no such attempt is made.

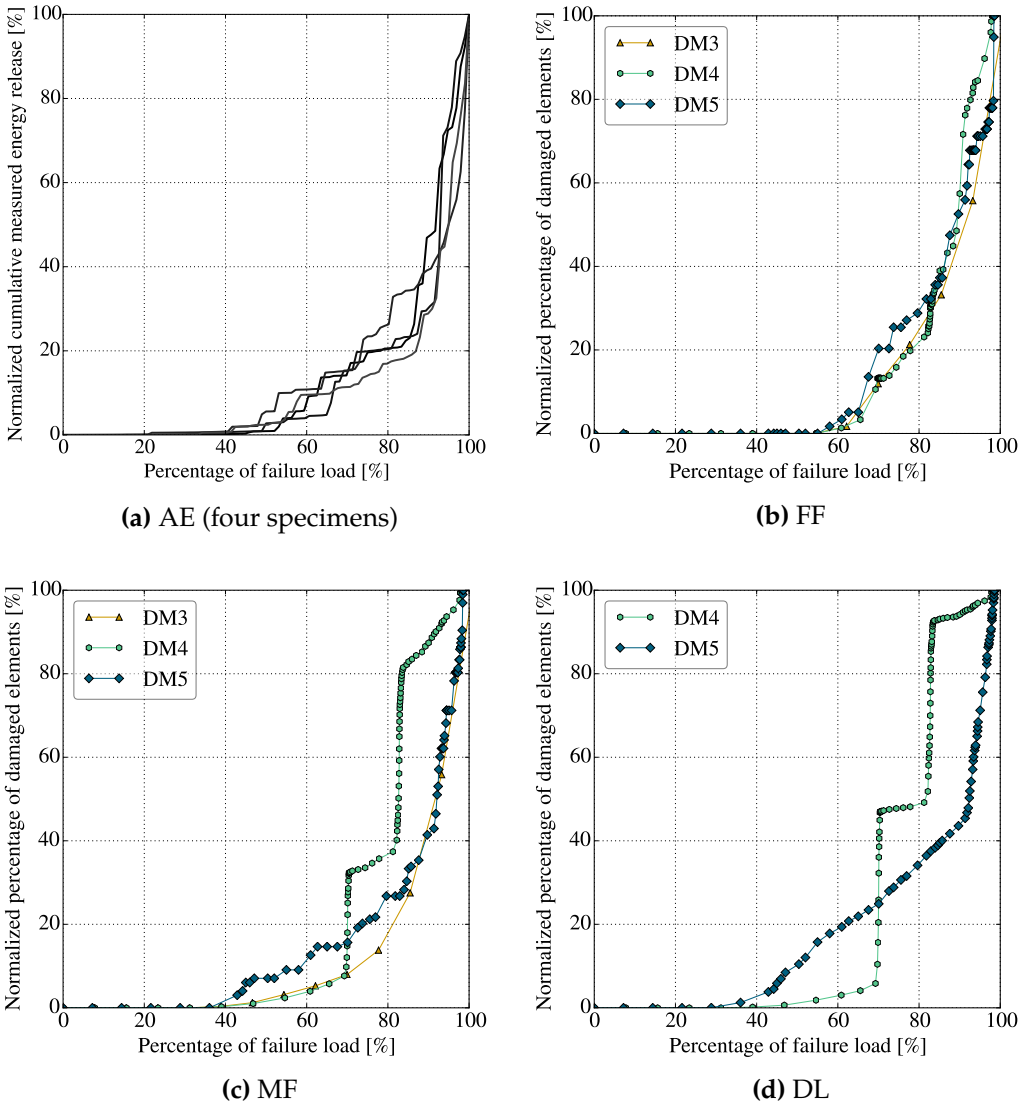

(a) AE (four specimens)

(b) FF

(c) MF

(d) DL

Figure 7.31: Predicted damage evolution experimental test case

Qualitative comparison shows decent agreement between the general trend of damage evolution between model predictions and AE data. Firstly, damage is initiated (at an initially slow rate) at 40 % of the failure load, predicted in the form of MF and DLs. Secondly, the increase in damage growth rapidity from roughly 80 % onwards is captured by all models.

Distinguishing between models is difficult in this qualitative comparison. Still, the steep increase in MF and DL at 70 % and 80 % of the failure load predicted by DM4 is not distinctly visible in AE measurements. This can be linked to the unrealistic damage patterns observed earlier, the jump at 70 % corresponding to extensive $0°/90°$ and $90°/45°$ DL coupled with significant MF in $90°$ and $45°$ plies, and the jump at 80 % to extensive $-45°/0°$ and $45°/-45°$ DL coupled with significant MF in $\pm 45°$ plies.

7.5 Conclusions and recommendations

A blended method has been developed using a stress-strain based approach to FF, modelling MF using cohesive elements inserted by XFEM on the basis of Puck initiation and modelling DLs through cohesive zones. This methodology is implemented in the form of a UMAT subroutine for material constitutive behaviour and FF modelling, complemented by a UDMGINI subroutine to initiate XFEM cracks to represent MF and cohesive zones pre-inserted at ply interfaces for modelling DLs. Use of XFEM for modelling matrix cracks yields significantly greater versatility than would be obtained by pre-inserted cohesive interfaces, relying on prior, accurate knowledge of crack locations.

The developed methodology has been validated on a set of ply-blocked laminates displaying DL driven failure, yielding the following conclusions:

- The blended method is much better able to capture the size effect inherent in ply-blocked laminates, related to the amount of DLs induced by interlaminar stiffness discontinuities, than the stress-strain based model. Even when complementing the stress-strain model by cohesive zones for DL modelling, this size effect is poorly represented and errors are significant.
- X-ray CT scans highlight the underlying reason. Only the blended method is well capable of modelling the dominant MF-DL interaction, exemplified by the resulting damage patterns. Stress-strain based models are not capable of modelling this interaction, resulting in failure patterns that are off.

An experimental campaign has been conducted to further validate the models developed. Six CFRP OHT specimens have been tested, using AE and DIC to assess damage growth and strain field representation respectively. This experimental campaign has led to the following conclusions:

- All models are capable of predicting final failure with good accuracy, errors within 10 % of the experimental average failure load.
- DIC observations of the local strain field contradict stress-strain based models in the sense that smeared stiffness degradation is imperceptible, up to the point of final failure.
- Damage patterns are well predicted by the blended model, showing correspondence to the main failure mechanisms of pull-out failure observed experimentally. Stress-strain models show poorer correspondence.
- AE observations show good qualitative correspondence of the measured energy release to model predictions of damage growth.

In spite of the promising results, there are still issues that require addressing. Recommendations are the following:

- Making the blended method and the convergence framework more robust. Cohesive zones for DL modelling cause consistent difficulty in convergence, whereas the XFEM implementation of MF can sporadically cause abrupt divergence.
- Investigating the use of parameters for MF modelling. In-situ strengths are not fully valid and predicted matrix crack lag behind experimental observations. Still, adopting non in-situ strengths showed deviating failure patterns and premature matrix crack development, already significant due to thermal loading.
- Validation on a more extensive set of test cases covering a variety of loading, material and geometry configurations, accompanied by detailed data (such as X-ray CT scans) on local damage patterns.

Chapter 8

Conclusions and recommendations

PDA of FRPs has been investigated, evaluated and performed firstly on a stress-strain basis. The insight yielded thereby has pinpointed a number of shortcomings of stress-strain based methodologies and the state-of-the-art of PDA in general, partially addressed through blending with a fracture mechanics based approach in the form of CZM and XFEM for a more accurate representation of delaminations and matrix cracking. The developments made, and those proposed to further the state-of-the-art, are listed hereafter per key topic.

Constitutive modelling and fundamentals of failure

In terms of constitutive modelling and fundamentals of FRP failure the following conclusions are reached:

- A linear constitutive model allows accurate and versatile modelling of FRP constitutive behaviour. Spline fits, or a Hahn-Tsai fit, offer pragmatic means to model non-linearity, particularly pronounced in shear.
- The effect of ply thickness and embeddedness on observed strength is captured by the concept of in-situ strengths. Analytical determination based on slit crack analyses offer a versatile method to estimate in-situ strengths.
- FRP heterogeneity and anisotropy necessitate a mode-dependent approach to failure, on a mesolvel distinguished as matrix failure, fiber failure and delaminations.

A number of fundamental flaws is to be addressed, as per the following recommendations:

- Interaction effects between stress and strain in various directions are to be taken into account, to guide extrapolation of stress-strain curves, for which extensive multiaxial testing campaigns are recommended.
- The in-situ effect remains relatively unexplored, although effects can be pronounced, hence experimental campaigning and in-depth investigation of this phenomenon is recommended.
- A stochastic approach to failure, and composite behaviour in general, is recommended to capture the probabilistic nature of input data and failure processes.
- An overall lack of physical understanding of failure processes marks the current state-of-the-art, for which extensive testing and evaluation of failure on a micromechanical level are key recommended activities.

Stress-strain based methods

State-of-the-art stress-strain based methodologies have been critically reviewed and evaluated, on the basis of an extensive trade-off and a number of test cases from the First World-Wide Failure Exercise, distinguishing damage initiation and propagation models. A trio of models has been implemented in FEM, by means of a user subroutine (UMAT) in ABAQUS, and validated with respect to a number of case studies from literature. This has yielded the following insights:

- Significant advancements have been made to move away from heuristical propositions to more physically based theories. Still, a lack of physical understanding of failure processes shows through even in the state-of-the-art Puck and LaRC damage initiation criteria, and even more so in damage propagation models. Delamination modelling is particularly ill-treated by stress-strain arguments.
- Puck, LaRC05 and the more empirical Cuntze criteria offer significantly improved predictive accuracy over heritage criteria, such as Hashin and Hashin-Rotem criteria, for a number of test cases from the First World-Wide Failure Exercise.
- Stress-strain based methods offer an effective method to predict laminate global behaviour, for cases with few delaminations. In particular, bilinear softening for damage propagation, in conjunction with LaRC05 damage initiation, offers consistently accurate final failure predictions. McCarthy et al. and Camanho and Matthews propagation models, coupled to respectively Puck and Cuntze criteria, show less consistent accuracy.
- None of the stress-strain based models are capable of accurately predicting local failure patterns, due to the inherent flaw of not taking into account fiber-matrix microstructure and excessive damage smearing.

To address shortcomings, the following recommendations are made:

- Failure processes occur on a microlevel and evaluation on a mesolevel inherently fails to capture these accuracy. A micromechanical approach may be more appropriate, complemented by experimental campaigning.
- Validation on an increased number of test cases covering a variety of loading, geometry and material configurations is recommended. Although attempts have been made to include numerous configurations, full validation necessitates significantly more experimental campaigning.

Blended stress-strain and fracture mechanics method

To forego the heuristical basis that lies at the heart of stress-strain based damage propagation and supplement delamination modelling, fracture mechanics has been blended into the developed stress-strain model. Matrix cracks are modelled by cohesive segments inserted using XFEM on the basis of Puck initiation, and cohesive interface elements are used to model delaminations. This blended method shows the following characteristics:

- Due to XFEM implementation, high versatility in capturing matrix cracks wherever these originate and however these grow, contrary to implementations with pre-inserted cohesive interfaces for which accurate knowledge of crack locations is required.

- Significantly improved ability to capture matrix cracks correctly, enforced to grow along fibers and in close correspondence to experimental X-ray CT scans, and to DIC scans conducted on an experimental campaign.
- Capability to accurately predict failure, even in the presence of dominant matrix crack - delamination interaction.
- Limited mesh dependency, but strong convergence issues. Even with viscous regularization, severe convergence issues still cause abrupt termination in some cases.

Recommendations for improvement of the blended method are the following:

- A more robust convergence framework to alleviate the numerical issues of the blended method.
- Experimental and numerical investigation into strength and fracture toughness values for the cohesive models used, both for matrix crack and delamination modelling.
- As previously pointed out for stress-strain models, extensive validation based on experimental campaigning.

Publications

Thesis contents have been adapted into two scientific publications:

- One paper has been submitted to and is, at the time of writing, under review at the *Journal of Composite Materials*, centered around the evaluation, selection and practical FEM implementation of stress-strain based approaches for PDA of FRPs [90]. This covers Chapters 4, 5 and 6.
- A second paper is, at the time of writing, being prepared for submission to *Composite Structures*, centered around the proposed blended methodology for PDA of FRPs and validation thereof through the conducted experimental campaign [91]. This covers mainly Chapter 7 and parts of earlier Chapters (foremostly 4, 5 and 6), as well as a fracture mechanics perspective from [6].

Appendix A

Classical Laminate Theory

For the purpose of preliminary analysis, CLT is a powerful tool. It is capable of analysing a laminate consisting of unidirectional plies while obviating the extensive work of a FEM. It is associated, however, with the drawback of a limitation to two dimensions in its formulation. This Appendix gives an abridged overview of CLT and its use in the preliminary analysis. Firstly, the laminate stiffness formulation is addressed. This is followed upon by laminate stress and strain acquisition and concluded by ply stress and strain acquisition.

A.1 Equivalent laminate stiffness

The stiffness matrix can be formulated for each layer. The (compliance and) stiffness matrix for a single layer is calculated in CLT under the assumption of plane stress. The stiffness matrix is given as, for each layer [14]

$$\mathbf{Q} = \begin{bmatrix} \frac{E_1}{1-\mu_{12}\,\mu_{21}} & \frac{\mu_{12}E_2}{1-\mu_{12}\,\mu_{21}} & 0 \\ \frac{\mu_{12}\,E_y}{1-\mu_{12}\,\mu_{21}} & \frac{E_2}{1-\mu_{12}\,\mu_{21}} & 0 \\ 0 & 0 & G_{12} \end{bmatrix} \tag{A.1}$$

The in-plane stiffness and compliance matrix of the laminate can be found as the thickness-weighted average of layer stiffness matrices, that is [14]

$$\mathbf{C} = \frac{1}{H}\sum_{k=1}^{n} \mathbf{Q_k} t_k \tag{A.2}$$

for n layers indexed k with thickness t_k and total laminate thickness H.

For this purpose ply alignment needs to be taken into account. Since each ply can be oriented in a different direction, denoted by angle ζ, these need to be transformed to the laminate axis system through transformation matrix [14]

$$\boldsymbol{M}_\zeta = \begin{bmatrix} m^2 & n^2 & 2\,mn \\ n^2 & n^2 & -2\,mn \\ -mn & mn & m^2 - n^2 \end{bmatrix} \tag{A.3}$$

for

$$m = \cos(\zeta) \tag{A.4}$$

$$n = \sin(\zeta) \tag{A.5}$$

Hereby the ply stiffness matrices can be calculated in the laminate axis system through [14]

$$\mathbf{C_k} = \mathbf{M_k Q_k M_k^T} \tag{A.6}$$

to obtain the laminate stiffness matrix via Equation A.2. Inversion of this matrix yields the laminate compliance matrix, that is [14]

$$\mathbf{S} = \mathbf{C}^{-1} \tag{A.7}$$

A.2 Laminate stress and strain

For a global applied stress, laminate strain can be obtained through the laminate compliance matrix. That is, through [14]

$$\begin{bmatrix} \varepsilon_1 \\ \varepsilon_2 \\ \gamma_{12} \end{bmatrix}_{laminate} = \mathbf{S} \begin{bmatrix} \sigma_1 \\ \sigma_2 \\ \tau_{12} \end{bmatrix}_{laminate} \tag{A.8}$$

Central to the use of CLT is the assumption that all layers are equally strained, such that laminate strain corresponds to ply strain.

A.3 Ply stress and strain

The laminate stress and strain are defined in the laminate axis system. To define these in the principal axis system of each ply, another transformation over ply angle φ is in order. Ply strains are then obtained as [14]

$$\begin{bmatrix} \varepsilon_1 \\ \varepsilon_2 \\ \gamma_{12} \end{bmatrix}_{ply} = (\mathbf{M_k^T})^{-1} \begin{bmatrix} \varepsilon_1 \\ \varepsilon_2 \\ \gamma_{12} \end{bmatrix}_{laminate} \tag{A.9}$$

Ply stresses in the ply axis system can be obtained from ply strains through use of the layer stiffness matrix $\mathbf{Q_k}$, i.e. [14]

$$\begin{bmatrix} \sigma_1 \\ \sigma_2 \\ \tau_{12} \end{bmatrix}_{ply} = \mathbf{Q_k} \begin{bmatrix} \varepsilon_1 \\ \varepsilon_2 \\ \gamma_{12} \end{bmatrix}_{ply} \tag{A.10}$$

Appendix B

Experimental determination of strength and fracture toughness

Evaluating failure inherently involves a comparison of the actual state with respect to a failure threshold. From the perspective of stress and strain, strengths fulfill this role of maximum allowable. For fracture mechanics, fracture toughness characterization is key. This Appendix gives an abridged overview of material parameter determination.

B.1 Strength characterization

Uni-axial testing is the predominant method for obtaining stress-strain curves and extracting (directional) material stiffnesses, Poisson's ratio's and strengths [14]. Inherent loss of uni-axial testing is the interaction between various strains, an effect that can be pronounced [29, 45]. Tests for properties in various directions are as follows

B.1.1 In-plane tensile properties

In-plane tensile properties are determined by loading (unidirectional laminate) coupons to failure under uniaxial tension (following the ASTM D3039M-14). Axial and transverse strains are recorded by strain gauges to yield the normal stress-strain curves in longitudinal and transverse directions. [14]

B.1.2 In-plane compressive properties

Longitudinal and transverse compressive strength are commonly determined using the IIT Research Institute fixture (following ASTM D3410M-16). Global buckling and end crushing make this a notoriously difficult test. [14]

B.1.3 In-plane shear properties

For determination of in-plane shear properties a number of test methods is used, the first being uniaxial tension on an eight-ply $[\pm 45^\circ]_{ns}$ coupon (following ASTM D3518M-13), the second the 10° off-axis test, the third the rail shear test (following ASTM D4255M-15) and the fourth the torsion test. [14]

B.1.4 Through-thickness tensile and compressive properties

Similar to in-plane uniaxial tension and compression through-thickness properties are determined, although specimens differ. These are waisted blocks or straight-sided blocks with square or rectangular cross-section. [14]

B.1.5 Through-thickness shear properties

Through-thickness shear properties can be determined by a modified Iosipescu impact V-notch specimen under shear. [14]

B.2 Fracture toughness characterization

The resistance to DL is captured in the fracture toughness [11]. The fracture toughness signifies the energy release rate corresponding to crack propagation [11, 14, 29]. Three modes are distinguished with separate fracture toughnesses: mode I (tensile opening), II (in-plane shear) and III (out-of-plane shear) [11]. Methods to determine these are the following.

B.2.1 Mode I

A Double Cantilever Beam (DCB) specimen (following ASTM D5528-13) is most often used to determine the mode I fracture toughness. An initial crack with Teflon insert is subjected to a tensile opening force applied through piano hinges. [14]

B.2.2 Mode II

The End-Notched Flexure (ENF) test can be used to determine the mode II fracture toughness. The (DCB) specimen is loaded in three- or four-point bending and mode II fracture toughness is extracted from three data points on the load-deflection curve. Mode I and II fracture toughnesses can also be determined by mixed-mode testing, combining DCB and ENF tests following ASTM D6671M-13. [14]

B.2.3 Mode III

Mode III fracture toughness is notoriously difficult to determine, although a singly split or doubly split DCB specimen or an Edge-Cracked Torsion (ECT) test offers possibilities. By lack of standardisation and proven test methods, this fracture toughness is not readily available, however. [14] In fact, it is difficult to distinguish between mode II and III crack opening in practice and the fracture toughnesses are often combined in a shear mode fracture toughness [12].

Appendix C

Intralaminar damage initiation criteria: theory and equations

An abridged overview of the theory and equations underlying the considered damage initiation criteria is given in this Appendix, implemented in the preliminary CLT analysis and UMAT subroutine. For specific details, please see the original papers [15, 20–22, 42–45].

C.1 Hashin-Rotem

The first to make a real distinction in failure modes, Hashin and Rotem proposed the following failure criteria. These criteria, distinguishing MFT, MFC, FFT and FFC incited a surge of methods posed on a similar basis.

C.1.1 Matrix failure

Hashin and Rotem predict MFC and MFT by the following two equations respectively [22]

$$(\frac{\sigma_1}{X_C})^2 + (\frac{\tau_{12}}{S_{12}})^2 > 1 \tag{C.1}$$

and for MFT [4, 22]

$$(\frac{\sigma_1}{X_T})^2 + (\frac{\tau_{12}}{S_{12}})^2 > 1 \tag{C.2}$$

Sun et al. proposed an empirical modification to yield a criterion much like Puck's (in two dimensions) by accounting for the friction caused by the normal stress, although still not considering the fracture plane angle [37].

C.1.2 Fiber failure

FFT and FFC are predicted by the maximum stress criterion, i.e.

$$|\sigma_1| > |X| \tag{C.3}$$

with $X = X_T$ if $\sigma_1 > 0$ and $X = X_C$ if $\sigma_1 < 0$.

C.2 Hashin

In the wake of the Hashin-Rotem criteria, Hashin went on to propose failure criteria on the basis of failure mechanisms observed and stressing the need thereof. These are the following criteria, discussed subsequently for MF and FF.

C.2.1 Matrix failure

Hashin considers MFC if [43]

$$\frac{1}{Y_C}[(\frac{Y_C}{2S_{23}})^2 - 1](\sigma_2 + \sigma_3) + \frac{1}{4S_{23}^2}(\sigma_2 + \sigma_3)^2 + \frac{1}{S_{23}^2}(\tau_{23}^2 - \sigma_2\sigma_3) + \frac{1}{S_{12}^2}(\tau_{12}^2 + \tau_{13}^2) > 1 \tag{C.4}$$

and MFT if [4, 43]

$$\frac{(\sigma_2 + \sigma_3)^2}{Y_T^2} + \frac{\tau_{12}^2 + \tau_{13}^2}{S_{12}^2} + \frac{\tau_{23}^2 - \sigma_2\sigma_3}{{S_{23}}^2} > 1 \tag{C.5}$$

based on a fracture plane. Unable to properly predict the fracture plane angle, this angle will always be 45° for this criterion, irrepresentative of reality [43].

C.2.2 Fiber failure

The FFT criterion follows from a quadratic assumption, not physically based, as

$$(\frac{\sigma_1}{X_T})^2 + \frac{1}{S_{12}^2}({\tau_{12}}^2 + \tau_{13}^2) > 1 \tag{C.6}$$

and FFC is predicted by the same maximum stress criterion as for the Hashin-Rotem criterion [22], see Equation C.3.

C.3 Puck

The first truly physically based damage initiation model for FRPs was founded by Puck and Schürmann [42]. In particular, the MF criteria based on the Mohr-Coulomb fracture hypothesis for brittle materials have a sound physical basis.

C.3.1 Matrix failure

Puck proposed MF criteria on the basis of the Mohr-Coulomb hypothesis [45]. This hypothesis states that fracture is only influenced by the stresses acting on that fracture plane (also called the master fracture plane). In a plane stress state, the Mohr-Coulomb fracture criterion was applied with the stresses those in the fracture plane, see Figure C.1. Now, considering the fracture envelope depicted in this Figure, and on the basis of Mohr-Coulomb theory, Puck arrived at the following criterion for MFT [42]

$$\max_{-\frac{\pi}{2} \le \theta \le \frac{\pi}{2}} \sqrt{[(\frac{1}{Y_T} - \frac{p^t_{\perp\psi}}{R^A_{\perp\psi}})\sigma_n(\theta)]^2 + (\frac{\tau_{nt}(\theta)}{R^A_{\perp\perp}})^2 + (\frac{\tau_{n1}(\theta)}{S_{12}})^2} + \frac{p^t_{\perp\psi}}{R^A_{\perp\psi}}\sigma_n(\theta) > 1 \tag{C.7}$$

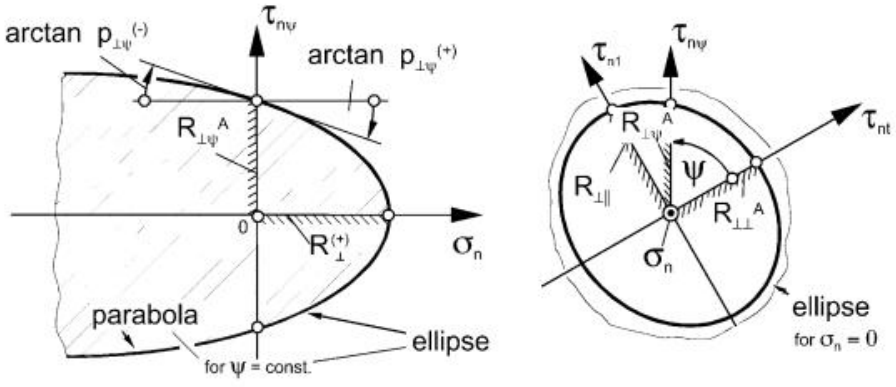

Figure C.1: Masture fracture body sections Puck failure theory, from [16, p.373]

Stresses on the fracture plane are calculated as [42]

$$\begin{cases} \sigma_n(\theta) = \sigma_2 \cos^2\theta + \sigma_3 \sin^2\theta + 2\tau_{23}\sin\theta\cos\theta \\ \tau_{nt}(\theta) = (\sigma_3 - \sigma_2)\sin\theta\cos\theta + \tau_{23}(\cos^2\theta - \sin^2\theta) \\ \tau_{n1}(\theta) = \tau_{31}\sin\theta + \tau_{21}\cos\theta \end{cases} \tag{C.8}$$

Moreover, parameters are defined as [16]

$$\frac{p^t_{\perp\psi}}{R^A_{\perp\psi}} = \begin{cases} \frac{1}{\tau^2_{nt}+\tau^2_{nl}}\left(\tau^2_{nt}\frac{p^t_{\perp\perp}}{R^A_{\perp\perp}} + \tau^2_{n1}\frac{p^t_{\perp\parallel}}{S_{12}}\right) & \text{if } \tau^2_{nt}+\tau^2_{nl} > 0 \\ 0 & \text{if } \tau^2_{nt}+\tau^2_{nl} = 0 \end{cases} \tag{C.9}$$

$$\frac{p^c_{\perp\psi}}{R^A_{\perp\psi}} = \begin{cases} \frac{1}{\tau^2_{nt}+\tau^2_{nl}}\left(\tau^2_{nt}\frac{p^c_{\perp\perp}}{R^A_{\perp\perp}} + \tau^2_{n1}\frac{p^c_{\perp\parallel}}{S_{12}}\right) & \text{if } \tau^2_{nt}+\tau^2_{nl} > 0 \\ 0 & \text{if } \tau^2_{nt}+\tau^2_{nl} = 0 \end{cases} \tag{C.10}$$

The following considerations for the strengths are relevant, the first two already implemented in the above equations [45]

- If solely a normal stress acts on the fracture plane, then the fracture resistance $R^{t\,A}_{\perp} = Y_T$ for unidirectional plies
- Shearing transverse-longitudinal to the fracture plane only affects fracture in this plane, hence $R^A_{\perp\parallel} = S_{12}$
- The transverse-transverse fracture resistance of the action plane is given by

$$R^A_{\perp\perp} = \frac{Y_C}{2(1+p^c_{\perp\perp})} \tag{C.11}$$

The inclination parameters are determined experimentally from the (σ_2, τ_{12}) fracture envelope. $p^c_{\perp\parallel}$ and $p^t_{\perp\parallel}$ are defined by the slope of the envelope, the former for a compressive σ_2 and the latter for a tensile σ_2, determined at $\sigma_2 = 0$. We can do so since $\theta_{fp} = 0°$ for both and hence we have $\sigma_n = \sigma_2, \tau_{n1} = \tau_{21}$. Direct experimental determination of $p^c_{\perp\perp}$ and $p^t_{\perp\perp}$ is not possible, although we can extract the former indirectly from a transverse compression test as [16]

$$p^c_{\perp\perp} = \frac{1}{2\cos^2\theta^c_{fp}} - 1 \tag{C.12}$$

with θ_{fp}^{c} the fracture angle in pure transverse compression. $p_{\perp\perp}^{t}$ or any of the other factors not experimentally determined are mostly chosen to be equal to the others [16]. Estimates for the slope parameters are given by Puck et al. [16] and Deuschle [13].

Let us consider that we can only find the fracture plane angle θ_{fp} iteratively for the general case, being the angle for which the left-hand side in Equation C.7 is maximum. Only in the case of plane stress we can find it explicitly if we assume a coupling between some of the experimental parameters

$$\frac{p_{\perp\perp}^{c}}{R_{\perp\perp}^{A}} = \frac{p_{\perp\parallel}^{c}}{S_{12}} = \frac{p}{R} = \text{constant} \tag{C.13}$$

The coupling is deemed acceptable from Puck's experience. Whilst there is no physical grounding for this coupling, there are no physical reasons against it [16]. A minor accuracy loss induced by this approximation is deemed acceptable in view of the significant amount of work reduction, obviating the iterative calculation of θ_{fp}. The angle of the fracture plane, θ, is then zero for matrix tension and on the basis thereof, we have a so-called Mode A matrix cracking. For this state of plane stress, MFT occurs if [45]

$$\sqrt{(\frac{\tau_{12}}{S_{12}})^2 + (1 - \frac{p_{\perp\parallel}^{t}}{Y_T})^2(\frac{\sigma_2}{R_{\perp\perp}^{A}})^2} + \frac{p_{\perp\parallel}^{t}}{S_{12}}\sigma_2 > 1 \tag{C.14}$$

Puck bases his criterion for MFC similarly on the Mohr-Coulomb fracture hypothesis [45]

$$\max_{\theta}(\frac{\tau_{nt}}{R_{\perp\perp}^{A} - p_{\perp\perp}^{c}\sigma_n})^2 + (\frac{\tau_{n1}}{S_{12} - p_{\perp\parallel}^{c}\sigma_n})^2 > 1 \tag{C.15}$$

and notes that for better agreement with experimental results this is to be adapted to [45]

$$\max_{\theta} \frac{\tau_{nt}^2}{(R_{\perp\perp}^{A})^2 - 2p_{\perp\perp}^{c}R_{\perp\perp}^{A}\sigma_n} + \frac{\tau_{n1}^2}{S_{12}^2 - 2p_{\perp\parallel}^{c}S_{12}\sigma_n} > 1 \tag{C.16}$$

In the absence of bi-axial experimental data he assumes a coupling

$$\frac{p_{\perp\perp}^{c}}{R_{\perp\perp}^{A}} = \frac{p_{\perp\parallel}^{c}}{S_{12}} = \frac{p}{R} = \text{constant}$$

based on experience [45], yielding MFC if (upon substitution in Equation C.16)

$$\max_{\theta}(\frac{\tau_{nt}}{R_{\perp\perp}^{A}})^2 + (\frac{\tau_{n1}}{S_{12}})^2 + 2\frac{p}{R}\sigma_n > 1 \tag{C.17}$$

The stresses on the fracture plane depend on the unknown fracture angle θ as given by Equation C.8. For a three-dimensional case, this angle is found by iteratively finding the angle for which the above factor is maximum. Note that Maimí et al. reduce the search for the fracture angle by allowing the fracture angle to take only one of two discrete values, $0°$ or $53°$, based on the premise that the fracture angle diminishes from approximately $53°$ to $40°$ and suddenly to $0°$ with increasing in-plane shear τ_{12} [10].

Cases where $\theta = 0°$ correspond to mode B fracture in which τ_{12} causes fracture; for $\theta \neq 0°$ mode C fracture occurs. In uniaxial tension, this angle is usually slightly higher than $45°$, reported by multiple authors [12, 21, 45]. This is slightly higher due to friction caused by compressive stress on the fracture surfaces, tending to oppose fracture, and this friction decreases with the fracture plane angle [15].

C.3.2 Fiber failure

Puck and Schürmann formulated their criteria on the premise of the maximum stress criterion and thereafter linking this to the tensile strength of a fibre embedded in a composite [42, 45]. Based on the assumption of equal strain in matrix and fibre, reasonable in view of the good bonding of these components, this yields FFT when [4, 42, 45]

$$\varepsilon_1 + \frac{\nu_{f12}}{E_{f1}} m_{\sigma f} \sigma_2 > \varepsilon_1^{tu} \tag{C.18}$$

Contrary to the previous criteria, this is a more physically-based criterion. A disadvantage is the additional required use of the mean magnification factor for the transverse stress for the fiber, although estimates of 1.3 for glass fibres and 1.1 for carbon fibres yield good results [45]. Moreover, it is a two-dimensional criterion. Fibre Poisson's ratio and elastic modulus are readily obtained from material data. Agreement is at the least not very different from the maximum stress and strain criteria, lying in between the predictions thereof [42].

We can consider a three-dimensional stress state as well, which adds an additional Poisson's contraction component to the axial strain in the fibers. This translates, via analogous derivation as by Puck [45], to a 3D criterion [92]

$$\varepsilon_1 + \frac{\nu_{f12}}{E_{f1}} m_{\sigma f} (\sigma_2 + \sigma_3) > \varepsilon_1^{tu} \tag{C.19}$$

if we assume that the Poisson's ratio is the same in 12 and 13 planes. This extension does not limit the validity of the equation, but merely extends it to cases where σ_3 is appreciable. The above form has been written in terms of ultimate strains in following the original formulation [45], although we can write it in terms of stresses as well [92].

In analogy to the treatment of FFT, Puck proposes a FFC criterion based on the maximum stress criterion but derived on a more physical basis. The derivation is analogous to that for FFT, difference lying in the fact that the compressive ultimate strength is now used, yielding that FFC occurs if [45]

$$|\varepsilon_1 + \frac{\nu_{f12}}{E_{f1}} m_{\sigma f} \sigma_2| > |\varepsilon_1^{cu}| \tag{C.20}$$

This would neglect, however, the shearing behaviour of FFC and Puck recognizes the shortcomings of this criterion [45]. To correct for this, Puck proposes a purely empirical correction for this shear interaction to yield

$$|\varepsilon_1 + \frac{\nu_{f12}}{E_{f1}} m_{\sigma f} \sigma_2| + (10\gamma_{12})^2 > |\varepsilon_1^{cu}| \tag{C.21}$$

The inclusion of this term casts some doubts as to the correctness of this criterion and strongly diminishes the physical basis, contrary to approaches taken in the formulation of the LaRC criteria for one [12, 21]. These criteria include a rigorous treatment of fiber kinking. Moreover, this is a plane stress criterion. Extension to a three-dimensional criterion can be done analogously to the case of FFT, but the empirical addition then becomes an issue. Without this addition, however, decent results have been obtained in the three-dimensional case through the criterion [3, 92]

$$|\varepsilon_1 + \frac{\nu_{f12}}{E_{f1}} m_{\sigma f} (\sigma_2 + \sigma_3)| > |\varepsilon_1^{cu}| \tag{C.22}$$

C.4 Cuntze

Cuntze describes damage on the basis of the FMC. Five modes are distinguished on the basis of material symmetry [44]. With each mode corresponding to one failure mechanism and one failure condition, each mode is governed by one strength. The criteria are then formulated on the basis of invariants, in analogy to Hashin's work [43].

Although five modes are distinguished, damage initiation is dictated by a mode interaction that activates based on all five modes [44]. Thereby, the damage criteria are interactive and evaluation takes place in all five modes simultaneously (although modes are evaluated independently). The interaction is based on a spring model, damage initiated if [93]

$$Eff_{\text{res}} = (Eff_{\text{mode 1}}^{m_{Cuntze}} + Eff_{\text{mode 2}}^{m_{Cuntze}} + Eff_{\text{mode 3}}^{m_{Cuntze}} + Eff_{\text{mode 4}}^{m_{Cuntze}} + Eff_{\text{mode 5}}^{m_{Cuntze}})^{\frac{1}{m_{Cuntze}}} \quad \text{(C.23)}$$

based on an empirically determined rounding-off exponent m_{Cuntze}. The maximum of the damage criteria for the five modes dictate the applicable damage mode. In these equations, the Eff variables denote the stress effort. If the resultant stress effort exceeds 1, damage is initiated.

C.4.1 Matrix failure

Cuntze distinguishes three modes for matrix failure. Although based on the same premise as Puck, Cuntze takes an empirical approach to formulate the criteria for these modes and poses the following criteria. For MFC the following criteria apply [93]

$$Eff_{\text{mode 1}} = \frac{(b_{\perp}^{\tau} - 1)(\sigma_2 + \sigma_3) + b_{\perp}^{\tau}\sqrt{\sigma_2^2 - 2\sigma_2\sigma_3 + \sigma_3^2 + 4\tau_{23}^2}}{Y_C} \quad \text{(C.24)}$$

$$Eff_{\text{mode 2}} = \sqrt{\frac{b_{\perp\parallel} I_{23-5} + \sqrt{{b_{\perp\parallel}}^2 I_{23-5}^2 + 4S_{12}^2(\tau_{31}^2 + \tau_{21}^2)^2}}{2S_{12}^3}} \quad \text{(C.25)}$$

and for MFT [93]

$$Eff_{\text{mode 3}} = \frac{(\sigma_2 + \sigma_3) + \sqrt{\sigma_2^2 - 2\sigma_2\sigma_3 + \sigma_3^2 + 4\tau_{23}^2}}{2Y_T} \quad \text{(C.26)}$$

where [93]

$$I_{23-5} = 2\sigma_2\tau_{21}^2 + 2\sigma_3\tau_{31}^2 + 4\tau_{23}\tau_{31}\tau_{21} \quad \text{(C.27)}$$

Herein a number of curve fitting parameters ($b_{\perp\parallel}$ and $b_{\perp\parallel}$) appear. Although estimates can be extracted, this requires statistical calibration based on an experimental failure envelope [44, 93]. In the absence of such data, these parameters are difficult to determine and rough estimates are to be made based on experience for similar materials. This highly limits the versatility of the Cuntze criteria.

C.4.2 Fiber failure

FFT and FFC are defined by maximum stress criteria, in two separate modes respectively as follows [93]

$$Eff_{\text{mode 4}} = \frac{\sigma_1}{X_T} \quad \text{(C.28)}$$

$$Eff_{\text{mode 5}} = \frac{-\sigma_1}{X_C} \quad \text{(C.29)}$$

C.5 LaRC03

In the wake of the Puck criteria [16, 45], the LaRC damage criteria for FRP composites [15, 20, 21] were developed. These are formulated in likeness to the Puck criteria, with a strong underlying physical basis. In particular, FFC is modelled on a more physical basis than with the previously considered maximum stress criteria.

C.5.1 Matrix failure

The LaRC03 criterion for MFT is modelled by an equivalent crack, a macroscopic representation of micromechanical matrix-fiber debonds [21]. In this formulation fracture mechanics was adopted to find an expression for crack initiation on the basis of stresses. For the assumption of plane stress, mode I and mode II fracture are considered whereas mode III is neglected due to the fact that it is impeded by fibers [33]. Linking the energy release rates to the stresses present, the following criterion is proposed as to their combined effect in determining MFT [4, 21]

$$(1-g)\frac{\sigma_2}{Y_T}+g(\frac{\sigma_2}{Y_T})^2+(\frac{\tau_{12}}{S_{12}})^2>1 \tag{C.30}$$

where g is a material constant determined as [21, 33]

$$g=\frac{\Lambda_{22}^0}{\Lambda_{44}^0}(\frac{Y_T}{S_{12}})^2 \tag{C.31}$$

for a thin embedded ply and

$$g=1.12^2\frac{\Lambda_{22}^0}{\Lambda_{44}^0}(\frac{Y_T}{S_{12}})^2 \tag{C.32}$$

otherwise.

Here [21, 33]

$$\Lambda_{22}^0=2(\frac{1}{E_2}-\frac{v_{yx}^2}{E_1}) \tag{C.33}$$

$$\Lambda_{44}^0=\frac{1}{G_{12}} \tag{C.34}$$

Notable is that the form of the criterion was proposed on the basis of glass- and graphite-epoxy systems and hence the interaction between modes I and II is not entirely physically based [33]. Moreover, let us consider that if $g=1$ (fracture toughnesses independent of loading mode) we attain the Hashin criterion for MFT (albeit using in-situ strengths). In practice, however, $g\approx 0.1$ for epoxy plies [33]. Computational effort for this criterion evaluation is limited, as opposed to Puck's criterion.

The LaRC03 criterion bases MFC similar to Puck on Mohr-Coulomb theory for brittle materials [21]. In fact, the two criteria display a number of similarities. Recasting Puck's criterion in the terminology used for LaRC03 yields MFC if [12]

$$\max_\alpha(\frac{\tau_T}{S_{23}-\eta^T\sigma_n})^2+(\frac{\tau_L}{S_{12}-\eta^L\sigma_n})^2>1 \tag{C.35}$$

whereas the LaRC03 criterion proposes [21]

$$\max_\alpha(\frac{\langle|\tau_T|+\eta^T\sigma_n\rangle^+}{S_{23}})^2+(\frac{\langle|\tau_L|+\eta^L\sigma_n\rangle^+}{S_{12}})^2>1 \tag{C.36}$$

adopting Macaulay brackets $\langle x \rangle^+ = max(0, x)$, noting that whereas Puck considers σ_n to increase effective strength (in view of sign of the friction coefficients), LaRC03 considers this to effect a decrease in effective shear stress [12]. The current implementation effects an overestimation of friction stresses, since the friction component is not corrected for the angle at which it acts [15]. Here the components acting on the fracture plane are (normal stress, transverse and longitudinal shear stress) [12, 21]

$$\begin{cases} \sigma_n = \sigma_2 \cos^2 \alpha \\ \tau_T = -\sigma_2 \cos \alpha \sin \alpha \\ \tau_L = \tau_{12} \cos \alpha \end{cases} \tag{C.37}$$

For the case of biaxial compression, Equation C.36 is evaluated in the misalignment frame. The angle thereof is found as described in the criterion for FFC and components acting on the fracture plane are transformed from the stresses in this misalignment frame as opposed to the ply axis system used in the above set of equations, in analogous fashion. Consequently, for biaxial compression MFC occurs if

$$\max_{\alpha}\left(\frac{\langle |\tau_T^m| + \eta^T \sigma_n^m \rangle^+}{S_{23}}\right)^2 + \left(\frac{\langle |\tau_L^m| + \eta^L \sigma_n^m \rangle^+}{S_{12}}\right)^2 > 1 \tag{C.38}$$

where

$$\begin{cases} \sigma_n^m = \sigma_2^m \cos^2 \alpha \\ \tau_T^m = -\sigma_2^m \cos \alpha \sin \alpha \\ \tau_L^m = \tau_{12}^m \cos \alpha \end{cases} \tag{C.39}$$

The threshold for biaxial compression is set at $|\sigma_1| > |Y_C|$, indicating moderate transverse compression. This threshold is based on experimental data, but is not extensively established [21].

Let us briefly review the notation of Puck and LaRC03 criteria, observing

$$\begin{cases} p^c_{\perp\perp} = \eta^T \\ p^c_{\perp\parallel} = \eta^L \\ \tau_{nt} = \tau_T \\ \tau_{n1} = \tau_L \\ R^A_{\perp\perp} = S_2 3 \\ R^A_{\perp\parallel} = S_1 2 \end{cases}$$

and hence the fact that the coupling assumed by Puck can also be written for the LaRC03 criterion, as adopted by Dávila et al. [21]

$$\frac{\eta^L}{S_L} = \frac{\eta^T}{S_T} \tag{C.40}$$

and the LaRC criteria gathers the friction coefficients from uniaxial testing in pure compression, with α_0 the angle of the fracture plane in that case [21]

$$\eta^T = \frac{-1}{\tan 2\alpha_0} \tag{C.41}$$

which allows us to attain the shear strength when considering the effective transverse shear at failure as [21]

$$S_2 3 = Y_C \cos \alpha_0 (\sin \alpha_0 + \frac{\cos \alpha_0}{\tan 2\alpha_0}) \tag{C.42}$$

thereby giving

$$\eta^L = \frac{-S_L \cos 2\alpha_0}{Y_C \cos^2 \alpha_0} \tag{C.43}$$

C.5.2 Fiber failure

For FFT, LaRC03 takes the pragmatic approach of the maximum stress criterion, see Equation C.3. This criterion is used for its good agreement in past implementations [21].

For FFC, a more physically based criterion is proposed on the basis of fiber kinking and matrix failure in the proximity thereof [21]. The LaRC03 criterion for FFC [21] takes a plane stress approach to a local region of waviness in fibers. In a three-dimensional setting, this is depicted in Figure C.2. At FFC, the stresses are expressed in the misalignment coordinate frame (superscript m) for misalignment angle φ as follows [21]

$$\begin{cases} \sigma_1^m = \cos^2\varphi\,\sigma_1 + \sin^2\varphi\,\sigma_2 + 2\cos\varphi\sin\varphi\,|\tau_{12}| \\ \sigma_2^m = \sin^2\varphi\,\sigma_1 + \cos^2\varphi\,\sigma_2 - 2\cos\varphi\sin\varphi\,|\tau_{12}| \\ \tau_{12}^m = -\cos\varphi\sin\varphi\,\sigma_1 + \cos\varphi\sin\varphi\,\sigma_2 + (\cos^2\varphi - \sin^2\varphi)|\tau_{12}| \end{cases} \tag{C.44}$$

and considering a case of axial compression wherein $\sigma_1 = -X_C$ and other stress components are zero. We then find, for the misalignment angle in pure compression φ_C, expressions for σ_2^m and τ_{12}^m. These are then substituted in the MFT and MFC criteria, expressed in the misalignment frame. Reason for this is that the matrix fails prior to the kinking, accommodating the latter.

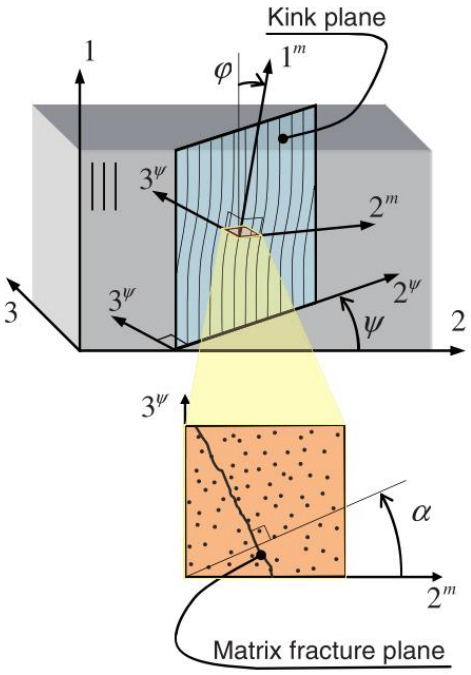

Figure C.2: Three-dimensional kink plane considered in LaRC criteria, from [20, p.2324]

The resulting equations are then solved for the misalignment angle [21]

$$\varphi_C = \tan^{-1}\frac{1 - \sqrt{1 - 4(S_{12}/X_C + \eta^L)(S_{12}/X_C)}}{2(S_{12}X_C + \eta^L)} \tag{C.45}$$

wherein the misalignment angle for pure compression features, solved for in the matrix failure criteria as [21]

$$\varphi = \frac{|\tau_{12}| + (G_{12} - X_C)\varphi_C}{G_{12} + \sigma_1 - \sigma_2} \tag{C.46}$$

under the premise of a linear elastic material. This is a limitation in view of shear nonlinearity of FRP composites.

This yields for the case of matrix tension ($\sigma_2^m \geq 0$) [4, 21]

$$\langle \frac{|\tau_{12}^m| + \eta^L \sigma_2^m}{S_{12}} \rangle^+ > 1 \tag{C.47}$$

and for the case of matrix compression ($\sigma_2^m < 0$) [4, 21]

$$(1-g)(\frac{\sigma_2^m}{Y_T}) + g(\frac{\sigma_2^m}{Y_T})^2 + (\frac{\tau_{12}^m}{S_{12}}) > 1 \tag{C.48}$$

the two criteria for FFC.

C.6 LaRC04

In many ways, LaRC04 is similar to LaRC03. It primarily extends the criteria to three dimensions and addresses overestimation of friction stresses in LaRC03.

C.6.1 Matrix failure

LaRC04 extended upon LaRC03 by inclusion of out-of-plane stresses, primarily component τ_{23} and moreover considering the non-linearity of shear to a greater extent through incorporation of Sandhu's strain energy failure concept [94]. As opposed to the plane stress state, mode III crack opening is now no longer neglected and instead mode II and mode III are combined in a shear mode. By similar reasoning as for LaRC03, but now considering this out-of-plane component and moreover the shear non-linearity, the following criterion is formulated for MFT [15]

$$(1-g)\frac{\sigma_2}{Y_T} + g(\frac{\sigma_2}{Y_T})^2 + \frac{\chi(\gamma_{12}) + \Lambda_{23}^0 \tau_{23}^2}{\chi(\gamma_{12}^u)} > 1 \tag{C.49}$$

where

$$g = \frac{\Lambda_{22}^0 (Y_T)^2}{\chi(\gamma_{12}^u)} \tag{C.50}$$

$$\Lambda_{23}^0 = \frac{1}{G_{23}} \tag{C.51}$$

$$\chi(\gamma_{12}^u) = \int_{\gamma_{12}^u} \tau_{12} \mathrm{d}\gamma_{12} \tag{C.52}$$

$$\chi(\gamma_{12}) = \int_{\gamma_{12}} \tau_{12} \mathrm{d}\gamma_{12} \tag{C.53}$$

This criterion is more accurate than LaRC03 in the sense that non-linearity is better addressed and moreover 3D behaviour is accounted for, on a similar basis as used in VCCT techniques [15]. Computational work is, however, greater, due to the integration required for the shear strain although this can be reduced depending on the representation of non-linearity, as for the Yamada-Sun criterion. Still, this criterion does not require the need to find a fracture plane angle as for Puck in 3D cases. Furthermore, the criterion obviates the need for the fitting parameters of Puck's criterion, making it more generally applicable.

In the LaRC04 formulation of MFC, the shortcoming in LaRC03 in relation to the friction was addressed by considering orthotropic friction, i.e. including the fact that only part of the normal stress σ_n induces friction [12, 15], to yield the following criterion

$$\max_{\alpha}(\frac{\tau_T}{S_{23}-\eta^T\sigma_n})^2+(\frac{\tau_L}{S_{12}-\eta^L\sigma_n})^2>1 \tag{C.54}$$

in exact correspondence to results obtained by Puck's criterion [15]. In fact, the equations are identical and to obtain the stresses on the fracture plane Equation C.8 can be used (replacing θ by α if we are to keep the notation as presented by the authors in LaRC presentation).

For the case of biaxial compression, that is $\sigma_1 < -Y_C$ (as in LaRC03), the above equation is evaluated in the misalignment frame, i.e. [15]

$$\max_{\alpha}(\frac{\tau_T^m}{S_{23}-\eta^T\sigma_n^m})^2+(\frac{\tau_L^m}{S_{12}-\eta^L\sigma_n^m})^2>1 \tag{C.55}$$

The procedure is analogous to that in LaRC03, although determining the misalignment frame orientation is different and the matrix stresses are obtained in a three-dimensional case, through [15]

$$\begin{cases} {\sigma_n}^m = \frac{\sigma_2^m+\sigma_3^\psi}{2}+\frac{\sigma_1-\sigma_2^\psi}{2}\cos 2\varphi+\tau_{12}^\psi\sin 2\varphi \\ {\tau_T}^m = -\frac{\sigma_2^m-\sigma_3^\psi}{2}\sin 2\alpha+\tau_{23}^m\cos 2\alpha \\ {\tau_L}^m = \tau_{12}^m\cos\alpha+\tau_{31}^m\sin\alpha \end{cases} \tag{C.56}$$

This is elaborated upon in the FFC criterion.

C.6.2 Fiber failure

The LaRC04 criteria follow as a generalization of the LaRC03 criteria, considering a 3D kinking plane [15]. Consequently, there is now an additional misalignment angle in the 23 plane, denote ψ, see Figure C.2. This additional angle is determined by arguing that the σ_3^ψ stress component in the 3D misalignment frame should be minimal, the σ_2^ψ component maximal. A negative stress σ_3^ψ would namely tend to close microcracks in planes other than the one at ψ, whereas σ_2^ψ tends to open microcracks within this plane. On the basis of microcracks being the initial cause for kinking through matrix failure, these assumptions are reasonable. Moreover, for the kinking to occur in a plane the τ_{23}^ψ component should be zero, supported by experiments [15].

This yields a condition for the out-of-plane misalignment angle

$$\tan 2\psi = \frac{2\tau_{23}}{\sigma_2-\sigma_3} \tag{C.57}$$

If the above considerations were not made, this angle would have to be determined iteratively (to maximimize the resulting failure criterion) at significant computational cost [15].

Within this plane we can then find the rotated stresses, that is [15]

$$\begin{cases} \sigma_2^\psi = \frac{\sigma_2+\sigma_3}{2}+\frac{\sigma_2-\sigma_3}{2}\cos 2\psi+\tau_{23}\sin 2\psi \\ \sigma_3^\psi = \sigma_2+\sigma_3-\sigma_2^\psi \\ \tau_{12}^\psi = \tau_{12}\cos\psi+\tau_{13}\sin\psi \\ \tau_{23}^\psi = 0 \\ \tau_{13}^\psi = \tau_{13}\cos\psi-\tau_{12}\sin\psi \end{cases} \tag{C.58}$$

and for constitutive relation

$$\tau_{12}^m = \tau_{12}^m(\gamma_{12}^m) \tag{C.59}$$

and the shear stress as given above, we can solve for the shear strain, relating the initial misalignment angle in the 2D plane φ_0 (due to e.g. manufacturing imperfections) and the shear strain (can be interpreted as an angle), to define the 2D misalignment plane as follows by solving iteratively [15]

$$\tau_{12}^m = \tau_{12}^m(\gamma_{12}^m) = \frac{-\sigma_1 - \sigma_2^\psi}{2} \sin 2(\varphi_0 + \gamma_{12}^m) + \tau_{12}^\psi \cos 2(\varphi_0 + \gamma_{12}^m) \tag{C.60}$$

to then obtain in-plane misalignment angle [15]

$$\varphi = \text{sgn}(\tau_{12}^\psi)\,(\varphi_0 + \gamma_{12}^m) \tag{C.61}$$

thereby gaining a full definition of the misalignment plane through (φ,ψ).

Next, for the case of matrix failure induced FCC or kinking (i.e. if the shear strain can be solved for), we can find the stresses in this kinking frame [15]

$$\begin{cases} \sigma_1^m = \frac{\sigma_1 + {\sigma_2}^\psi}{2} + \frac{\sigma_1 - \sigma_2^\psi}{2} \cos 2\varphi + \tau_{12}^\psi \sin 2\varphi \\ \sigma_2^m = \sigma_1 + \sigma_2^\psi - \sigma_1^m \\ \tau_{12}^m = -\frac{\sigma_1 - \sigma_2^\psi}{2} \sin 2\varphi + \tau_{12}^\psi \cos 2\varphi \\ \tau_{23}^{m\psi} = {\tau_{23}}^\psi \cos\varphi - \tau_{13}^\psi \sin\varphi \\ \tau_{13}^{m\psi} = {\tau_{13}}^\psi \cos\varphi \end{cases} \tag{C.62}$$

and plug these into the LaRC04 matrix failure criteria, again distinguishing uniaxial and biaxial compression cases. For matrix compression ($\sigma_2^m < 0$), $\alpha = 0$ for kinking to occur and FFC occurs if [4, 15]

$$\frac{\tau_{12}^m}{S_L - \eta^L \sigma_2^m} > 1 \tag{C.63}$$

For matrix tension ($\sigma_2^m \geq 0$), kink formation and FFC occur if [4, 15]

$$(1-g)\frac{\sigma_2^m}{Y_T} + g(\frac{\sigma_2^m}{Y_T})^2 + \frac{\Lambda_{23}^0[\tau_{23}^{m\psi}]^2 + \chi(\gamma_{12}^m)}{\chi(\gamma_{12}^u)} > 1 \tag{C.64}$$

FFT is predicted by the maximum stress criterion, see Equation C.3. This criterion was adopted for its good agreement in past implementations [15].

C.7 LaRC05

The latest installment of the LaRC criteria, LaRC05 is at the forefront of current damage initiation criteria and offers a solid physical basis much akin to Puck and LaRC03/04 criteria. MF and FF are predicted as follows by the LaRC05 criteria.

C.7.1 Matrix failure

For LaRC05, the crack treatment in LaRC04 is omitted in preference for a single expression indicating both MFC and MFT failure, distinguishing the cases by considering the normal traction opening a matrix crack if it is positive only [20]. The following criterion is proposed

$$\max_\alpha \; (\frac{\tau_T}{S_{23} - \eta^T \sigma_n})^2 + (\frac{\tau_L}{S_{12} - \eta^L \sigma_n})^2 + (\frac{\langle \sigma_n \rangle^+}{Y_T})^2 > 1 \tag{C.65}$$

Upon consideration of this expression for the case of MFT, i.e. $\sigma_n \geq 0$, we can notice a glaring similarity to Puck's proposition [45]. Finding the fracture plane angle again requires an iterative approach within the range of $0° - \alpha_0$, making the evaluation of this criterion computationally comparable to the Puck criterion.

C.7.2 Fiber failure

LaRC05 considers the same three-dimensional kinking plane as LaRC04, yet the kink band angle ψ is determined iteratively to maximize the left-hand side of the failure criterion rather than analytically through the considerations made in LaRC04 [20]. This increases the computational effort, while accuracy can be expected to increase.

The angle φ is found considering Equation C.61 and iteratively solving for φ_0

$$\varphi_0 = \varphi_C - \gamma(\frac{X_C}{2}\sin 2\varphi_0) \tag{C.66}$$

where the $\gamma()$ indicates the dependency of (in-plane) shear strain on the shear stress (argument). φ_C is given by Equation C.45. The stresses in the misalignment can then be determined to evaluate the failure criterion for FFC [20]

$$\max_{\psi} \ (\frac{\tau_{23}^m}{S_T - \eta^T \sigma_2^m})^2 + (\frac{\tau_{12}^m}{S_L - \eta^T \sigma_2^m})^2 + (\frac{\langle \sigma_2^m \rangle^+}{Y_T})^2 \tag{C.67}$$

Again, FFT is predicted by the maximum stress criterion of Equation C.3. A similar reasoning as for LaRC03 and LaRC04 is adopted.

Appendix D

WWFE-I test cases

This Appendix briefly describes the test cases of the first Worldwide Failure Exercise [2], used for two-dimensional PDA. Firstly, material properties used in the analysis are discussed. Secondly, test cases are outlined.

D.1 Material properties

In the first Worldwide Failure Exercise, four fiber/matrix combinations are used. Relevant properties are given in Table D.1, extracted from the instructions of the exercise [2]. For the E-Glass/LY556, strengths are taken based on experimental data in the plot of test case 1 [2], as given by Pinho et al. [15], for the improved agreement over the uniaxial data given in the instructions of the Exercise.

Table D.1: Material properties of the first Worldwide Failure Exercise test cases, adapted from [2] and [15]

	AS4/3501−6	T300/BSL914C	E-glass/LY556	E-glass/MY750
E_1 [GPa]	126	138	53.5	45.6
E_2 [GPa]	11	11	17.7	17.2
G_{12} [GPa]	6.6	5.5	5.83	5.83
ν_{12} [−]	0.28	0.28	0.278	0.278
X_T [MPa]	1950	1500	1140	1280
X_C [MPa]	1480	900	570	800
Y_T [MPa]	48	27	37.5	40
Y_C [MPa]	200	200	130.3	145
S_{12} [MPa]	79	80	66.5	73
ε_1^{tu} [%]	1.38	1.087	2.132	2.807
ε_1^{cu} [%]	1.175	0.652	1.065	1.754
ε_2^{tu} [%]	0.436	0.245	0.197	0.246
ε_2^{cu} [%]	2.0	1.818	0.644	1.2
γ_{12}^{u} [%]	2	4	3.8	4
E_{f1} [GPa]	225	230	80	74
ν_{f12} [GPa]	0.2	0.2	0.2	0.2

D.1.1 Stress-strain curves

For the purpose of in-situ strength estimation, a Hahn-Tsai polynomial is fitted to uniaxial test data [18]

$$\gamma_{12} = \frac{1}{G_{12}}\tau_{12} + \beta\tau_{12}^3 \tag{D.1}$$

A least squares fit of the above polynomial results in Figure D.1, for fit parameter β as in the plots. Good correspondence is achieved with Camanho et al. [29]. It is readily apparent that the Hahn-Tsai polynomial decently approximates the shear non-linearity for the materials considered. As compared to the spline fits hereafter, the Hahn-Tsai offers less accuracy as the spline is fit locally whereas the Hahn-Tsai is applied globally. However, the Hahn-Tsai polynomial is easier to handle and allows the formulation of analytical solutions taking into account shear non-linearity.

For the more general case, a spline fit is applied to the uniaxial test data by Kaddour et al. [2]. The order of the splines is particularly influential for the extrapolation of the stress-strain curves. This inter- and extrapolation, based on first order splines, is shown in Figure D.2. The extrapolation is subjectively done, in good agreement with extrapolation by Pinho et al. [20].

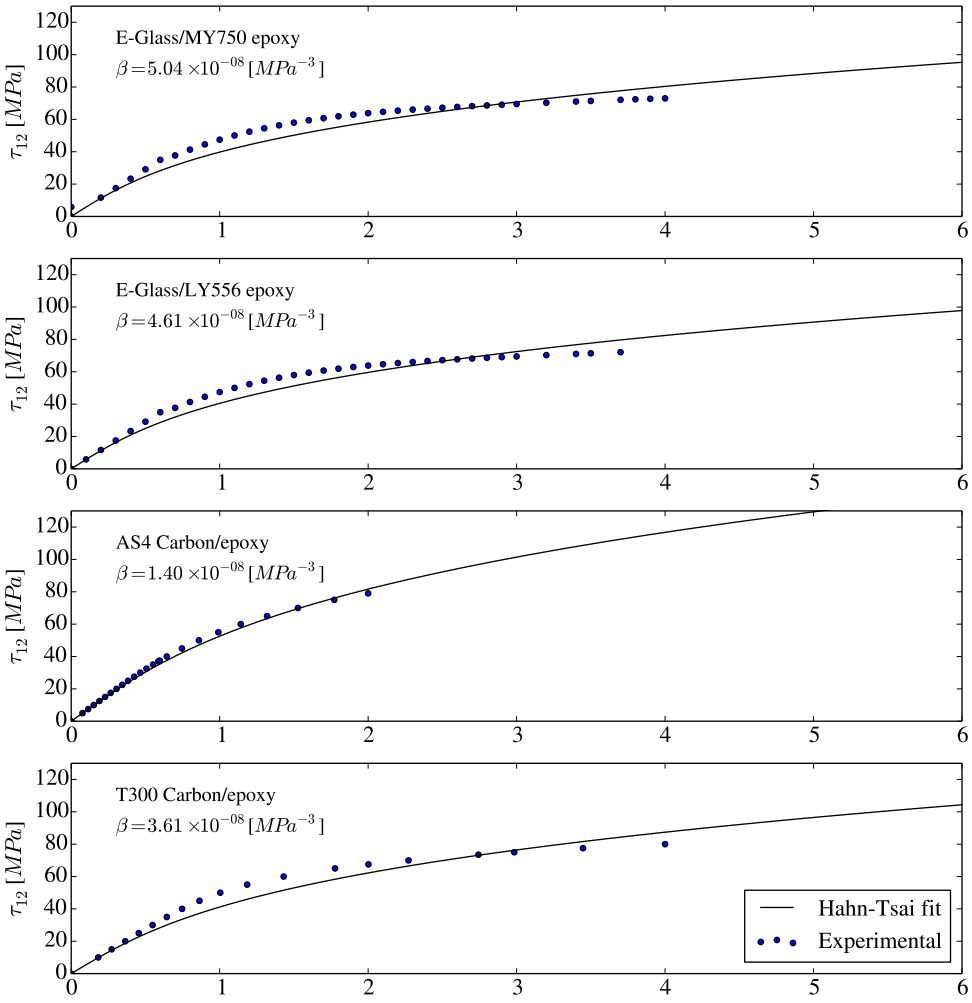

Figure D.1: Hahn-Tsai inter- and extrapolation of in-plane shear stress-strain curves

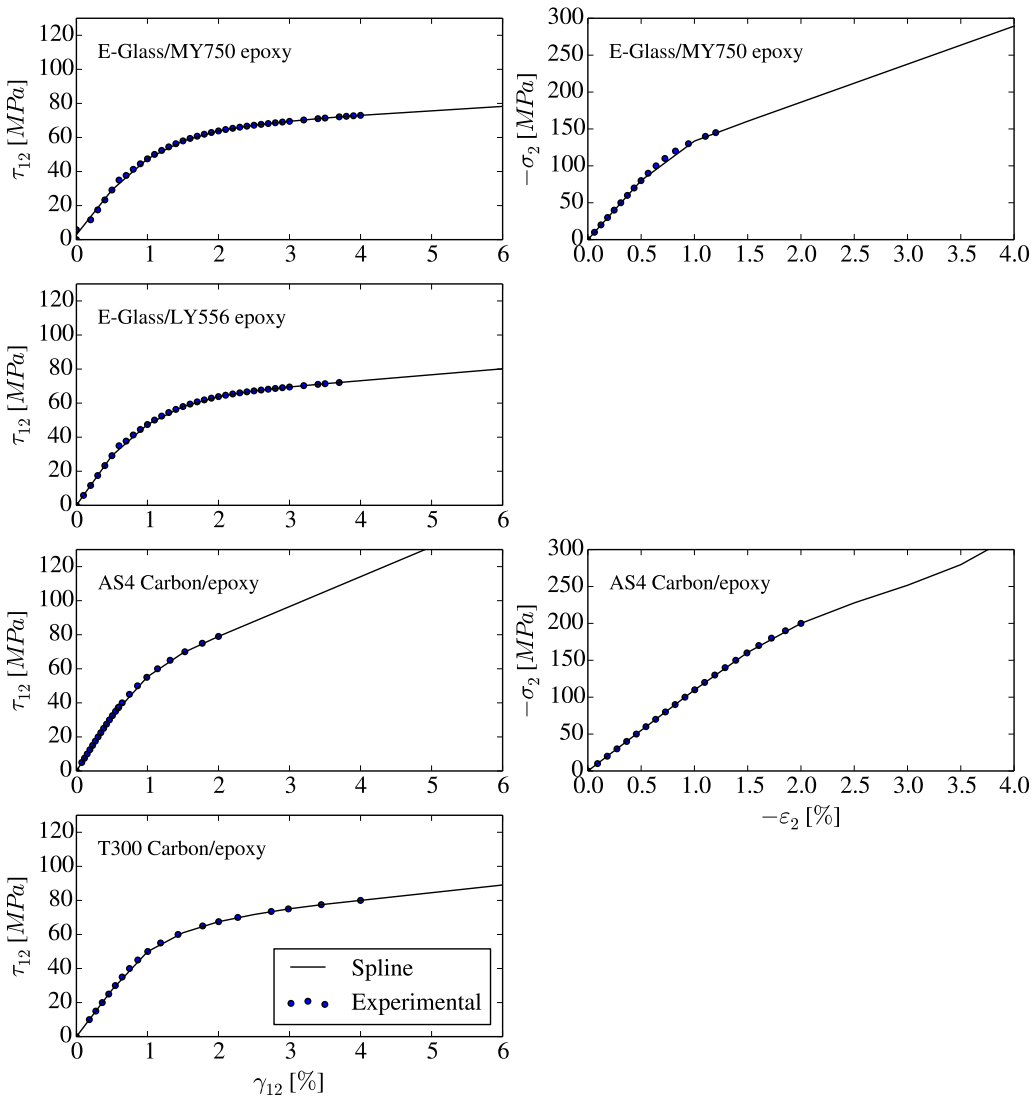

Figure D.2: Spline inter- and extrapolation of transverse longitudinal and in-plane shear stress-strain curves

D.1.2 Fracture toughness

Mode I and mode II interlaminar fracture toughness are extracted from DCB and ENF tests respectively. Assumed values for the four material combinations are listed in Table D.2. For the CFRP composites, these are assumed on the basis of Pinho's work [12]. For the GFRP composites, these are assumed on the basis of work by Girão Coelho [25].

Table D.2: Interlaminar fracture toughness of materials

	AS4/3501−6	T300/BSL914C	E-glass/LY556	E-glass/MY750
G_{Ic} [N/mm]	0.258	0.258	0.18	0.18
G_{IIc} [N/mm]	1.080	1.080	0.36	0.36

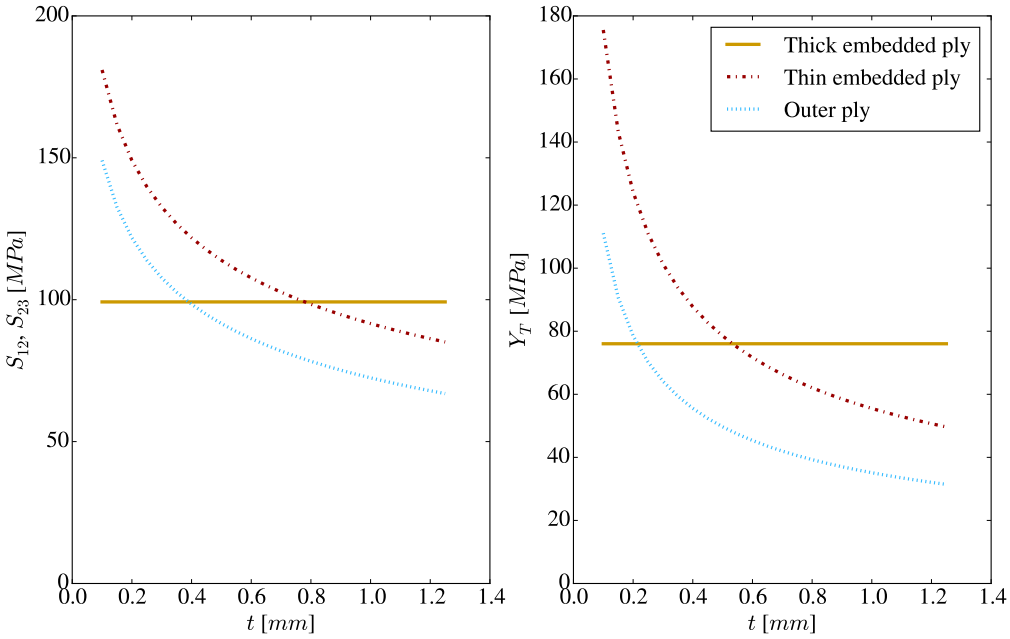

Figure D.3: In-situ strength model for AS4/3501−6 carbon epoxy lamina

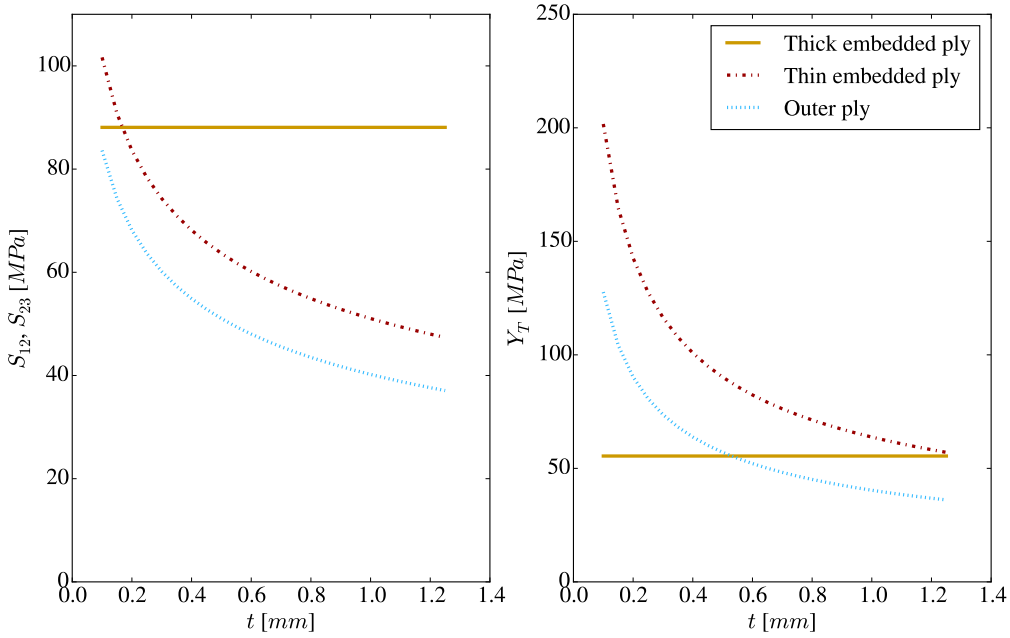

Figure D.4: In-situ strength model for T300/BSL914C carbon epoxy lamina

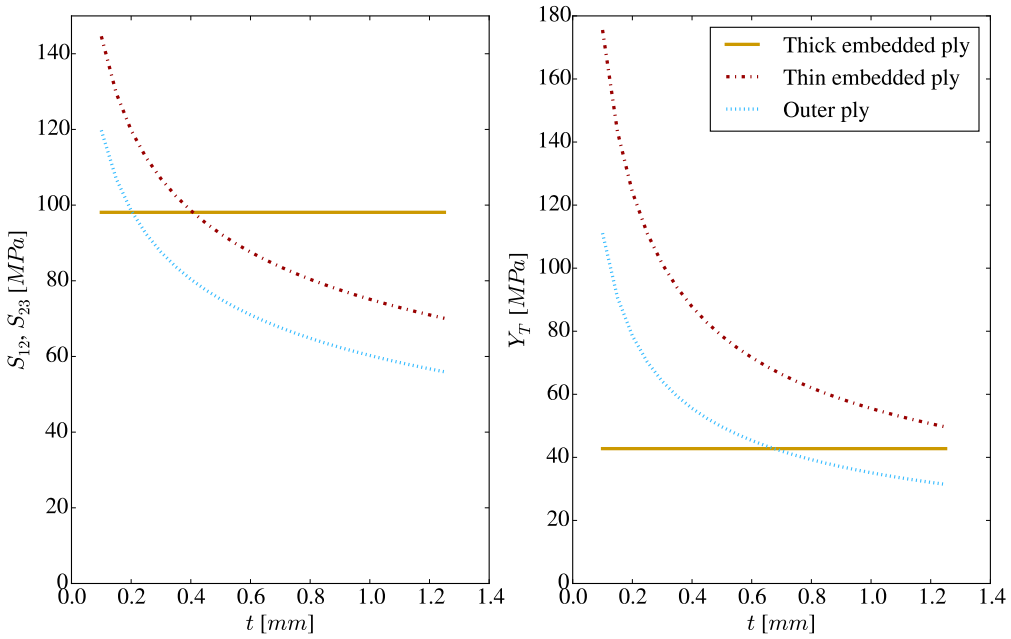

Figure D.5: In-situ strength model for E-glass/LY556 glass epoxy lamina

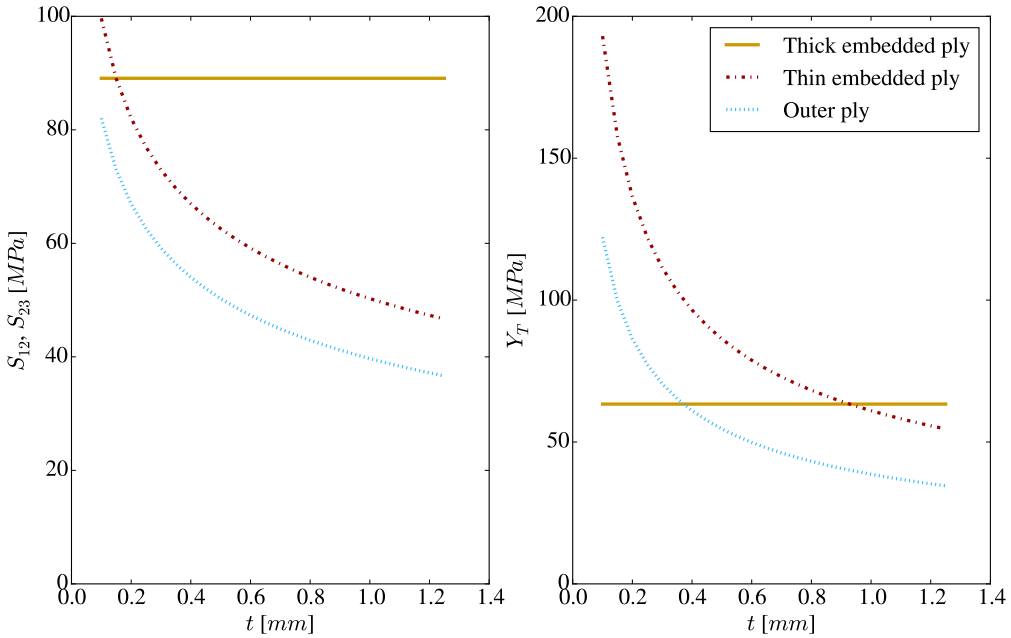

Figure D.6: In-situ strength model for E-glass/MY750 glass epoxy lamina

D.1.3 In-situ strength

For the input parameters as listed above, the in-situ strength model outlined in Section 3.3 yields results as given in Figures D.3-D.6. The intersection of thin and thick embedded ply models denotes the transition from a thin to a thick ply, i.e. the thick ply model forms a lower bound

on the strength of embedded plies.

D.1.4 Inclination parameters Puck

The inclination parameters for the Puck model are estimated based on guidelines by Deuschle [13] after the work by Puck and Knops [16]. These are summarized in Table D.3. For the range given for $p^t_{\perp\perp}$ and $p^c_{\perp\perp}$, the mean value is taken.

Table D.3: Suggested inclination parameters Puck failure theory, from [13, p.57] (after [16])

	$p^t_{\perp\parallel}$	$p^c_{\perp\parallel}$	$p^t_{\perp\perp}$, $p^c_{\perp\perp}$
CFRP	0.30	0.25	0.20-0.25
Glass Fiber Reinforced Polymer (GFRP)	0.35	0.30	0.25-0.30

D.1.5 Friction coefficients LaRC

Friction coefficients for LaRC criteria are extracted as per instructions by the authors, following from uniaxial test data as [15, 21]

$$\eta_L = \frac{-S_{12}\cos 2\alpha_0}{Y_C \cos {\alpha_0}^2} \tag{D.2}$$

$$\eta_T = \frac{-1}{\tan 2\alpha_0} \tag{D.3}$$

For all calculations, $\alpha_0 = 53^\circ$ as an approximation based on experimental observations [21, 45].

D.1.6 Fit and inclination parameters Cuntze

The fit parameter m_{Cuntze} is taken as 3.1 for the test cases, following Cuntze's submissions [44]. Analogously, $b_{\perp\parallel}$ and $b^r_\perp$ are estimated at 0.13 and 1.5 for all materials, similar to Cuntze [44].

Although these parameters can be determined from experimental data, this requires knowledge of (part of) the experimental failure envelope in advance. Since this is generally not available, the parameters are estimated, in this case on the basis of Cuntze's experience.

D.2 Test case description

In the first Worldwide Failure Exercise, a total of fourteen cases feature on a number of different laminates of a number of different fiber/matrix combinations and loading cases.These are summarized in Table D.4. The cases are briefly discussed hereafter.

Table D.4: Overview of test cases first Worldwide Failure Exercise, adapted from [2, p.44]

TC	Laminate	Material	Loading
1		E-Glass/LY556 epoxy	(σ_2, τ_{12}) envelope
2	$0°$	T300 Carbon/epoxy	(σ_1, τ_{12}) envelope
3		E-Glass/MY750 epoxy	(σ_2, σ_1) envelope
4	$(90°/\pm 30°/90°)$	E-Glass/LY556 epoxy	(σ_2, σ_1) envelope
5			(σ_2, τ_{12}) envelope
6			(σ_2, σ_1) envelope
7	$(0°/\pm 45°/90°)_s$	AS4 Carbon/epoxy	Stress strain curve $(\varepsilon_2, \sigma_2)$
8			Stress strain curve $(\varepsilon_2, \sigma_2)$ with $\sigma_2 = \sigma_1$
9			(σ_2, σ_1) envelope
10	$\pm 55°$ angle ply	E-Glass/MY750 epoxy	Stress strain curve $(\varepsilon_2, \sigma_2)$
11			Stress strain curve $(\varepsilon_2, \sigma_2)$ with $\sigma_2 = \sigma_1$
12	$(0°/90°)_s$ cross ply	E-Glass/MY750 epoxy	Stress strain curve $(\varepsilon_1, \sigma_1)$
13	$\pm 45°$ angle ply	E-Glass/MY750 epoxy	Stress strain curve $(\varepsilon_2, \sigma_2)$ with $\sigma_2 = \sigma_1$
14			Stress strain curve$(\varepsilon_2, \sigma_2)$ with $\sigma_2 = -\sigma_1$

D.2.1 Test case 1, 2 and 3

A unidirectional lamina is evaluated, thereof without the complications of in-situ strength and interply failure. Key feature is the interaction between shear and normal stresses in test cases 1 and 2, and between normal stresses in test case 3. Apparent from experimental results is an increase of shear failure stress due to transverse tensile loading, and vice versa a decrease fo shear failure stress under longitudinal tensile loading.

D.2.2 Test cases 4 and 5

A multidirectional laminate is evaluated, thereby requiring consideration of ply interaction as well as in-situ strengths. In terms of the former, whereas for a unidirectinoal laminate first ply failure entails final failure; for the case of a multidirectional laminate a failure sequence results that requires analysis of damage progression. Key features are a decrease in biaxial strength under combined tension-compression loading and a decrease in axial strength due to shear stress.

D.2.3 Test cases 6, 7 and 8

A multidirectional laminate is evaluated. Much of the same remarks as in the previous cases apply. In addition, evaluation of stress strain curves is involved. For test case 7, relatively linear behaviour was found. For test case 8, a stiffness decrease was observed near final failure.

Notable is that for the biaxial compression part of test case 6, buckling is the suspected mode of failure. This is a failure mode not considered in most of the models.

D.2.4 Test cases 9, 10 and 11

For test cases 9 up to 11, weepage (fluid leakage through thin, unlined tubes) is evaluated as well as final failure. The former is an indication of non-final failure. Both weepage and final failure show a biaxial strength larger than the uniaxial strength as a key feature.

D.2.5 Test case 12

Key features in this test case are the reduction in longitudinal modulus, accompanied by an increase in transverse crack density and the observed onset of transverse matrix cracking in the 90° plies. Final failure by fibre fracture was observed.

D.2.6 Test cases 13 and 14

These cases display much the same behaviour as test case 12. For test case 14, however, highly non-linear behaviour was observed. In addition, information on initial failure is lacking for test case 14.

Appendix E

Material data validation cases

Material data used for the modelling of validation cases is given in Tables E.1 and E.2. For T300-1034C, properties are taken from Maimí et al. [10, 34], including in-situ strengths as per the theory by Camanho et al. [29]. For the Glare GFRP, input values are as reported by Lapczyk and Hurtado [9]. For IM7/8552, ply material properties are taken from Camanho et al. [71]. For AS4/8552, material properties are taken from [89, 95, 96]. Theory-specific parameters follow as dictated in Appendix D.

Cohesive zone parameters, used for the blended models, are given in Table E.1. For IM7/8552, these are taken from [11, 79]. For AS4/8552, these are taken from [95].

Table E.1: Cohesive zone parameters (for DL and MF modelling)

Material	$\sigma_I^{\max}$ [MPa]	$\sigma_{II}^{\max}$ [MPa]	G_{Ic} [N/mm]	G_{IIc} [N/mm]	η_{BK} [-]
IM7/8552	60	90	0.2	1.0	1.0
AS4/8552	80.7	114.5	0.2	1.0	2.08

Table E.2: Material properties for lamina used in test cases (hyphens denote unavailable properties)

	T300-1034C	Glare GFRP	IM7/8552	AS4/8552
General				
E_1 [GPa]	147	55	171	135
E_2 [GPa]	11.4	9.5	9.1	9.5
ν_{12} [-]	0.30	0.33	0.33	0.32
ν_{23} [-]	0.49	0.45	0.40	0.45
G_{12} [GPa]	6.2	5.5	5.3	4.9
G_{23} [GPa]	2.2	3.0	3.2	3.2
X_T [MPa]	1724	2500	2324	2207
X_C [MPa]	1379	2000	1200	1531
Y_T (thin embedded ply) [MPa]	159	50	160	145
Y_T (thick embedded ply) [MPa]	105	-	113	82
Y_T (outer ply) [MPa]	101	-	101	96
Y_C [MPa]	268	150	200	200
S_{12} (thin embedded ply) [MPa]	110	50	130	133
S_{12} (thick embedded ply) [MPa]	73	-	107	111
S_{12} (outer ply) [MPa]	90	-	107	111
β [$\times 10^{-8}$ MPa^{-3}]	3.20	-	2.98	3.00
α_0 [deg]	53	53	53	53
Bilinear softening				
G_{fft} [N/mm]	52.5	12.5	81.5	92.0
G_{ffc} [N/mm]	45.8	12.5	106.3	80.0
G_{mft} [N/mm]	0.13	1.0	0.28	0.20
G_{mfc} [N/mm]	0.45	1.0	0.80	0.80
Puck				
$p^c_{\perp\perp}$ [-]	0.225	0.275	0.225	0.225
$p^t_{\perp\perp}$ [-]	0.225	0.275	0.225	0.225
$p^c_{\perp\parallel}$ [-]	0.25	0.30	0.25	0.25
$p^t_{\perp\parallel}$ [-]	0.30	0.35	0.30	0.30
$m_{\sigma f}$ [-]	1.1	1.3	1.1	1.1
ν_{f12} [-]	0.20	0.20	0.20	0.25
E_{f1} [GPa]	231	87	276	225
Cuntze				
m_{Cuntze} [-]	3.1	3.1	3.1	3.1
$b^\tau_\perp$ [-]	1.3	1.3	1.3	1.3
$b_{\perp\parallel}$ [-]	0.13	0.13	0.13	0.13
$b^\tau_{\perp\parallel}$ [-]	0.4	0.4	0.4	0.45

References

[1] U. Icardi, S. Locatto, and A. Longo, "Assessment of Recent Theories for Predicting Failure of Composite Laminates," *Applied Mechanics Reviews*, vol. 60, no. 2, p. 76, 2007.

[2] A. S. Kaddour, M. J. Hinton, and P. D. Soden, eds., *Failure Criteria in Fibre Reinforced Polymer Composites: The World-Wide Failure Exercise*. Oxford: Elsevier Ltd, 1st ed., 2004.

[3] A. S. Kaddour and M. J. Hinton, "Maturity of 3D failure criteria for fibre-reinforced composites: Comparison between theories and experiments: Part B of WWFE-II," *Journal of Composite Materials*, vol. 47, no. 6-7, pp. 925–966, 2013.

[4] A. C. Orifici, I. Herszberg, and R. S. Thomson, "Review of methodologies for composite material modelling incorporating failure," *Composite Structures*, vol. 86, no. 1-3, pp. 194–210, 2008.

[5] J. A. Pascoe, R. C. Alderliesten, and R. Benedictus, "Methods for the prediction of fatigue delamination growth in composites and adhesive bonds - A critical review," *Engineering Fracture Mechanics*, vol. 112-113, pp. 72–96, 2013.

[6] A. van Oostrum, *Application of fracture mechanics in a blended methodology for Progressive Damage Analysis of Fiber-Reinforced Polymers in FEM*. Msc thesis, Delft University of Technology, to be published (September 2017).

[7] M. R. Garnich and V. M. K. Akula, "Review of Degradation Models for Progressive Failure Analysis of Fiber Reinforced Polymer Composites," *Applied Mechanics Reviews*, vol. 62, no. 1, pp. 010801–010801–33, 2008.

[8] L. B. Lessard and M. M. Shokrieh, "Two-Dimensional Modeling of Composite Pinned-Joint Failure," *Journal of Composite Materials*, vol. 29, no. 5, pp. 671–697, 1995.

[9] I. Lapczyk and J. A. Hurtado, "Progressive damage modeling in fiber-reinforced materials," *Composites Part A: Applied Science and Manufacturing*, vol. 38, no. 11, pp. 2333–2341, 2007.

[10] P. Maimí, P. P. Camanho, J. A. Mayugo, and C. G. Dávila, "A continuum damage model for composite laminates: Part I - Constitutive model," *Mechanics of Materials*, vol. 39, no. 10, pp. 897–908, 2007.

[11] F. P. Van der Meer, *Computational Modeling of Failure in Composite Laminates*. Phd thesis, Delft University of Technology, 2010.

[12] S. T. Pinho, *Modelling failure of laminated composites using physically-based failure models*. Phd thesis, Imperial College London, 2005.

[13] H. M. Deuschle, *3D Failure Analysis of UD Fibre Reinforced Composites: Puck's theory within FEA*. Phd thesis, Universität Stuttgart, 2010.

[14] I. M. Daniel and O. Ishai, *Engineering Mechanics of Composite Materials*. New York: Oxford University Press, 2nd ed., 2006.

[15] S. T. Pinho, C. G. Dávila, P. P. Camanho, L. Iannucci, and P. Robinson, "Failure Models and Criteria for FRP Under In-Plane or Three-Dimensional Stress States Including Shear Non-linearity," tech. rep., National Aeronautics and Space Administration, Hampton, Virginia, 2005.

[16] A. Puck, J. Kopp, and M. Knops, "Guidelines for the determination of the parameters in Puck's action plane strength criterion," *Composites Science and Technology*, vol. 62, no. 3, pp. 371–378, 2002.

[17] T. A. Bogetti, C. P. R. Hoppel, V. M. Harik, J. F. Newill, and B. P. Burns, "Predicting the nonlinear response and progressive failure of composite laminates," *Failure Criteria in Fibre-Reinforced-Polymer Composites*, vol. 64, no. 3, pp. 329–342, 2012.

[18] H. T. Hahn and S. W. Tsai, "Nonlinear Elastic Behavior of Unidirectional Composite Laminae," *Journal of Composite Materials*, vol. 7, no. 1, pp. 102–118, 1973.

[19] F. Chang, R. A. Scott, and G. S. Springer, "Failure Strength of Nonlinearly Elastic Composite Laminates Containing a Pin Loaded Hole," *Journal of Composite Materials*, vol. 18, no. 5, pp. 464–477, 1984.

[20] S. T. Pinho, R. Darvizeh, P. Robinson, C. Schuecker, and P. P. Camanho, "Material and structural response of polymer-matrix fibre-reinforced composites," *Journal of Composite Materials*, vol. 46, no. 20, pp. 2313–2341, 2012.

[21] C. G. Davila, N. Jaunky, and S. Goswami, "Failure Criteria for FRP Laminates in Plane Stress," *Journal of Composite Materials*, vol. 39, no. 4, pp. 323 – 345, 2005.

[22] Z. Hashin and A. Rotem, "A fatigue failure criterion for fiber-reinforced materials," *Journal of Composite Materials*, vol. 7, no. 4, pp. 448–464, 1973.

[23] C. Soutis, F. C. Smith, and F. L. Matthews, "Predicting the compressive engineering performance of carbon fibre-reinforced plastics," *Composites Part A: Applied Science and Manufacturing*, vol. 31, no. 6, pp. 531–536, 2000.

[24] C. R. Schultheisz and A. M. Waas, "Compressive failure of composites, Part I: Testing and micromechanical theories," *Progress in Aerospace Sciences*, vol. 32, no. 1, pp. 1–42, 1996.

[25] A. M. Girão Coelho, "Finite Element Guidelines for Simulation of Delamination Dominated Failures in Composite Materials Validated by Case Studies," *Archives of Computational Methods in Engineering*, vol. 23, no. 2, pp. 363–388, 2016.

[26] A. C. Garg, "Delamination- A damage mode in composite structures," *Engineering Fracture Mechanics*, vol. 29, no. 5, pp. 557–584, 1988.

[27] J. Berthelot, "Transverse cracking and delamination in cross-ply glass-fiber and carbon-fiber reinforced plastic laminates: Static and fatigue loading," *Applied Mechanics Reviews*, vol. 56, no. 1, pp. 111–147, 2003.

[28] A. Parvizi, K. W. Garrett, and J. E. Bailey, "Constrained cracking in glass fibre-reinforced epoxy cross-ply laminates," *Journal of Materials Science*, vol. 13, no. 1, pp. 195–201, 1978.

[29] P. P. Camanho, C. G. Dávila, S. T. Pinho, L. Iannucci, and P. Robinson, "Prediction of in situ strengths and matrix cracking in composites under transverse tension and in-plane shear," *Composites Part A: Applied Science and Manufacturing*, vol. 37, no. 2, pp. 165–176, 2006.

[30] F. K. Chang and M. H. Chen, "The In Situ Ply Shear Strength Distributions in Graphite/Epoxy Laminated Composites," *Journal of Composite Materials*, vol. 21, no. August 1987, pp. 708–733, 1987.

[31] D. L. Flaggs and M. H. Kural, "Experimental Determination of the In Situ Transverse Lamina Strength in Graphite/Epoxy Laminates," *Journal of Composite Materials*, vol. 16, no. 2, pp. 103–116, 1982.

[32] S. T. Pinho, G. Vyas, and P. Robinson, "Response and damage propagation of polymer-matrix fibre-reinforced composites: Predictions for WWFE-III Part A," *Journal of Composite Materials*, vol. 47, no. 20-21, pp. 2595–2612, 2013.

[33] G. J. Dvorak and N. Laws, "Analysis of Progressive Matrix Cracking In Composite Laminates II. First Ply Failure," *Journal of Composite Materials*, vol. 21, no. 4, pp. 309–329, 1987.

[34] P. Maimí, P. P. Camanho, J. A. Mayugo, and C. G. Dávila, "A continuum damage model for composite laminates: Part II - Computational implementation and validation," *Mechanics of Materials*, vol. 39, no. 10, pp. 909–919, 2007.

[35] S. W. Tsai, "Strength Characteristics of Composite Materials," tech. rep., National Aeronautics and Space Administration, Washington, DC, 1965.

[36] S. W. Tsai and E. M. Wu, "A General Theory of Strength for Anisotropic Materials," *Journal of Composite Materials*, vol. 5, no. 1, pp. 58–80, 1971.

[37] C. T. Sun, B. J. Quinn, and J. Tao, "Comparative Evaluation of Failure Analysis Methods for Composite Laminates.," tech. rep., U.S. Department of Transportation, Springfield, Virginia, 1996.

[38] R. Hill, "A Theory of the Yielding and Plastic Flow of Anisotropic Metals," *Proceedings of the Royal Society of London. Series A, Mathematical and Physical Sciences*, vol. 193, no. 1033, pp. 281–297, 1948.

[39] F. Paris, "A Study of Failure Criteria of Fibrous Composite Materials," tech. rep., National Aeronautics and Space Administration, Hampton, Virginia, 2001.

[40] O. Hoffman, "The Brittle Strength of Orthotropic Materials," *Journal of Composite Materials*, vol. 1, no. 2, pp. 200–206, 1967.

[41] C. C. Chamis, "Failure Criteria for Filamentary Composites," in *Testing and Design, ASTM STP 460*, pp. 336–460, Philadelphia: American Society for Testing and Materials, 1969.

[42] A. Puck and H. Schürmann, "Failure Analysis of FRP Laminates By Means of Physically Based Phenomenological Models," *Composites Science and Technology*, no. 62, pp. 1633–1662, 2002.

[43] Z. Hashin, "Failure Criteria for Unidirectional Fiber Composites," *Journal of Applied Mechanics*, vol. 47, no. 2, pp. 329–334, 1980.

[44] R. G. Cuntze, "The predictive capability of failure mode concept-based strength criteria for multi-directional laminates-Part B," *Composites Science and Technology*, vol. 64, no. 3, pp. 976–1025, 2004.

[45] A. Puck and H. Schürmann, "Failure analysis of FRP laminates by means of physically based phenomenological models," *Composites Science and Technology*, no. 58, pp. 1045–1067, 1998.

[46] J. D. Lee, "Three dimensional finite element analysis of damage accumulation in composite laminate," *Computers & Structures*, vol. I, no. 3, pp. 335–350, 1982.

[47] O. O. Ochoa and J. J. Engblom, "Analysis of progressive failure in composites," *Composites Science and Technology*, vol. 28, no. 2, pp. 87–102, 1987.

[48] R. S. Long, "Static Strength of Adhesively Bonded ARALL-1 Joints," *Journal of Composite Materials*, vol. 25, no. 4, pp. 391–415, 1991.

[49] M. M. Shokrieh, L. B. Lessard, and C. Poon, "Three-Dimensional Progressive Failure Analysis of Pin/Bolt Loaded Composite Laminates," in *83rd Meeting of the AGARD SMP on "Bolted/Bonded Joints in Polymeric Composites"*, (Florence, Italy), 1996.

[50] L. Tong, "An Assessment of Failure Criteria to Predict the Strength of Adhesively Bonded Composite Double Lap Joints," *Journal of Reinforced Plastics and Composites*, vol. 16, no. 8, pp. 698–713, 1997.

[51] M. E. Pachajoa, M. K. Frances, and J. D. Lee, "Stress and failure analysis of composite structures," *Engineering Fracture Mechanics*, vol. 50, no. 5, pp. 883–902, 1995.

[52] C. T. McCarthy, M. A. McCarthy, and V. P. Lawlor, "Progressive damage analysis of multi-bolt composite joints with variable bolt-hole clearances," *Composites Part B: Engineering*, vol. 36, no. 4, pp. 290–305, 2005.

[53] P. P. Camanho and F. L. Matthews, "A Progressive Damage Model for Mechanically Fastened Joints in Composite Laminates," *Journal of Composite Materials*, vol. 33, no. 24, pp. 2248–2280, 1999.

[54] K. I. Tserpes, G. Labeas, P. Papanikos, and T. Kermanidis, "Strength prediction of bolted joints in graphite/epoxy composite laminates," *Composites Part B: Engineering*, vol. 33, no. 7, pp. 521–529, 2002.

[55] C. Zhang, N. Li, W. Wang, W. K. Binienda, and H. Fang, "Progressive damage simulation of triaxially braided composite using a 3D meso-scale finite element model," *Composite Structures*, no. 125, pp. 104–116, 2015.

[56] Z. P. Bažant and B. H. Oh, "Crack band theory for fracture of concrete," *Matériaux et Construction*, vol. 16, no. 3, pp. 155–177, 1983.

[57] F. P. Van der Meer and L. J. Sluys, "Continuum Models for the Analysis of Progressive Failure in Composite Laminates," *Journal of Composite Materials*, vol. 43, no. 20, pp. 2131–2156, 2009.

[58] P. P. Camanho, W. S. Sanders, C. Davila, and J. A. Mayugo, "Progressive failure analysis of advanced composites," tech. rep., University of Porto, Department of Mechanical Engineering, Porto, Portugal, 2008.

[59] G. Vigueras, F. Sket, C. Samaniego, L. Wu, L. Noels, D. Tjahjanto, E. Casoni, G. Houzeaux, A. Makradi, J. M. Molina-Aldareguia, M. Vázquez, and A. Jérusalem, "An XFEM/CZM implementation for massively parallel simulations of composites fracture," *Composite Structures*, vol. 125, no. July, pp. 542–557, 2015.

[60] P. W. Harper and S. R. Hallett, "Cohesive zone length in numerical simulations of composite delamination," *Engineering Fracture Mechanics*, vol. 75, no. 16, pp. 4774–4792, 2008.

[61] A. S. Kaddour, M. J. Hinton, and P. D. Soden, "A comparison between the predictive capability of matrix cracking, damage and failure criteria for fibre reinforced composite laminates: Part A of the third world-wide failure exercise," *Journal of Composite Materials*, vol. 47, no. 20-21, pp. 2749–2779, 2013.

[62] D. S. Zarouchas, A. A. Makris, F. Sayer, D. van Hemelrijck, and A. M. van Wingerde, "Investigations on the mechanical behavior of a wind rotor blade subcomponent," *Composites Part B: Engineering*, vol. 43, no. 2, pp. 647–654, 2012.

[63] A. A. Makris, C. Ramault, D. van Hemelrijck, D. S. Zarouchas, E. Lamkanfi, and W. van Paepegem, "An investigation of the mechanical behavior of carbon epoxy cross ply cruciform specimens under biaxial loading," *Polymer Composites*, vol. 31, no. 9, pp. 1554–1561, 2010.

[64] N. F. Knight, "User-Defined Material Model for Progressive Failure Analysis," tech. rep., National Aeronautics and Space Administration, 2006.

[65] O. O. Ochoa and J. N. Reddy, *Finite Element Analysis of Composite Laminates*. Boston, MA: Kluwer, 1st ed., 1992.

[66] D. H. Robbins and J. N. Reddy, "Modelling of thick composites using a layerwise laminate theory," *International Journal for Numerical Methods in Engineering*, vol. 36, no. 4, pp. 655–677, 1993.

[67] F. K. Chang and K. Y. Chang, "A Progressive Damage Model for Laminated Composites Containing Stress Concentrations," *Journal of Composite Materials*, vol. 21, no. 9, pp. 834–855, 1987.

[68] J. B. Ransom and N. F. Knight, "Global/local stress analysis of composite panel," tech. rep., National Aeronautics and Space Administration, 1989.

[69] N. Germain, J. Besson, and F. Feyel, "Composite layered materials: Anisotropic nonlocal damage models," *Computer Methods in Applied Mechanics and Engineering*, vol. 196, no. 41-44, pp. 4272–4282, 2007.

[70] S. C. Tan, "A Progressive Failure Model for Composite Laminates Containing Openings," *Journal of Applied Mechanics*, vol. 25, no. May, pp. 556–577, 1991.

[71] P. P. Camanho, P. Maimí, and C. G. Dávila, "Prediction of size effects in notched laminates using continuum damage mechanics," *Composites Science and Technology*, vol. 67, no. 13, pp. 2715–2727, 2007.

[72] S. C. Tan, *Stress Concentrations in Laminated Composites*. Lancaster, Pennsylvania: Technomic Pub. Co., 1st ed., 1994.

[73] O. J. Nixon-Pearson, S. R. Hallett, P. W. Harper, and L. F. Kawashita, "Damage development in open-hole composite specimens in fatigue. Part 2: Numerical modelling," *Composite Structures*, vol. 106, pp. 890–898, 2013.

[74] O. J. Nixon-Pearson and S. R. Hallett, "An investigation into the damage development and residual strengths of open-hole specimens in fatigue," *Composites Part A: Applied Science and Manufacturing*, vol. 69, pp. 266–278, 2015.

[75] T. J. De Vries, *Blunt and sharp notch behaviour of Glare laminates*. PhD thesis, Delft University of Technology, 2001.

[76] A. B. De Morais, "Cohesive zone beam modelling of mixed-mode I-II delamination," *Composites Part A: Applied Science and Manufacturing*, vol. 64, no. September, pp. 124–131, 2014.

[77] P. Camanho and C. Davila, "Mixed-Mode Decohesion Finite Elements in for the Simulation Composite of Delamination Materials," tech. rep., National Aeronautics and Space Administration, Hampton, Virginia, 2002.

[78] A. Turon, C. G. Dávila, P. P. Camanho, and J. Costa, "An Engineering Solution for Solving Mesh Size Effects in the Simulation of Delamination with Cohesive Zone Models," *Engineering Fracture Mechanics Journal*, vol. 74, no. 10, pp. 1665–1682, 2007.

[79] S. R. Hallett, B. G. Green, W. G. Jiang, and M. R. Wisnom, "An experimental and numerical investigation into the damage mechanisms in notched composites," *Composites Part A: Applied Science and Manufacturing*, vol. 40, no. 5, pp. 613–624, 2009.

[80] R. Krueger, "Virtual crack closure technique: History, approach, and applications," *Applied Mechanics Reviews*, vol. 57, no. 2, p. 109, 2004.

[81] Q. Yang and B. Cox, "Cohesive models for damage evolution in laminated composites," *International Journal of Fracture*, vol. 133, no. 2, pp. 107–137, 2005.

[82] M. Elices, G. Guinea, J. Gómez, and J. Planas, "The cohesive zone model: advantages, limitations and challenges," *Engineering Fracture Mechanics*, vol. 69, no. 2, pp. 137–163, 2002.

[83] M. Jalalvand, G. Czél, J. D. Fuller, M. R. Wisnom, L. P. Canal, C. D. González, and J. LLorca, "Energy dissipation during delamination in composite materials - An experimental assessment of the cohesive law and the stress-strain field ahead of a crack tip," *Composites Science and Technology*, vol. 134, pp. 115–124, 2016.

[84] M. L. Benzeggagh and M. Kenane, "Measurement of mixed-mode delamination fracture toughness of unidirectional glass/epoxy composites with mixed-mode bending apparatus," *Composites Science and Technology*, vol. 56, no. 4, pp. 439–449, 1996.

[85] B. G. Green, M. R. Wisnom, and S. R. Hallett, "An experimental investigation into the tensile strength scaling of notched composites," *Composites Part A: Applied Science and Manufacturing*, vol. 38, no. 3, pp. 867–878, 2007.

[86] T. Fries and T. Belytschko, "The extended/generalized finite element method: An overview of the method and its applications," *International Journal for Numerical Methods in Engineering*, vol. 84, no. 3, pp. 253–304, 2010.

[87] Hexcel 8552, "Epoxy Matrix Product Datasheet." http://www.hexcel.com/user_area/content_media/raw/HexPly_8552_eu_DataSheet.pdf. [Online; accessed 01-02-2017].

[88] D. S. Zarouchas, A. E. Antoniou, F. Sayer, D. Van Hemelrijck, and A. M. van Wingerde, "Structural Integrity Assessment of blade's subcomponents using Acoustic Emission Monitoring.," in *Experimental and Applied Mechanics, Volume 6: Proceedings of the 2011 Annual Conference on Experimental and Applied Mechanics* (T. Proulx, ed.), pp. 511–518, New York, NY: Springer New York, 2011.

[89] N. Ersoy, T. Garstka, K. Potter, M. R. Wisnom, D. Porter, M. Clegg, and G. Stringer, "Development of the properties of a carbon fibre reinforced thermosetting composite through cure," *Composites Part A: Applied Science and Manufacturing*, vol. 41, no. 3, pp. 401–409, 2010.

[90] B. R. van Dongen and D. S. Zarouchas, "An evaluation of progressive damage analysis using stress-strain based methodologies for composites through FEM implementation," *Journal of Composite Materials*, submitted manuscript.

[91] B. R. van Dongen, A. van Oostrum, and D. S. Zarouchas, "Implementation and validation of a blended continuum damage and fracture mechanics method for Progressive Damage Analysis of Fiber-Reinforced Polymers using XFEM," *Composite Structures*, manuscript prepared for submission.

[92] H. M. Deuschle and A. Puck, "Application of the Puck failure theory for fibre-reinforced composites under three-dimensional stress: Comparison with experimental results," *Journal of Composite Materials*, vol. 47, no. 6-7, pp. 827–846, 2013.

[93] R. G. Cuntze, "The predictive capability of failure mode concept-based strength conditions

for laminates composed of unidirectional laminae under static triaxial stress states," *Journal of Composite Materials*, vol. 46, no. 19-20, pp. 2563–2594, 2012.

[94] R. Sandhu, "Nonlinear Behavior of Unidirectional and Angle Ply Laminates," *Journal of Aircraft*, vol. 13, no. 2, pp. 104–111, 1976.

[95] N. G. Perogamvros and G. N. Lampeas, "Experimental and numerical investigation of AS4/8552 interlaminar shear strength under impact loading conditions," *Journal of Composite Materials*, vol. 50, no. 19, pp. 2669–2685, 2016.

[96] P. Badalló, *Analysis and Optimization of Composite Stringers*. PhD thesis, Universitat de Girona, 2015.